Analysing the ability of the UniGrow method to assess the effect of the geometry of the weld excess on the fatigue life of butt-welded plates

T. M. de Bruijn

TU Delft

SIEMENS Gamesa
RENEWABLE ENERGY

Analysing the ability of the UniGrow method to assess the effect of the geometry of the weld excess on the fatigue life of butt-welded plates

by

T.M. de Bruijn

to obtain the degree of Master of Science
at the Delft University of Technology,
to be defended publicly on Thursday January 7th, 2021 at 13:00

Student number: 4730046

Project duration: December 4th 2019 – December 3rd 2020

Thesis committee:

Prof. M. Veljkovic	TU Delft, Chairman
Dr. H. Xin	TU Delft
Dr. ir. J. H. den Besten	TU Delft
J. Remijn	SGRE
M. Seidel	SGRE

TU Delft

Preface

Laying before you is the conclusion to my Master programme at the TU Delft. It was a time which I thoroughly enjoyed, and which allowed me to further focus on the direction of study I am interested in: the design of steel and timber structures. However, writing and conducting the Master thesis was no easy task in a year which was dominated by restrictions due to COVID-19. This makes me especially grateful for the people who have helped me through the past year in any way, shape or form.

As a start, I would like to thank Milan Veljkovic for finding an interesting thesis topic and for his useful input and feedback during our progress meetings. Thanks for pushing me to keep on delivering better results and improving my research. I would also like to thank Haohui Xin for his feedback and discussions during the progress meetings. Furthermore, I would like to thank Henk den Besten and Stephanie Röscher for their feedback on my thesis.

On the SGRE side, a huge thank you is in place for Joris Remijn. Our weekly discussions, be it in the office or through Teams, have helped greatly in pushing the thesis forwards. You provided very interesting insights and your trust in the thesis was very valuable. I would also like to thank Marc Seidel for providing great feedback and guidance for when I was stuck.

I would like to thank my mother, my father, my brother Paul and his girlfriend Ilse. Due to COVID-19 we spent many, many hours at home, together, and you made it work so well. You have always supported me and believed in me and I can't express how grateful I am for that.

Even though we haven't spent nearly as much time together as I would've liked to, I would also like to thank my friends. They provided the necessary distraction from my thesis during those fun days that we had together, be it in a theme park or at home.

A last and very special thank you goes to my girlfriend Femke, who was there for me when I needed it most and who has been so very supportive. This year has probably been one of the toughest years in my life and thanks to the many fun days we spent together, I was able to pull through. Thank you.

Abstract

Fatigue is one of the driving limit states in the design of wind turbines, as they are subject to varying loads from winds, waves and gusts. One such governing area is the butt-welded connection from the shell to the ring flange. To optimize the tower design and to help focus future research, more insight on the influence of material properties and geometrical features on the fatigue life of these butt welds is needed. Due to the costs associated with testing, SGRE stated the need for a model that could assess the total fatigue life of butt welds subject to Mode I cracking in a rather quick way. After literature study, it was proposed to use the UniGrow model.

The UniGrow method is a total fatigue life model in which the material is considered to consist of elementary blocks. Fatigue is modelled as a process of continuous crack initiation of the elementary block ahead of the crack tip. In this model, the plastic compressive residual stress ahead of the crack tip plays an important role in the determination of the crack growth speed. These plastic compressive residual stresses ahead of the crack tip can either be determined analytically (analytical UniGrow) or by using numerical methods such as FEA (numerical UniGrow). The plastic compressive residual stresses ahead of the crack tip are converted into a plastic residual SIF that is used to reduce the applied residual stress intensity factor (i.e. plasticity decreases crack growth speed). Due to the application of a number of methods such as the Creager-Paris equations, the current UniGrow implementation is solely valid for pure Mode I crack growth.

Validation of the UniGrow method in the crack propagation range has been performed with results from experiments on CT specimens made of S355 steel. Good correspondence between the experimental results and predicted crack growth rates were found for all stress ratios except R = 0.25. Both Analytical and Numerical Unigrow methods have been analysed. Based upon the results of the validation it was recommended to use a numerical method (elastoplastic FEA) to determine the plastic residual stresses ahead of the crack tip as this provides more physically accurate results. The analytical method can be used to obtain an initial guess of the elementary block size, as it is a much faster method. Furthermore, using the Morrow method for the determination of the fatigue life of the elementary block ahead of the crack tip was found to provide more accurate results than the SWT damage parameter. This is due to the fact that in the elementary block ahead of the crack tip, cyclic stress relaxation occurs and, therefore, mean stress effects need not be accounted for. For short cracks, the fatigue life of the elementary block is usually outside the LCF range ($N_f > 5*10^4$ cycles). Here, the use of the Morrow method without considering residual stresses is not recommended since cyclic stress relaxation does not occur due to limited plasticity.

The performance of the UniGrow method as total fatigue life was studied using literature research and a comparison to another total fatigue life model: Two-Stage-Model. In the studied literature, researchers tend to use the weight function method to determine the SIF in welded geometries. Analysis comparing the weight function method to FEA results showed that the WF method generally overpredicts the SIFs compared to FEA. For a flat plate, the difference was found to be a maximum of 3.5%, whereas for the welded geometry, the difference was up to 12%.

From the literature and the comparison of the UniGrow model to the Two-Stage-Model, it was concluded that the UniGrow model is incapable of predicting proper fatigue crack initiation lives as it is unable to capture the complexity of short crack growth. The model provides satisfactory results for cracks where crack propagation is a dominant part of the fatigue life (such as welded geometries and notched specimens in the LCF regime). It was proposed to use the UniGrow model to determine fatigue lives of notched specimens up to 10^5 cycles. It was found that this limit also depends on the SCF present in the specimen. For welded geometries, available results in literature showed good correspondence. However, the welds used by SGRE are of better quality (lower SCF) than the ones used in UniGrow research. This means that relatively more of the fatigue life will be spent in fatigue crack initiation. More research is therefore needed to examine whether this affects the functioning of the UniGrow method for welds.

The UniGrow method was lastly used to determine which of the parameters controlling the geometry of the weld excess (the weld flank angle, weld toe radius and weld excess height) is of greatest influence on the fatigue performance of a butt weld. From this analysis it was concluded that changing the weld excess height, followed by the weld flank angle has the most beneficial effect on the fatigue life. The results from this parametric study should be used with great care: the usage of the UniGrow method combined with neglecting the residual stresses could lead to incorrect predictions of fatigue crack initiation life. Simplifications of the material and crack type could also have had an influence on the results.

Contents

List of Figures

List of Tables

List of Abbreviations

FEA	Finite Element Analysis
HCF	High Cycle Fatigue
LC	Long Crack
LCF	Low Cycle Fatigue
SC	Short Crack
SCF	Stress Concentration Factor
SIF	Stress Intensity Factor
WF	Weight Function
XFEM	eXtended Finite Element Method

1 Introduction

1.1 Background Information

Wind turbines are subject to varying loads coming from gusts of winds or waves. In steel, of which the towers are made, these varying loads can cause fatigue failure even if the stresses are well below yield stress. Fatigue failure is due to the nucleation of microcracks at the surface of the material (crack initiation) and subsequent crack propagation by cyclic loading. This is especially a problem in welded areas because the weld profiles can be quite rough, causing stress concentrations. Also, the residual stresses caused by the cooling of the weld metal can cause fatigue cracks in nominally compressive joints.

Fatigue is considered as one of the limit states during tower design. Turbine tower design is, in most of the cases, said to be fatigue-controlled: the fatigue loads are governing for the dimensioning of the turbine tower. Currently, fatigue design at SGRE is done using S-N/FAT curves, where the fatigue life can be determined directly from the nominal stress. These have the issue of being very conservative, with a design factor of 1.25 on the load side causing the design life to be up to a half less than the characteristic life. Furthermore, S-N/FAT curves are based solely on a lot of historical experimental results, all with varying failure criteria, material data and so forth. There's thus no clear definition of *fatigue failure* as such and it also completely ignores any underlying physical processes.

SGRE has attempted to improve the fatigue life by crafting a new S-N curve specific for the butt welds used in their towers that are fabricated according to their weld quality requirements. This S-N curve, however, still inherits the same issues as mentioned in the previous paragraph.

The goal of SGRE is to get more insight in the physical process behind fatigue failure and the parameters that control them. The goal of SGRE is thus said to be twofold: implement and analyse a total fatigue life model capable of accounting for geometrical features of butt welds and analyse the effect of those geometrical features. This can be a valuable resource for SGRE in order to further focus research and optimize the tower design.

1.2 Research Objective

Considering the issues mentioned in chapter 1.1, the following objective has been developed for this thesis:

Implement and analyse the functioning of a total fatigue life model which can be used for analysis of the effect of the geometry of the weld excess on the fatigue life of butt-welded plates subject to Mode I cracks.

1.3 Research Questions

After a literature study, it was concluded that the model that will be implemented and analysed is the UniGrow model. This has led to the formation to the following main research question:

To what extent is the UniGrow method capable of predicting the influence of the weld geometry on the total fatigue life of butt welds subject to Mode I cracks?

With the following sub-questions:

1. How well does the analytical UniGrow model perform compared to the numerical UniGrow model in terms of prediction of plastic residual stresses ahead of the crack tip and crack growth speed of Mode I cracks in mild steel at various stress ratios?
2. How well does the UniGrow method perform in predicting crack growth rates of Mode I long cracks in mild steel at various stress ratios?
3. Which strain-life method used in the UniGrow method is most suitable for predicting the crack growth speed of Mode I cracks in mild steel at various stress ratios?
4. How well does the weight function method perform compared to FEA for predicting SIF of Mode I edge cracks in a butt weld geometry?
5. What are the results from other research that have used the UniGrow method to predict total fatigue life of Mode I cracks?

6. How does the UniGrow method perform compared to the Two-Stage-Model in predicting the total fatigue life of butt weld geometries made of mild steel with an edge crack loaded in tension?
7. What are the validity limits of use of the UniGrow model for Mode I cracks based on the results of this study and literature for the prediction of the fatigue life?
8. Which of the geometrical features of the weld excess does the implemented UniGrow method predict to be of greatest influence on the fatigue life of Mode I edge cracks in butt-welds made of mild steel?

1.4 Thesis Structure

The thesis is divided into six chapters, each with their own purpose. The structure of the thesis can be read below.

Chapter 2 presents an overview of the literature that is relevant to the current study. The literature study starts with an overview of fatigue and the relevant parameters influencing the fatigue life of butt-welded geometries. It is continued by methods that are used to model the two stages of fatigue, after which some total fatigue life models, such as the UniGrow method, are presented.

Chapter 3 discusses the implementation, verification and validation of the UniGrow method. In the first section of the chapter, an analytical version of the UniGrow method will be implemented and verified. The second section is focused on a numerical version of the UniGrow method. After verification of this method, validation of both the analytical and numerical methods has been done against crack growth data. This validation is limited to the crack propagation phase.

Chapter 4 analyses the functioning of the UniGrow model as a total fatigue life model. The chapter starts off with a literature study in which previous research that have used the UniGrow method to determine the total fatigue life of detail will be discussed. Subsequently, the UniGrow model will be compared to the Two-Stage-Model on prediction of total fatigue life of welded geometries without consideration of weld residual stresses. The chapter will be concluded by a proposal of the validity limits of the UniGrow model.

Chapter 5 presents the parametric study that has been conducted using the UniGrow method. Here, three parameters that influence the geometry of the weld excess will be examined on their effect on the total fatigue life of butt welds made of S355 steel.

Chapter 6 present the conclusions of the research and the recommendations.

2 Literature Overview

2.1 Fatigue

The classical definition of fatigue is: the progressive, localized and permanent structural change that occurs in a material that is subject to cyclic fluctuating stresses. These stresses may well be below the tensile strength of the material.

The growth of a fatigue crack can be divided into three stages: crack initiation, crack propagation and final fracture [71], as depicted in Figure 2.1. Crack initiation starts with the formation of microcracks at points of high stress concentrations due to surface flaws, geometrical discontinuities or weld defects. As microcracks grow, they coalesce to form one principal crack. In contrary to the microcracks, which are governed by shear, the principal crack will grow perpendicular to the direction of the stress. Once it is large enough, the crack enters the crack growth stage. After the propagation period, the crack growth becomes unstable and the specimen breaks.

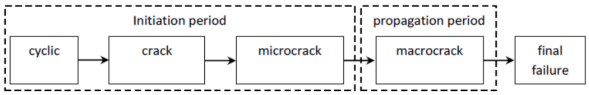

Figure 2.1 Stages of fatigue life [71]

Generally, at low levels of stress and strains or for unnotched or bluntly notched specimens, the total fatigue life is mainly spent on fatigue crack initiation [64]. At high levels of stresses/strains, the crack propagation dominates [20]. For welded specimens, initial defects and inclusions cause a major part of the fatigue life to be spent on crack propagation. Ramchandra et al [61] concluded that the fatigue propagation life was 75 - 89% of the total fatigue life of all welded specimens studied, whereas other researchers indicated that this could be as low as 50% [64].

The fatigue stages have different crack damage mechanics and therefore Miller [37] defined length scales of cracks:

- **Short crack (SC):** Cracks of up 0.5-1 mm in length. The short cracks are usually divided into microstructurally short crack (MSC) and physically short crack (PSC). Where the MSC is in the order of the grain size of the structure.
- **Long crack (LC):** Cracks longer than 0.5-1 mm.

The 0.5 – 1 mm range as transition point between crack initiation (SC) and crack propagation (LC) reflects very well what can be found in literature: researchers often use values in that range to define the end of the crack initiation period [64].

2.2 Factors affecting fatigue life

From literature, several factors that affect the fatigue life can be identified:

- **Load (stresses):** Residual stresses caused by welding, the stress ratio and notch effect from the weld geometry.
- **Resistance (material):** The material quality, i.e. its grain size, fracture toughness, yield/ultimate strength.

2.2.1 Weld notch

After creating a butt weld, several geometrical features can cause stress concentrations in the weld area. The most important ones and their effects are:

- **Excess weld material:** Excess weld material means a disruption in the stress flow from one plate to the other [50]. At the weld toe, stress concentrations will occur due to this weld material.
- **Undercut:** Similar to excess weld material, an undercut also causes a disruption in the stress flow and forms a stress concentration near the weld toe [50].

The important parameters for determining the effect that the notch has on the stress concentration is and their location can be found in Figure 2.2. A lot of research has been done about the effects of these parameters and the results of these researches will be discussed for each parameter.

- **Weld toe radius:** A larger radius means a smoother transition from one thickness to the other and thus less disruption in the stress flow. This hypothesis is supported by numerical studies on mild steel butt welds [12], [52], [56], [74] and also experimental research on mild steel cruciform joints and high strength steel butt welds by Lee et al [26] and Sanders et al [66] respectively. The researchers harmoniously conclude that a larger weld toe radius lowers the stress concentration at the weld toe and thus prolongs fatigue life.
- **Weld flank angle:** Starting from the stress flow concept, one would expect smaller stress concentration for smaller weld flank angles, because the stress flow would be disturbed less. Both numerical and experimental research on both butt welds and cruciform joints has concluded that a smaller angle is beneficial for the fatigue life [52], [26], [66]. Ninh et al [52] found that reducing the flank angle beyond 20° has a significant effect on fatigue life. This parameter is also used extensively by design codes in execution requirements of welds.
- **Undercut dimensions:** The undercut is defined as an irregular groove along the weld toe that is formed when the parent material is wasted and not filled by weld metal [12], [50]. Undercuts can form in butt welds but are most commonly found in fillet welds [12]. Numerical studies on butt welds by [74] and [7] found that the governing parameters are the undercut depth, undercut width and the undercut root radius. [7] especially emphasizes the effect of the depth to radius ratio (h/r ratio). When the h/r increases, it was found that the stress concentration increased dramatically. The effect was more pronounced for smaller undercut widths. [74] had similar findings. These numerical findings are supported by experiments done on the fatigue life of butt welds in [50] and [49] which show the same effect.

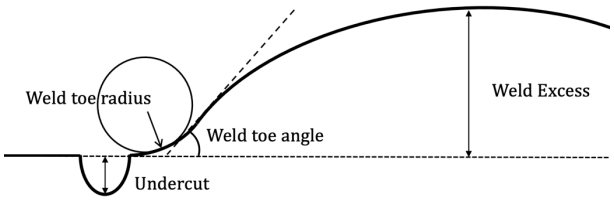

Figure 2.2 Schematic of typical butt-weld geometry

2.2.2 Mean stress and weld residual stress

Residual stress fields result from the welding and the subsequent cooling of a detail during which the weld metal contracts [29]. This creates tension field in the material that is often assumed to be of the magnitude of yield strength but can have varying stress values depending on certain parameters [52], [29], [40].

$$R = \frac{\sigma_{min}}{\sigma_{max}} \tag{2.1}$$

Residual stresses locally increase the mean stress that is "felt" by the material during cyclic loading. The mean stress is usually expressed in terms of the stress-ratio, which is defined by Eq. (2.1). Depending on the type of loading, the mean stress can have both a positive and negative effect. Fatigue life is shorter in regions where mean stresses are tensile, the opposite holds for regions where mean stresses are compressive. Numerical investigations validated with experimental results by Llavori et al [31] and Nguyen et al [50], on butt welds and experimental results on welded attachments with different filler materials. Experiments done by Harati et al [17] confirm this influence of the residual stress on the fatigue.

2.2.3 Thickness

For fatigue testing on butt welds, it was found that an increase in thickness decreases the fatigue life. In [58] a review of all experiments on butt welds was made. It was concluded that the size effect is a combination of the following three factors:

- **Geometrical:** This effect is twofold. Firstly, in thicker specimens the stress gradient will become less. This causes the stress field at the crack tip to be more intense and thus increases crack growth [51], [58]. Secondly, the local weld toe geometry doesn't scale with the thickness. Several researchers have found both numerically [12] and by reviewing 8 different experiments on butt welds [58] that when the radius to thickness ratio (r/t) decreases, the stress concentration increases and thus causes a reduction in the fatigue life. A positive observed geometric effect is

that the welds are less likely to be overfilled and thus the flank angle is less [58]. This, as stated before reduces the stress concentration and increases fatigue life.

- **Statistical:** In a larger element, a higher probability of weak location occurs. However, it was found by [58] after reviewing 8 different experiments that the weld length is a better indicator of the statistical size factor.
- **Technological:** The technological size effect is twofold: it can influence the residual stresses and misalignment. The residual stress is affected by size since for larger section size, more constraint is provided and thus higher residual stresses are able to build up [29], [58]. The misalignment aspect is a positive factor for increasing section sizes: a thick plate with the same misalignment as the thin plate has a smaller relative misalignment and thus reduces secondary bending stresses [58].

2.3 Crack Initiation

The first stage of crack growth is the crack initiation phase, often considered to be a complex stage of the crack growth. The preferred method for modelling this stage of crack growth is the so-called strain-life approach.

2.3.1 Strain-Life Approach

The strain-life approach is based on the assumption that the construction material in a component with a notch under repeated cyclic loading has the same structural mechanical behaviour as a smooth sample that is subjected to the same stress-strain state [27]. In other words, it is assumed that the material near the notch shows the same fatigue behaviour as a smooth specimen undergoing the same cyclic deformation [27].

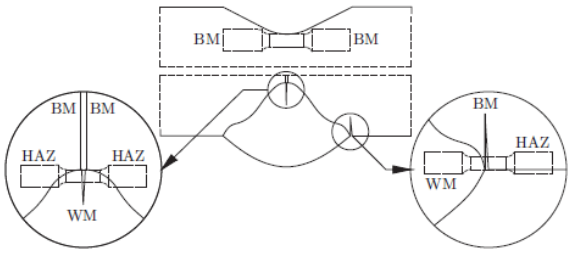

Figure 2.3 Illustration of fundamental assumption in strain-life approach [27]

Two equations usually govern the relationship between the local strain and the number of reversals till failure. These are the Coffin-Manson equation [32] given in Eq. (2.2) and the Basquin equation [2] given in Eq. (2.3), for elastic strain and plastic strains respectively. These relations were both found after fully reversed experiments.

$$\frac{\Delta\varepsilon_e}{2} = \frac{\sigma_f'}{E}\left(2N_f\right)^b \quad [Coffin - Manson] \tag{2.2}$$

$$\frac{\Delta\varepsilon_p}{2} = \varepsilon_f'\left(2N_f\right)^c \quad [Basquin] \tag{2.3}$$

The plastic strain range and elastic strain range are usually added to overcome the issue of separating elastic and plastic strains. The total fatigue life can subsequently be determined by means of Eq. (2.4). A visualization of adding these two equations is given in Figure 2.4. The equation holds for R=-1 (i.e. zero mean stress) [28] and is often referred to as the Morrow equation.

$$\frac{\Delta\varepsilon}{2} = \frac{\sigma_f'}{E}\left(2N_f\right)^b + \varepsilon_f'\left(2N_f\right)^c \tag{2.4}$$

Where:

- $\Delta\varepsilon$ = **strain range**
- σ_f' = **fatigue strength coefficient**
- ε_f' = **fatigue ductility coefficient**
- b = **fatigue strength exponent**
- c = **fatigue ductility exponent**
- N_f = **number of reversals**

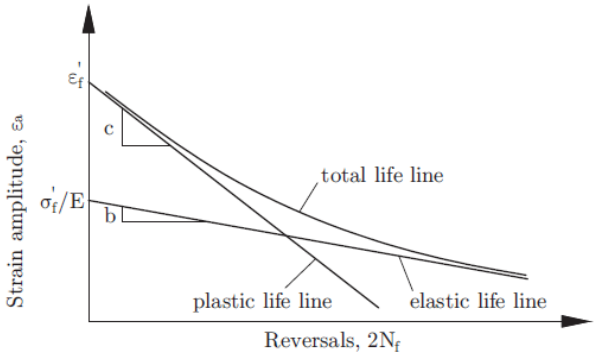

Figure 2.4 Typical strain-life curve [27]

2.3.2 Cyclic Behaviour

When steel is loaded with a monotonic load, the behaviour is described by the Ramberg-Osgood equation [62]. It describes both the elastic and plastic zones of material behaviour and is derived from the true stress – true plastic strain relationship as given in Figure 2.5 which was derived from experiments. Strain is composed of elastic and plastic strain, by rewriting the formula in Figure 2.5 and using the standard definition for elastic strain, the Ramberg-Osgood relationship given in Eq. (2.5) can be derived.

$$\varepsilon = \varepsilon_{el} + \varepsilon_{pl} = \frac{\sigma}{E} + \left(\frac{\sigma}{K}\right)^{\frac{1}{n}} \tag{2.5}$$

Where:

- ε = **strain**
- σ = **stress**
- K = **strength coefficient**
- n = **cyclic hardening coefficient**

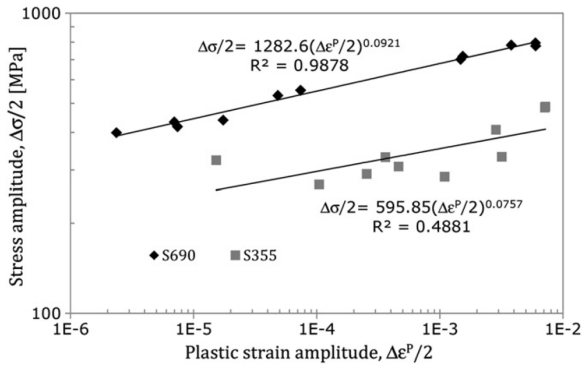

Figure 2.5 True plastic strain - stress relationship used as input for Ramberg-Osgood relationship

When the load is reversed, the hysteresis branch follows a path that is governed by Masing behaviour [64], which yields Eq. (2.6).

$$\Delta\varepsilon = \Delta\varepsilon_{el} + \Delta\varepsilon_{pl} = \frac{\Delta\sigma}{E} + 2\left(\frac{\Delta\sigma}{2K}\right)^{\frac{1}{n}} \tag{2.6}$$

When a metal is cyclically loaded, the material will tend to soften or harden, which changes the stress-strain relationship of that material. The position and shape of the curve will change slightly to eventually reach a steady state [24]. The hardening or softening will only take place in the 5-10 percent of the fatigue life [64] and therefore it is often assumed that the full life is spent in steady state behaviour, as is also proposed by, [27], [51], and [64] and many others. The equation then changes into the one given in Eq. (2.7).

$$\Delta\varepsilon = \frac{\Delta\sigma}{E} + 2\left(\frac{\Delta\sigma}{2K'}\right)^{\frac{1}{n'}} \; or \; \varepsilon = \frac{\sigma}{E} + \left(\frac{\sigma}{K'}\right)^{\frac{1}{n'}} \tag{2.7}$$

Where:

- K′ = **cyclic strength coefficient**
- n' = **cyclic hardening coefficient**

2.3.3 Elastoplastic Stress

As the notch grows sharper, the SCF at the notch increases and this could lead to the stress surpassing the yield limit of the material. Plasticity will occur and this needs to be accounted for before being able to determine the strain-life of a model. Researches such as [28], [51], [53], often fall back on the Linear Elastic FEM and applying plastic correction afterwards. Two methods are conventionally used for this: Neuber Hyperbola or the Molsky-Glinka method [24].

2.3.3.1 Neuber Hyperbola

The Neuber Hyperbola is based on the hypothesis that the elastic stress concentration factor is the geometric mean of the true stress and strain concentration factor [24].

$$K_\sigma = \frac{\sigma}{S} \text{ and } K_\varepsilon = \frac{\varepsilon}{e} \text{ which make } K_t = \sqrt{K_\sigma K_\varepsilon} \tag{2.8}$$

If both sides of the equation are squared and with some rewriting, the Neuber expression can be obtained. This expression is given in Eq. (2.9).

$$\sigma\varepsilon = K_t^2 Se \rightarrow \Delta\sigma\Delta\varepsilon = K_t^2 \Delta S \Delta e \tag{2.9}$$

Where:

- $(\Delta)\varepsilon$ = **local true notch strain (range)**
- $(\Delta)\sigma$ = **local true notch stress (range)**
- $(\Delta)e$ = **nominal strain (range)**
- $(\Delta)S$ = **nominal stress (range)**
- K_t = **elastic stress concentration factor**

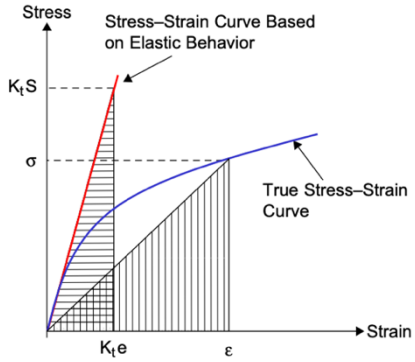

Figure 2.6 Graphical depiction of functioning of the Neuber Hyperbola

In essence, this formula equates the elastic strain energy density (including the notch effect) to an approximation of the elastoplastic strain energy density (a triangle). A graphical interpretation of this effect can be seen in Figure 2.6. For nominally elastic behaviour, where plasticity is local, $\Delta e = \Delta S/E$. Which yields Eq. (2.10).

$$\Delta\sigma\Delta\varepsilon = \frac{(K_t\Delta S)^2}{E} \tag{2.10}$$

Using Eq. (2.10) above and the Ramberg-Osgood relation (Eq. (2.5)), Eq. (2.11) can be found:

$$\Delta\frac{\Delta\sigma^2}{E} + 2\Delta\sigma\left(\frac{\Delta\sigma}{2K'}\right)^{\frac{1}{n'}} = \frac{(K_t\Delta S)^2}{E} = \frac{(\Delta\sigma_{LE})^2}{E} \; or \; \frac{\sigma^2}{E} + \sigma\left(\frac{\sigma}{K'}\right)^{\frac{1}{n'}} = \frac{(K_t S)^2}{E} = \frac{(\sigma_{LE})^2}{E} \quad (x) \tag{2.11}$$

When the stress is then calculated by elastic FEA, the $K_t\Delta S$ factor can be replaced by the stress that results from the model [51], [28]. This is because the stress concentration is already included in the calculation of the stress, due to the geometry of the model. The above equation can then be solved for $\Delta\sigma$ and using the Ramberg-Osgood relation, a value for $\Delta\varepsilon$ can be obtained.

2.3.3.2 Molsky and Glinka

The Molsky and Glinka method proposes a slightly different assumption. Here it is proposed that the elastoplastic strain energy density at the notch root is related by $K_t{}^2$ to the strain energy density from elastic calculation, the relation given in Eq. (2.12) [24]. As can be seen in Figure 2.7, this method is very similar to the Neuber Hyperbola, but instead takes the full area under the true stress-strain curve into account.

$$W_e = K_t^2 W_s \tag{2.12}$$

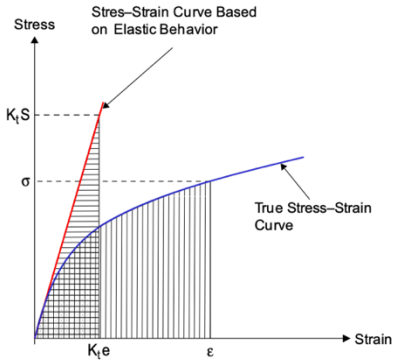

Figure 2.7 Graphical depiction of functioning of Molsky-Glinka method

The strain energy density from elastic calculation can be determined as given in Eq. (2.13).

$$W_s = \frac{1}{2} Se = \frac{1}{2}\frac{S^2}{E} \; or \; \Delta W_s = \frac{1}{2}\Delta S \Delta e = \frac{1}{2}\frac{\Delta S^2}{E} \tag{2.13}$$

The strain energy from the true stress-strain curve cannot be determined by direct integration of from zero to the required strain, this is because no closed form of the Ramberg-Osgood relationship expressed in strain is available. Therefore, the elastoplastic strain energy density can be determined with the integral given in Eq. (2.14).

$$W_e = \sigma_a \varepsilon_a - \int_0^{\sigma_a} \frac{\sigma}{E} + \left(\frac{\sigma}{K}\right)^{\frac{1}{n}} d\sigma \tag{2.14}$$

Which, when using $\varepsilon_a = \frac{\sigma_a}{E} + \left(\frac{\sigma_a}{K}\right)^{\frac{1}{n}}$ and evaluating the integral in Eq. (2.14), yields the elastoplastic strain energy density given in Eq. (2.15).

$$W_e = \frac{\sigma^2}{2E} + \frac{\sigma}{1+n}\left(\frac{\sigma}{K'}\right)^{\frac{1}{n'}} \; or \; \Delta W_e = \frac{\Delta\sigma^2}{2E} + \frac{2\Delta\sigma}{1+n}\left(\frac{\Delta\sigma}{2K'}\right)^{\frac{1}{n'}} \tag{2.15}$$

By equating $(\Delta)W_e$ and $(\Delta)W_s$, the equations for the determination of the true stress from the nominal stress are obtained. These are given in Eq. (2.16). When the stress is then calculated by elastic FEM, the $K_t \Delta S$ factor can be replaced by the stress that results from the model [51], [28].

$$\frac{\Delta\sigma^2}{E} + \frac{4\Delta\sigma}{1+n}\left(\frac{\Delta\sigma}{2K'}\right)^{\frac{1}{n'}} = \frac{(K_t\Delta S)^2}{E} = \frac{(\Delta\sigma_{LE})^2}{E} \; or \; \frac{\sigma^2}{E} + \frac{2\Delta\sigma}{1+n}\left(\frac{\sigma}{K'}\right)^{\frac{1}{n'}} = \frac{(K_t S)^2}{E} = \frac{(\sigma_{LE})^2}{E} \tag{2.16}$$

2.3.3.3 Comparison of correction methods

It can be seen from the equations that the Neuber and Molsky-Glinka method provide very similar correction equations. The two methods converge for small stress-values; however, the Neuber Hyperbola generates relatively higher elastoplastic stresses and strains than the Molsky-Glinka method. This is a direct cause of the definition of the Neuber Hyperbola: higher stress and strain are needed to obtain the same strain energy density as in the Molsky-Glinka method. It is usually said that the Neuber Hyperbola is an upperbound approach, whereas the Molsky-Glinka method is a lower bound approach [38].

2.3.4 Mean Stress Correction

The strain-life equations have been derived for R=-1, however, as shown in section 2.2.2, the mean stress plays a significant role in the fatigue life of specimens. Therefore, correction needs to be done for other mean stresses. The most frequently used approach is the Smith-Watson-Topper damage formula [72]. In this method, it is assumed that the equivalent stress amplitude is equal to the geometric mean of the stress amplitude and maximum stress [81]. This is presented in Eq. (2.17).

$$\sigma_{ar} = \sqrt{\sigma_{max}\sigma_a} \tag{2.17}$$

After applying the equation into the strain-life equation, it was found that plotting the fatigue life against $\sqrt{\sigma_{max}\varepsilon_a E}$ reduced the data of tests with different stress ratios to a single curve [72]. It was proposed that at a given life, $\sigma_{ar}\varepsilon_{ar}$ for an equivalent fully reversed test is equal to $\sigma_{max}\varepsilon_a$ for a mean stress test [72]. After equating and some rewriting, it yields Eq. (2.18).

$$P_{WST} = \sqrt{\sigma_{n,max}\varepsilon_{1,a}E} = \sqrt{\sigma_f'^2\left(2N_f\right)^{2b} + \sigma_f'\varepsilon_f' E\left(2N_f\right)^{b+c}} \tag{2.18}$$

Where:

- σ_{max} = **maximum stress**
- ε_a = **strain amplitude**
- n_p = **support factor**
- σ_f' = **fatigue strength coefficient**
- ε_f' = **fatigue ductility coefficient**
- b = **fatigue strength exponent**
- c = **fatigue ductility exponent**
- N_f = **number of reversals**

A limitation of this method is the inability to provide accurate results when the material undergoes nominal pressure [28]. Since most fatigue details experience tensile residual stress, it is expected that this method is applicable to the butt weld in case.

2.4 Linear Elastic Fracture Mechanics

Once the crack is initiated, it will start growing in the direction perpendicular to the applied load. The crack enters the crack propagation stage which can be described physically by fracture mechanics.

2.4.1 Crack modes

There are three modes in which a crack can extend [67], an illustration of which has been given in Figure 2.8:

- **Mode I:** Mode in which the crack faces move apart. Crack growth occurs due to stresses perpendicular to the crack.
- **Mode II:** In-plane shearing or sliding mode; the crack surfaces slide apart perpendicular to the crack front. Crack growth occurs due to in-plane shear stresses.
- **Mode III:** Tearing or anti-plane shear mode; the crack surface slide apart parallel to the crack front. Crack growth occurs due to anti-plane shear stresses.

In the case of the crack growth in butt welds, mainly Mode I crack growth is dominating. This is due to the fact that shear cracks quickly grow to be perpendicular to the applied stress direction.

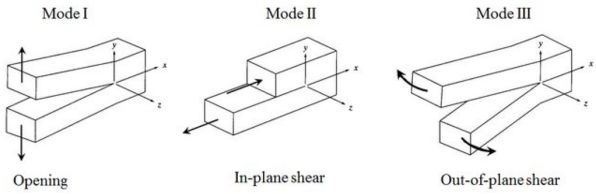

Figure 2.8 Different modes of crack growth [77]

2.4.2 Basis of Fracture Mechanics

Once a crack grows large enough to become a long crack (LC), fracture mechanics approaches can be used to describe the growth of the crack. Fracture mechanics can be divided into Linear Elastic Fracture Mechanics (LEFM) and Elastic Plastic Fracture Mechanics (EPFM). LEFM assumes linear elastic material behaviour: the stresses around the crack tip are calculated with the theory of elasticity. EPFM assumes non-linear material behaviour and thus accounts for plasticity around the crack tip. In LEFM, the stresses around the crack tip tend to infinity, which will not be possible in reality due to plasticity. If the plastic zone that is formed is small enough, LEFM can be applied [67]. The discussed theories are applicable to LEFM.

2.4.2.1 Griffith Criterion

The Griffith Criterion is as follows: *"crack growth will occur, when there is enough energy available to generate new crack surface"* [67]. The criterion is based on the energy balance of the entire cracked body and is therefore often considered to be a global criterion. The energy balance as function of the crack length is given by Eq. (2.19), the external supplied energy must be converted into several types of internal energy.

$$\frac{dU_e}{da} = \frac{dU_i}{da} + \frac{dU_a}{da} + \frac{dU_d}{da} + \frac{dU_k}{da} \tag{2.19}$$

Where:

- U_e = mechanical energy supplied to a material volume (due to work from external forces)
- U_i = internal elastic energy
- U_a = surface energy (due to generation of new surfaces)
- U_d = dissipated energy (due to plastic deformation and friction)
- U_k = kinetic energy (due to material velocity)

The crack growth often takes place at slow speeds and therefore the kinetic energy can often be neglected. For brittle materials, the dissipated energy is often neglected as little to no plasticity takes place in the material. However, for ductile materials, the dissipated energy may not be neglected [67]. Griffith assumed brittle material behaviour and thus the equation can be rewritten to Eq. (2.20), where U_p is the potential energy of the body [78].

$$\frac{dU_e}{da} - \frac{dU_i}{da} = \frac{dU_a}{da} \rightarrow -\frac{dU_p}{da} = \frac{dU_a}{da} \tag{2.20}$$

Where

$$U_p = U_i - U_e \tag{2.21}$$

Griffith then defined the energy release rate (G) and the crack resistance force (R) as given in Eq. (2.22). Here B is the thickness of the material and γ is the energy required to form a unit surface of material.

$$G = -\frac{1}{B}\frac{dU_p}{da} \; and \; R = \frac{1}{B}\frac{dU_a}{da} = 2\gamma \tag{2.22}$$

Equating the two, yields Eq. (2.23). Simply said, the equation above states that sufficient potential energy is needed to be able to generate new free surfaces and thus grow the crack.

$$G = R = 2\gamma \tag{2.23}$$

2.4.2.2 Stress intensity factor

The crack growth criterion can also be based on the elastic stress state at the crack tip, the growth criterion is then characterized by the so-called stress intensity factor (SIF). This crack growth criterion is often classed as local, since solely the stress state at the crack tip is considered [67]. The stress intensity factor is a measure of the stress intensity at the crack tip. This parameter depends on the applied stress, geometry (often accounted for by Y) and crack length and can be described by Eq. (2.24).

$$K = Y\sigma\sqrt{\pi a} \tag{2.24}$$

The SIF at which the crack growth becomes unstable and the critical energy release rate (G_c) is reached is called the fracture toughness (K_c). The local crack growth parameter K can be related to the global crack growth parameter G. This relation is found by equating the released energy by extending the crack by δa to the work required to close the small opening again without any external work variation [67]. This results in the relation as given in Eq. (2.25) and Eq. (2.26).

$$G = \frac{1}{E}(K_I^2 + K_{II}^2) + \frac{1+v}{E}K_{III}^2 \tag{2.25}$$

$$G = \frac{1-v^2}{E}(K_I^2 + K_{II}^2) + \frac{1+v}{E}K_{III}^2 \tag{2.26}$$

2.4.3 Paris Law

Several phenomenological models have been formulated to predict the fatigue life of structures. The crack growth rate da/dN is related to a certain load, which is often expressed by the stress intensity factor. Since fatigue is often assumed to occur in the high cycle fatigue regime, stresses are low and the use of LEFM is justified [67].

In LEFM, the crack growth rate da/dN is mostly related to ΔK through the Paris Law, introduced by Paris and Erdogan [57]. After conducting experiments, Paris and Erdogan found that the crack growth could be divided into three regions:

- **Region I: Threshold crack propagation regime**
- **Region II: Stable crack propagation regime / Paris region**
- **Region III: Unstable crack propagation regime**

$$\frac{da}{dN} = C(\Delta K)^m \tag{2.27}$$

The Paris Law, a linear log-log relationship given by Eq. (2.27) (and illustrated in Figure 2.9), is only valid for Region II crack growth. In the threshold crack propagation regime, the crack grows slower than predicted by the Paris Law. Stress intensity factor ranges below the vertical threshold asymptote denoted by ΔK_{th} are considered to be too low to cause crack growth. In the unstable propagation regime, the stress intensity factor K slowly reaches the critical stress intensity factor K_c (i.e. material toughness) and the material fails. The crack growth accelerates and is higher than predicted by the Paris Law. The parameters C and m can be determined from tests and depend on the material and stress ratio R.

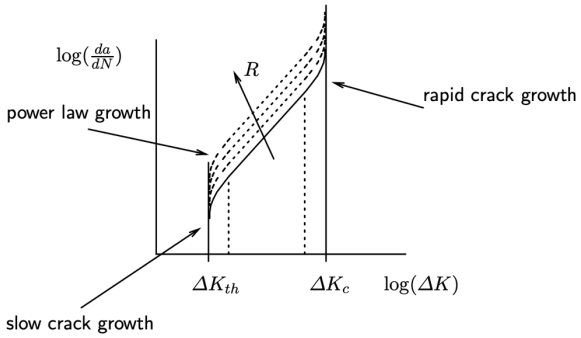

Figure 2.9 Graphical depiction of Paris-Law crack growth

2.4.4 Similitude concept and short cracks

In Fracture Mechanics the implicit assumption is made that cracks of different lengths, subject to different stresses, will have the same crack growth speed as long as the applied SIF range is the same. This notion is called the similitude concept and is fundamental for crack growth calculations. However, the similitude concept breaks down in the case of [75]:

- Crack sizes that approach microstructural dimensions
- Crack sizes that are comparable to the extent of local plasticity
- Different out of plane stresses
- Different crack extension mechanisms
- Different fatigue crack closure

This list is not complete but lists some of the important instances. The focus of this part will be on the first two: short cracks. It has been widely accepted that a SC subject to a certain SIF range will have a higher crack growth speed than a LC subject to that same SIF range. This can be seen in Figure 2.10 where the crack growth rates are several orders of magnitude higher than that would be predicted if one would extrapolate Paris Law to SC. As can be seen from Figure 2.10, cracks can also grow below the typical threshold SIF. For shorter cracks, this threshold is said to decrease; for very short cracks it even approaches the fatigue limit stress of a smooth bar.

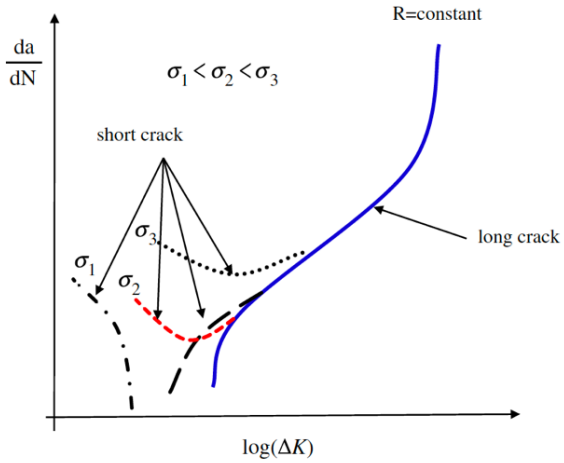

Figure 2.10 Crack growth rates of SC compared to LC [1]

In literature, one can find several explanations for this short crack phenomena, two of which will be shortly discussed here. These are the crack closure concept, first postulated by Newman [43], and the Unified Approach that was postulated by Vasadavon et al [76].

According to the crack closure concept, the higher crack growth speeds can partly be explained by crack closure and partly by microstructural features [75]. The effect of crack closure would be caused by smaller cracks having a smaller plastic wake and therefore experiencing almost no crack closure, similar to crack growth speeds of specimens at high R. This can also be used to explain why crack growth speeds tend to decrease as SC grows longer. Microstructural features such as grain boundaries also impede crack growth [19]. As the crack size increases, and so the size of the plastic wake, some cracks will arrest due to low stress and crack closure effects, others will decrease in crack growth speed. The behaviour of the cracks is highly dependent on the maximum stress that is applied. According to this theory, the crack growth speed can be defined by the parameter ΔK which is corrected to ΔK_{eff} by subtracting the SIF (K_o) at which the crack opens.

Sadananda et al argue that the crack closure concept views LC as being the anomaly, since crack growth speed for LC has to be corrected due to crack closure effects. The SC growth is then viewed as being intrinsic to fatigue. However, Sadananda et al [65] argue that larger scatter in SC growth results than in LC growth results, means that it could not possibly intrinsic material behaviour, since one would expect less scatter as it is free of crack closure. Furthermore, the effect would be caused by plastic crack closure effects, which have been experimentally shown to not be a major contributing factor to the crack closure effect [76].

According to Sadananda et al [65], SC show anomalous behaviour due to augmented internal stresses. These internal stresses arise from notches or holes and as the crack grows away from them, their effect decreases and thus the crack growth speed decreases. If the applied stress is not high enough, the driving force from the increasing crack length will not increase fast enough and thus the crack will arrest, which can be seen in Figure 2.10. Since the internal stresses increase the maximum and minimum SIF, the local stress ratio will increase as compared to the nominal applied stress ratio. This could be the reason why short cracks show similar crack growth speeds as cracks at high R-ratios. According to this theory, the crack speed can be defined by two parameters: ΔK and K_{max} that are augmented by internal stresses due to *notches or inclusions*. The theory is called the Unified Approach.

2.4.5 Determination of stress intensity factor

When using LEFM, accurate determination of the stress intensity factor is needed to provide proper estimation of the crack growth rate using for example the Paris Law. Over the years, several methods for the determination of the stress intensity factor have been developed. Some of these methods will now be discussed.

2.4.5.1 Newman-Raju Equation

The Newman-Raju equation, Eq. (2.28), was one of the first empirical relationships for determining the stress-intensity factor as a function of angle (φ), crack depth (a), crack width (c), plate thickness (t) and distance to nearest edge (b) [47]. An overview of the geometry is given in Figure 2.11. It has been derived for semi-elliptical surface cracks in flat plates. The stress-intensity factors needed to form these equations were obtained using 3D finite element analysis.

$$K_I = (S_t + HS_b)\sqrt{\frac{\pi a}{Q}}F\left(\frac{a}{c}, \frac{a}{t}, \frac{c}{b}, \varphi\right) \tag{2.28}$$

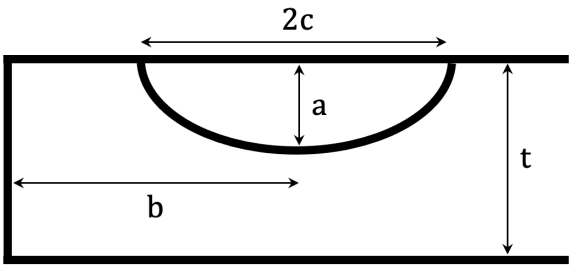

Figure 2.11 Dimensions of the semi-elliptical crack used in the Newman-Raju equation

Tensile (S_t) and bending (S_b) stress components of the applied stress are considered separately. The complete equations for the bending factor (H), boundary-correction factor (F) and the shape factor (Q) are given in Appendix A.1. The validity limits of the equation are given below. Interesting to see here is that the equations are also valid for $a/c = 0$, which can be considered an edge crack. The semi-elliptical crack results and edge crack were within 5% of the finite element results [47].

- $0 \leq a/c \leq 1$
- $0 \leq a/t \leq 0.8$
- $c/b < 0.5$
- $0 \leq \varphi \leq \pi$

2.4.5.2 Weld Magnification Factor

Stress concentration caused by for example the presence of welds increases the stress-intensity factor. Bowness and Lee [4] defined this increase by the magnification factor as defined in Eq. (2.29).

$$M_k = \frac{K_{(in\ plate\ with\ stress\ concentration)}}{K_{(in\ same\ plate\ but\ with\ no\ stress\ concentration)}} \tag{2.29}$$

This factor is usually combined with an analytical solution for a flat plate (such as the Newman-Raju equation) to obtain SIF values for welded geometries. The general equation for determining stress-intensity factors in plates with stress concentrations has been derived by Hobbacher [18] as in Eq. (2.30).

$$K = \sqrt{\pi a}\left(\sigma_m Y_m M_{k,m} + \sigma_b Y_b M_{k,b}\right) \tag{2.30}$$

Geometry factors Y and magnification factors M_k can be found in literature, an example of which is the Newman-Raju equation that was discussed in the previous section.

2.4.5.3 Weight Function

Bueckner [5] and Rice [63] have first introduced the weight function method. The most important feature of the weight function method lies in the fact that once the weight function for a cracked body is determined, the stress-intensity factor for another, possibly more complex stress field can be determined by means of evaluating the integral given in Eq. (2.31) [16].

$$K = \int_0^a \sigma(x) m(x,a) dx \tag{2.31}$$

If a reference stress-intensity factor K_r and a corresponding reference displacement field u_r are known, the weight function can simply be determined [16]. The issue lies not in determining this reference stress-intensity factor, but in the displacement field, which is often unknown. Petroski and Achenbach [59] proposed a general approximate crack opening displacement function $u_r(x,a)$ as given in Eq. (2.32).

$$u_r(x,a) = \frac{\sigma_0}{H\sqrt{2}}\left[4F\sqrt{a(a-x)} + \frac{G(a-x)^{\frac{3}{2}}}{\sqrt{a}}\right] \quad where \quad F = \frac{K_r}{\sigma_0\sqrt{\pi a}} \tag{2.32}$$

It can be shown that this leads to the weight function in Eq. (2.33), which can be used to approximate analytical weight functions [16].

$$m(x,a) = \frac{2}{\sqrt{2\pi(a-x)}}\left[1 + M_1\left(1-\frac{x}{a}\right) + M_2\left(1-\frac{x}{a}\right)^2\right] \tag{2.33}$$

Eq. (2.33) has been shown to not yield accurate results for very non-uniform or discontinuous reference stress fields [16]. Furthermore, it was found that the three-term variant didn't always yield accurate results, leading to a more general form of this weight function given in Eq. (2.34) derived by Fett et al [13]

$$m(x,a) = \frac{2}{\sqrt{2\pi(a-x)}}\left[1 + M_1\left(1-\frac{x}{a}\right) + M_2\left(1-\frac{x}{a}\right)^2 + \ldots + M_n\left(1-\frac{x}{a}\right)^n\right] \tag{2.34}$$

Sha and Yang [68], alternatively proposed a weight function in the form of Eq. (2.35).

$$m(x,a) = \frac{2}{\sqrt{2\pi(a-x)}}\left[1 + M_1\left(1-\frac{x}{a}\right)^{1/2} + M_2\left(1-\frac{x}{a}\right) + \ldots + M_n\left(1-\frac{x}{a}\right)^{n/2}\right] \tag{2.35}$$

Eq. (2.34) and Eq. (2.35) have been shown to be able to approximate weight functions of one- and two-dimensional cracks, such as edge cracks in finite bodies. These weight functions are therefore usually called the Universal Weight Functions [16]. To derive the weight function for a semi-elliptical crack, a typical crack type emanating from the weld toe, Shen et al [70] based their derivation on the analytical solution of a weight function for an embedded circular crack in an infinite body.

For a semi-elliptical crack in a finite body, it was proposed to use the four-term version of Eq. (2.34) to approximate the weight function in the deepest point of the crack [70]. This was proposed because the form of the weight function of the embedded circular crack in an infinite body is similar to that of Eq. (2.34). For that same reason, Shen et al [70] proposed to use the Eq. (2.36) to approximate the weight function for the surface point of the crack.

$$m(x,a) = \frac{2}{\sqrt{\pi x}}\left[1 + M_1\left(\frac{x}{a}\right)^{1/2} + M_2\left(\frac{x}{a}\right) + M_3\left(\frac{x}{a}\right)^{3/2}\right] \tag{2.36}$$

The values for M_1, M_2, M_3 have been determined by Shen and Glinka [69] by solving a set of equations for the surface and deepest point. These were subsequently validated with numerical data, yielding an accuracy of better than 2% for the surface points and better than 5% for the deepest point of the crack [69].

2.5 Total Fatigue Life Modelling

In previous sections, methods for the determination of crack initiation life and crack propagation life have been discussed. This section will discuss some of the methods that are used to determine the total fatigue life of a specimen.

2.5.1 S-N Method

The current practice for calculation of fatigue life is by using so-called S-N or Wöhler-curves. S-N curves describe the relationship between the applied stress range (S) and the number of cycles till failure (N_f). The curves are based on curve fitting a line to fatigue experiments done on (welded) details. An example of such an S-N curve is given in Figure 2.12. In EN 1993-1-9 [41], 14 equally spaced S-N curves are given. Welded details are subsequently assigned to a given detail category, of which the number relates to the stress range at 2 million cycles.

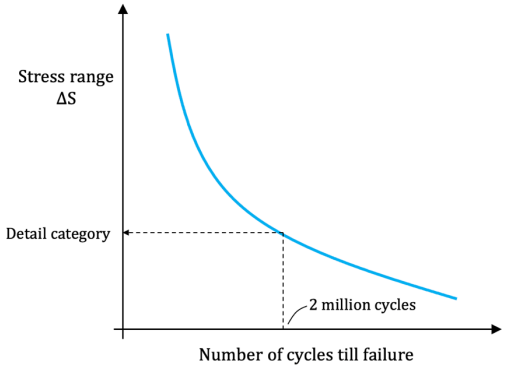

Figure 2.12 Example of S-N curve

The S-N method is a so-called global fatigue approach: the nominal stress in the cross section is used to determine the fatigue life. Stress-raising effects from local eccentricity, misalignment or other macro-geometric features should be considered when determining this stress. All other influencing parameters are taken into account by the detail category. These can include weld shape, discontinuities, imperfections and weld residual stresses. Some disadvantages of this method are:

- **Failure definition:** It is not defined clearly whether S-N curves define the fatigue crack initiation life or the total fatigue lifetime. The most common viewpoint is that the S-N curves describe initiation life. However, in the many, mostly historical, experimental results on which the curves are based, many different failure definitions may have been used.
- **No insight in fatigue process:** Considering the aforementioned point, S-N curves are therefore also not able to determine the extent of a fatigue crack at a given point in time and ignore any underlying physical processes at work.
- **Conservative:** S-N curves are based solely on a lot of historical experimental results. The uncertainty in the experiments increases scatter of the data and thus lowers the fatigue strength of the detail category.

2.5.2 Two-Stage Model

The two-stage model was proposed by Röscher and Knobloch [64]. It is a local model, capable of modelling the entire fatigue process. The basis of the model is considering the fatigue life as two distinct stages with each their own modelling approach. By adding the fatigue life of the crack of the two stages, fatigue crack initiation (N_i) and fatigue crack propagation (N_p), the total fatigue life can be found. The following methods were used for the determination of the fatigue life in the two respective stages:

- **Fatigue Crack Initiation:** This stage is modelled using the strain-life approach. The crack initiation location is identified from linear FEA as the point where the highest principal stress is observed. Using Neuber's rule and the Smith-Watson-Topper damage parameter, the crack initiation life is determined.
- **Fatigue Crack Propagation:** This stage is modelled using LEFM combined with eXtended FEM. The crack propagation phase is assumed to start at a crack length of 0.5 mm. This crack is introduced in the model where the highest principal stress was observed, its direction being perpendicular to the principal stress direction. Crack growth is based on Paris Law. XFEM is used to be able to model the crack growth independent from the mesh. The crack direction is governed by the principal stress direction ahead of the crack tip.

2.5.3 UniGrow model

The UniGrow model was first introduced by Noroozi et al [53]. It is a local, residual-stress based model, based on the Unified Approach that was postulated by Vasedavan et al [76]. It is based on the idea that the fatigue process near cracks and notches is governed by concentrated strains and stress in the crack tip region [34]. It uses the stress and strain ahead of the crack tip, combined with the strain life approach to determine the fatigue life.

2.5.3.1 Basis of the model

The model is based on the following assumptions and computational rules [53]:

- **The material is a medium made of elementary blocks:** An elementary block has been defined by Neuber [42] as the smallest material volume to which the mechanics of continuum and bulk material properties can be applied. The assumed material characteristics are displayed in Figure 2.13. It is often postulated that the elementary block size is related to the grain size [8], however, no clear relationship has been defined. This same idea has been postulated by Forsyth [15]. An important consequence of these assumptions is that the size of these elementary blocks controls the fatigue crack propagation rates. The elementary block size is thus an important tuning parameter for the UniGrow method.

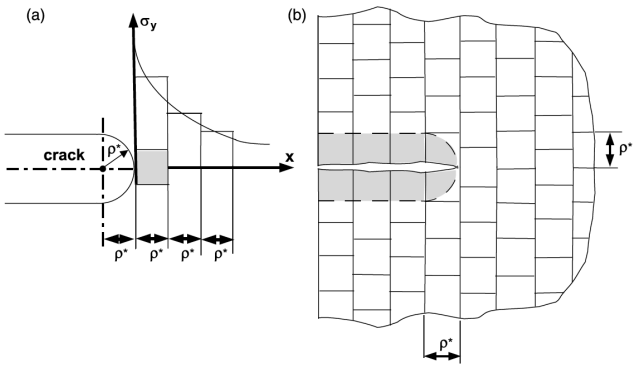

Figure 2.13 Material and crack assumptions [53]

- **The crack tip assumed to have a finite radius (rho*) equal to the elementary block size:** In classical fracture mechanics solutions, crack tips are assumed to be sharp. This leads to a singular point which cannot be used for the determination of the stresses and strains ahead of the crack tip. To overcome this issue, Noroozi et al [53] postulated to model the crack tip as having a finite radius. Notch theories can now be applied, such as the Creager-Paris equations, which yield non-singular solutions for stresses and strains ahead of the crack tip.
- **The fatigue crack growth can be considered as a process of successive crack initiations:** The crack tip shape in this model is similar to that of a small notch. Therefore it was proposed by Noroozi et al [53] to determine the fatigue crack life of the first elementary block ahead of the crack tip using the strain-life approach.
- **Stress distribution ahead of crack tip is altered by residual stresses:** When a load is first applied on a cracked body, the first reversal can cause plastic deformations at the crack tip. The material will start to plastically deform at point B' in Figure 2.14. In the subsequent reversal, the load is released, and the material will deform back. However, due to the Bauschinger effect, the plastic deformation in this reversal will be smaller than in the initial reversal. This causes a part near the crack tip to stay plastically deformed [53].

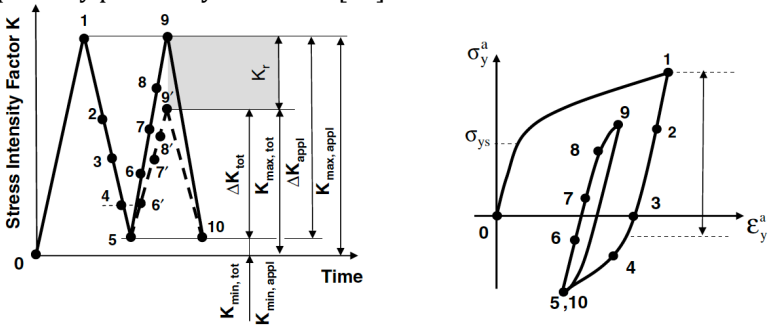

Figure 2.14 SIF as a function of time and stress-strain curve

The increased stiffness of this plastic zone at the crack tip prevents closure of the material just behind the crack tip [54]. This phenomenon has been observed both experimentally and numerically [53], [54]. One way of modelling this crack opening is by symmetrically applying the compressive part of the residual stress ahead of the crack tip onto the crack faces just behind the circular crack tip [53].

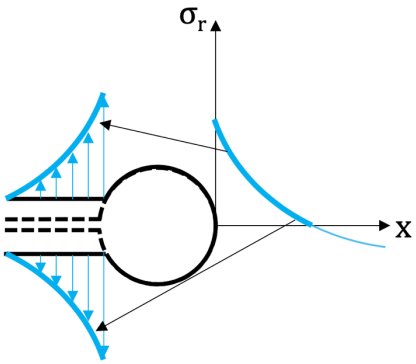

Figure 2.15 Mirroring of the residual stress ahead of the crack tip to the crack surface behind the crack tip

Due to the residual stresses created in the first two reversals, the maximum stress ahead of the crack tip can't be reached in the third reversal [54]. This can be modelled by quantifying the effect of the residual stress as a stress intensity factor K_r. K_r is determined using the weight function method and the stress applied to the crack faces just behind the crack tip. The maximum stress-intensity factor that is 'felt' by the material at the crack tip is given by Eq. (2.37).

$$K_{max,tot} = K_{max} + K_{res} \tag{2.37}$$

The resultant minimum stress-intensity factor is unaltered. This means that the stress-intensity factor range now has to be determined using Eq. (2.38).

$$\Delta K_{tot} = K_{max,tot} - K_{min,tot} = \Delta K + K_{res} \tag{2.38}$$

Note that this method is, in its basis, very similar to the one proposed in the Unified Approach. In the Unified Approach, it is assumed that the crack growth speed can be described by two driving variables, K_{max} and ΔK. It is then postulated that internal stresses augment K_{max} and K_{min}. As ΔK remains the same, the local stress ratio at the crack tip alters as opposed to the nominally applied one.

2.5.3.2 Calculation Procedure

The calculation procedure proposed by Noroozi et al [53] can be divided into roughly five steps. These are given in Figure 2.16 and described below.

1. **Determination of the stress-intensity factor:** Noroozi et al [53] propose evaluating the stress-intensity factor using the weight function method. First, the stresses in the proposed crack plane have to be determined using LE FEA. Then the SIF can be determined by applying the weight function.
2. **Determination of the elastoplastic stress distribution ahead of the crack tip:** In the UniGrow model, the crack tip is assumed to have a finite radius. Therefore, Noroozi et al [53] argue that the Creager-Paris equations can be used to determine the elastic stress distribution ahead of the crack tip. FEA calculations by De Jesus et al [10] show this to be a good assumption. It is subsequently proposed to transfer these elastic stresses into elastoplastic stresses by using the multiaxial plasticity correction postulated by Moftakhar et al [38]. General uniaxial Neuber correction is not applicable, because the stress state ahead of the crack tip is multiaxial.
3. **Determination of the residual stress distribution and residual SIF ahead of the crack tip:** The residual stress distribution ahead of the crack tip can be determined with Eq. (2.39) [53].
$$\sigma_r(x) = \sigma_{max}(x) - \Delta\sigma(x) \tag{2.39}$$
This is then symmetrically applied to the crack face, as has been discussed before. Using the same weight function as in the first step, the residual stress intensity factor can be determined.
4. **Determination of the elastoplastic stress and strain on first elementary block ahead of the crack tip:** After calculating the corrected maximum SIF and SIF range according to the formulas

before, the Creager-Paris equations can again be used to determine the linear elastic stress ahead of the crack tip. Noroozi et al [53] then proposes to take the average of the elastic stress on the first elementary block. This can subsequently be converted into an elastoplastic stress and strain range using the uniaxial Neuber Method [53].

5. **Determination of the initiation life of the elementary block ahead of the crack tip:** Using the elastoplastic stresses and strains, the fatigue life can be determined using a strain-life method. Noroozi et al [53] propose to use the Smith-Watson-Topper damage parameter.
6. **Extend crack by one elementary block and go back to step 1.**

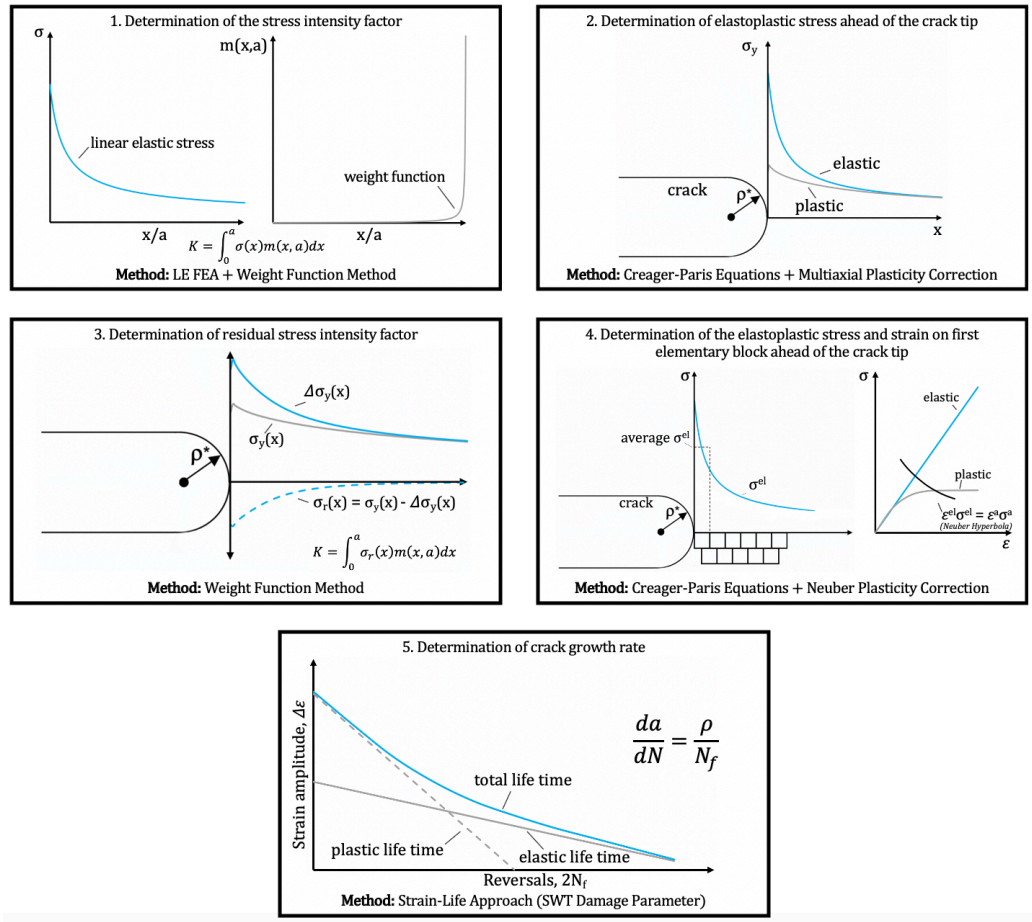

Figure 2.16 Global procedure used in the UniGrow method as proposed by Noroozi et al [53]

3 Implementation, Verification and Validation of the UniGrow Method

Before any calculations can be made using the UniGrow method, the model first needs to be implemented. Even more important is the verification of the model with previous research to make sure it functions well. One such research has been conducted by De Jesus and Correia [10]: the UniGrow method was implemented to generate crack growth results for CT specimens made of P355NL1 steel. Detailed data from this research is available and will be used for the verification of the implemented UniGrow method.

Two versions of the UniGrow method will be implemented to see how the two versions behave compared to each other. The main difference between the two being the method for calculating the plastic residual stress ahead of the crack tip. This can be done analytically (relatively quick method) or numerically (more thorough, time-consuming method). The analytical UniGrow implementation (referred to as analytical UniGrow) will be based on the original UniGrow method by Noroozi et al [53]. The numerical UniGrow implementation (referred to as numerical UniGrow) is based on the UniGrow method that has been used by De Jesus and Correia [10].

Both analytical and numerical UniGrow implementation will then be used to predict crack growth rates in CT specimens made from S355 steel. This is the validation part of this chapter. The data on the specimens and crack growth rates will be taken from De Jesus et al [11], which have conducted fatigue tests at several stress ratios from R = 0.0 to R = 0.75.

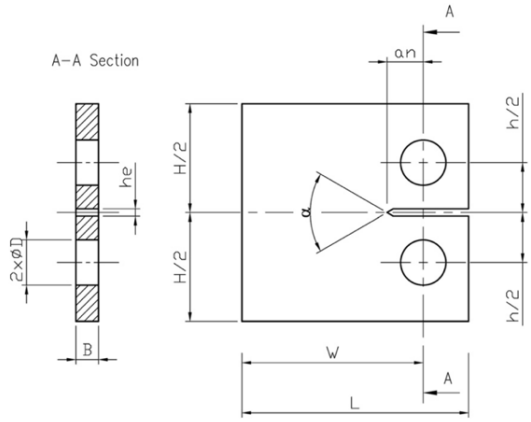

Figure 3.1 Dimensions of a CT specimen [11]

The main geometry that will be researched in this chapter is the Compact Tension (CT) specimen. CT specimens are rectangular plates of steel with a pre-cut slot and two holes where a load is applied. An example of a CT specimen is given in Figure 3.1. Due to their geometry, low forces cause high SIF values. Combined with their relatively small size, they are especially suitable for fatigue testing. CT specimens are used to evaluate the crack growth rates in materials and determine the Paris Law parameters.

The highly standardized testing and fabrication procedure and the absence of weld residual stresses mean that data from these tests provides an excellent starting point for the evaluation of the UniGrow method. Pre-cracking of the CT specimens means that the crack is always in the crack propagation or LC regime. Verification and validation done in this chapter is thus solely valid for crack growth rate prediction when the crack is in the crack propagation stage.

This chapter is divided into four parts. It will start with the verification of the analytical UniGrow implementation, followed by the verification of the numerical UniGrow implementation. Lastly, the validation of the UniGrow method against experimental results from De Jesus et al [11] will be presented.

3.1 Verification of analytical UniGrow implementation

As one of the main objectives of this research is to obtain a method which can be used for quick computation of the fatigue life, the analytical version of the UniGrow method is implemented first. This implementation determines crack growth rates without the aid of FEA and is based solely on analytical methods. First the validation data will be presented, then the implemented UniGrow model is discussed and lastly the results are presented and discussed.

3.1.1 Model description and model data

De Jesus et al [10] have done fatigue tests on CT specimens made of P355NL1 steel, its dimensional characteristics are given in Figure 1. The material data is given in Table 3.1. The strain life parameters and the material properties were determined from 43 fatigue tests on smooth specimens under R = 0 and R = -1. The correlation between the fitted parameters and the data was high: $R^2 > 0.91$ for σ_f' and b and $R^2 > 0.95$ for the other parameters. The material block size, ρ^*, was found to be 3 x 10^{-5} m. This will be taken as true, since this section is aimed at verifying the model rather than validating the model.

Dimensions		Material parameters		Strain-life parameters	
$\boldsymbol{W}$	40 mm	E	205.2 GPa	σ_f'	1005.5 MPa
$\boldsymbol{a_n}$	8 mm	v	0.275	b	-0.1033
$\boldsymbol{B}$	4.35 mm	K'	948.35 MPa	ε_f'	0.3678
$\boldsymbol{L}$	50 mm	n'	0.1533	c	-0.5475
$\boldsymbol{H}$	48 mm				
$\boldsymbol{h}$	22 mm				

Table 3.1 Material parameters and dimensions of the CT specimens [10]

The Paris law constants were obtained from tests on a total of five CT specimens: two under R = 0, two under R = 0.5 and one under R = 0.7. Correlation between fitted parameters and the data is high: $R^2 > 0.95$ for all stress ratios.

De Jesus et al [10] have implemented the five steps of the UniGrow model as follows:

1. **Determination of the elastoplastic stress distribution ahead of the crack tip:** Has been done using a 2D elastoplastic FEA model of half the CT specimen. The authors used plane stress quadratic triangular elements, Mises yield theory with multilinear kinematic hardening to model the plastic behaviour.
2. **Determination of the plastic residual stress intensity factor:** Using the residual stress from the previous step, K_{res} was determined using the universal weight function.
3. **Determination of the elastoplastic stress and strain on first elementary block ahead of the crack tip:** This has been done using the Creager-Paris equations in combination with the Neuber uniaxial plasticity correction.
4. **Determination of the initiation life of the first elementary block ahead of crack tip:** The initiation life was determined using the Smith-Watson-Topper damage parameter.

The verification data has been determined with a more advanced, numerical implementation of the UniGrow model. However, the difference is limited to the determination of the plastic residual SIF. If the outcome of this step shows large differences with the model by De Jesus et al [10], the relations given by De Jesus et al can be used to verify the last step.

3.1.2 Global UniGrow implementation

The global steps of the UniGrow method will be performed as follows:

1. **Determination of the applied stress intensity factor:** The applied stress intensity factor will be established using an analytical equation derived by Newman and Srawley [73]. This topic will be further addressed in chapter 3.1.3.1.
2. **Determination of the elastoplastic stress distribution ahead of the crack tip:** The elastic stresses ahead of the stress tip will be determined using Creager-Paris equations. These will then be corrected for using analytical elastoplastic correction method. This topic will be further addressed in chapter 3.1.3.2.

3. **Determination of the residual stress intensity factor:** Using the weight function method and the elastoplastic stresses from the previous step, the plastic residual SIF will be determined. Further background on this will be given in chapter 3.1.3.3.
4. **Determination of the elastoplastic stress and strain on first elementary block ahead of the crack tip:** This will be done using the Creager-Paris equations in combination with the Neuber uniaxial plasticity correction. This will be further discussed in chapter 3.1.3.4 for background.
5. **Determination of the initiation life of the first elementary block ahead of crack tip:** The initiation life will be determined using the Smith-Watson-Topper damage parameter. This will be further addressed in chapter 3.1.3.5.

These steps have been discussed in more detail in section 2.5.3 and apart from the first step, all steps will be implemented as recommended by Noroozi et al [53] in order to see how the initially proposed UniGrow method performs. Moreover, the initially proposed UniGrow method is almost analytical and therefore also the computationally least intensive method.

The first step will be altered because the determination of the stress intensity factor of the CT specimen with a weight function is considered outside of the scope of this research. The weight function method will be replaced by an empirical formula derived by Newman [44] and Srawley [73]. This can be seen in the altered calculation procedure in Figure 3.2.

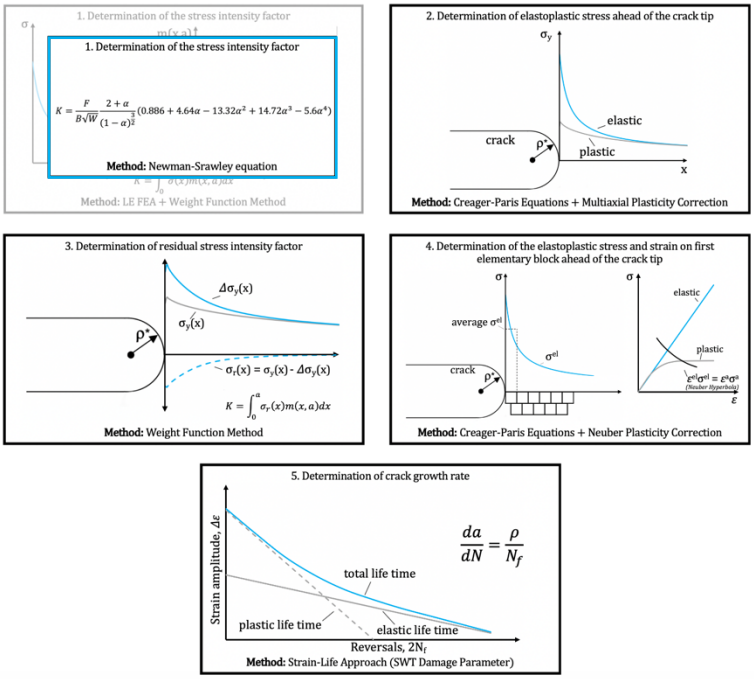

Figure 3.2 Global calculation procedure of analytical UniGrow method

3.1.3 Implemented methods

The UniGrow model roughly consists of five modules for the determination of the instantaneous crack growth rate, the implementation of the modules for this case is:

3.1.3.1 Determination of stress intensity factor

Analytical formulas are available for the determination of the stress intensity factor of a CT specimen. The most commonly used equation is the empirical relation by Newman [44] and Srawley [73] given in Eq. (3.1). This equation is recommended by ASTM E647 Standard for use in fracture mechanics calculations. The determination of the stress intensity factor from 2D equations is a slight simplification of the actual case: in actuality the SIF varies along the crack front [80], where the centre value is slightly higher than the values on the edges. The Newman-Srawley equation presents an average over the thickness.

The equation is fitted to data from three papers that have conducted an analytical evaluation of the stress intensity factor of a CT Specimen. It has been based on the assumption that crack growth takes place at the end of the slot perpendicular to the applied force, which is generally the case for CT specimens. The accuracy of the equation proposed by Srawley [73] is ±0.4%. The equation is valid in the range $0.2 < \alpha < 1$.

$$K_I = \frac{F}{B\sqrt{W}} \frac{2+\alpha}{(1-\alpha)^{\frac{3}{2}}} (0.886 + 4.64\alpha - 13.32\alpha^2 + 14.72\alpha^3 - 5.6\alpha^4) \; where \; \alpha = \frac{a}{W} \tag{3.1}$$

3.1.3.2 Determination of elastoplastic stress distribution ahead of crack tip

The second step in the analytical UniGrow model is the determination of the elastoplastic stresses ahead of the crack tip. These play a vital role in the determination of the plastic residual SIF. In the analytical method, the elastic stresses are determined first, after which a correction method is used to determine the elastoplastic stresses.

Elastic Stress

The elastic stress ahead of the crack tip will be determined using the Creager-Paris equations, as was proposed by Noroozi et al [53]. The Creager-Paris equations have been derived after observations that blunting of the crack tip takes place in stress corrosion cracks (cracks caused by stress and environmental factors) [9]. Blunting of the crack tip has also been observed in cracks that undergo cyclic plasticity, hence it has been proposed by Noroozi et al [53] to use these formulas for the calculation of elastic stresses ahead of the crack tip.

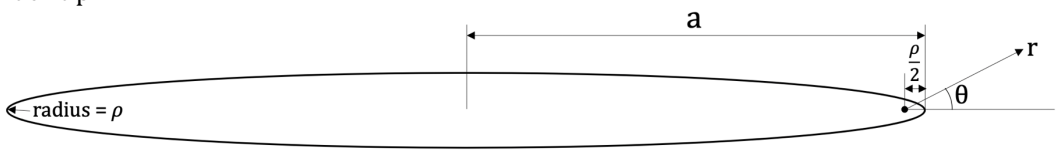

Figure 3.3 Model of elliptical crack used for determination of Creager-Paris equations

The analytical equations are based on a crack in the shape of an elliptical notch, as displayed in Figure 3.4. Here, the tip of the notch with a radius of ρ, resembles the blunt crack tip. The origin of the equations lies at the focal point of the ellipse, which, if $\rho \ll a$, lies at approximately $\rho/2$. The equations are therefore only considered to be valid for long cracks with a notch of a finite radius. For mode I cracking, the formulas are given in Eq. (3.2) - (3.4) [9].

$$\sigma_x = \frac{K_I}{\sqrt{2\pi r}} \left(\cos\frac{\theta}{2} \left[1 - \sin\frac{\theta}{2} \sin\frac{3}{2}\theta \right] - \frac{\rho}{2r} \cos\frac{3}{2}\theta \right) \tag{3.2}$$

$$\sigma_y = \frac{K_I}{\sqrt{2\pi r}} \left(\cos\frac{\theta}{2} \left[1 + \sin\frac{\theta}{2} \sin\frac{3}{2}\theta \right] + \frac{\rho}{2r} \cos\frac{3}{2}\theta \right) \tag{3.3}$$

$$\tau_{xy} = \frac{K_I}{\sqrt{2\pi r}} \left(\sin\frac{\theta}{2} \cos\frac{\theta}{2} \cos\frac{3}{2}\theta - \frac{\rho}{2r} \sin\frac{3}{2}\theta \right) \tag{3.4}$$

These stress fields are very similar to the Westergaard solution for a Mode I sharp crack in an infinite plane [79] given in Eq. (3.5) - (3.7). They differ only by the last term, which is dependent on the radius of curvature of the crack tip. For $r \gg \rho$, the term can be neglected. This implies that blunting of the notch disturbs the stress field of a planar crack in the region near the notch. Further away from the notch, the stress field is similar to the one described by the Westergaard equations for sharp crack tips.

$$\sigma_x = \frac{K_I}{\sqrt{2\pi r}} \cos\frac{\theta}{2} \left[1 - \sin\frac{\theta}{2} \sin\frac{3}{2}\theta \right] \tag{3.5}$$

$$\sigma_y = \frac{K_I}{\sqrt{2\pi r}} \cos\frac{\theta}{2} \left[1 + \sin\frac{\theta}{2} \sin\frac{3}{2}\theta \right] \tag{3.6}$$

$$\tau_{xy} = \frac{K_I}{\sqrt{2\pi r}} \sin\frac{\theta}{2} \cos\frac{\theta}{2} \cos\frac{3}{2}\theta \tag{3.7}$$

A simplification of the Creager-Paris equations can be made based upon the fact that solely the stresses in a straight line ahead of the crack tip (i.e. $\theta = 0$) are considered to drive fatigue crack growth. The Creager-Paris equations reduce to a simple function of the distance ahead of the crack tip as given in Eq. (3.8) - (3.10).

$$\sigma_x = \frac{K_I}{\sqrt{2\pi r}}\left(1 - \frac{\rho^*}{2x}\right) \tag{3.8}$$

$$\sigma_y = \frac{K_I}{\sqrt{2\pi r}}\left(1 + \frac{\rho^*}{2x}\right) \tag{3.9}$$

$$\tau_{xy} = 0 \tag{3.10}$$

Shear stress is responsible for changes in crack direction by altering the direction of the principal stresses ahead of the crack tip. By only considering the stresses in the plane directly ahead of the crack tip (θ = 0), the shear stress reduces to zero. The calculated stresses ahead of the crack tip, σ_x and σ_y, are thus the principal stresses. This leads to the following implication: due to the absence of shear stresses, the crack is only able to grow in a straight line. This implication fits well with the UniGrow method; if the crack would change direction, the weight function method, would no longer be applicable. The current implementation of the UniGrow method thus seems solely suitable for crack growth in one plane, i.e. pure Mode I crack propagation.

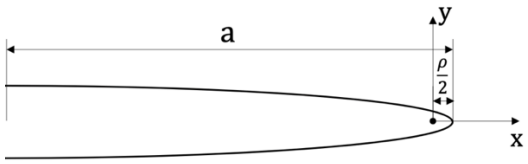

Figure 3.4 Elliptical crack with x-y coordinate system at the tip

Elastoplastic stress

From Eq. (3.8) it becomes clear that the stress at the crack tip is uniaxial, since the σ_x reduces to zero at the crack tip (free surface). The stress state ahead of the crack tip, however, is multiaxial: biaxial for plane stress cases and triaxial for plane strain cases, the directions given in Figure 3.5. This implies that the uniaxial Neuber rule, introduced in section 2.3.3. cannot be applied to determine the plastic stresses ahead of the crack tip. Two widely applied methods are available for this correction: the Hoffmann-Seeger method [24] and the method by Moftakhar et al [38].

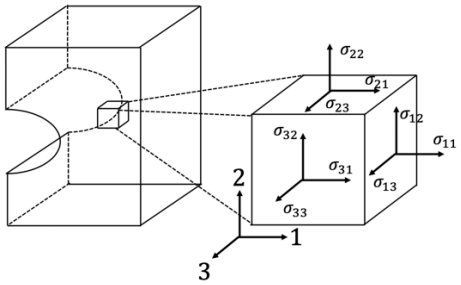

Figure 3.5 Stress state ahead of the crack tip

The two methods are very similar in their basis, both extend the Neuber rule, albeit in different ways:

- **Hoffmann-Seeger:** Based on equating the Von Mises equivalent elastic strain density to the equivalent plastic strain density. The Neuber rule is modified by changing the elastic and plastic stresses/strains to Von Mises equivalent elastic and plastic stresses/strains.

$$\sigma_{eq}^a \varepsilon_{eq}^a = \sigma_{eq}^e \varepsilon_{eq}^e \tag{3.11}$$

- **Moftakhar et al**: Based on equating the total elastic strain energy density to the total plastic strain energy density. The Neuber rule is applied as a summation of all strain energy density.

$$\sigma_{ij}^a \varepsilon_{ij}^a = \sigma_{ij}^e \varepsilon_{ij}^e \tag{3.12}$$

  For the principal directions, this equation reduces to:

$$\sigma_1^a \varepsilon_1^a + \sigma_2^a \varepsilon_2^a + \sigma_3^a \varepsilon_3^a = \sigma_1^e \varepsilon_1^e + \sigma_2^e \varepsilon_2^e + \sigma_3^e \varepsilon_3^e \tag{3.13}$$

The two methods shall now be discussed.

Hoffmann-Seeger method

Hoffmann and Seeger developed a method to determine the notch stresses and strains. The following assumptions have been made by the authors:

- **Hencky's flow rule holds**
- **Equivalent stress:** Von Mises equivalent stress is generally assumed to hold for steels.
- **Proportional loading:** This means that it is assumed that the ratio of in-plane principal strains is constant. This generally holds for notch strains [38], but not for other situations.
- **Plane stress:** Out-of-plane principal stress is zero.
- **Principal stresses and strain axes are fixed in orientation:** Since plane stress is assumed, the out-of-plane shear stresses are zero. The in-plane shear stress directly ahead of the crack tip is zero (see Eq. (3.10)). This means that the elastic stresses are in fact principal stresses.

First, the Von Mises equivalent elastic stress and strain has to be determined using Eq. (3.14) and (3.15).

$$\sigma_{eq}^{e} = \sqrt{(\sigma_1^e)^2 + (\sigma_2^e)^2 - \sigma_1^e \sigma_2^e} \tag{3.14}$$

$$\varepsilon_{eq}^{e} = \frac{\sigma_{eq}^{e}}{E} \tag{3.15}$$

The equivalent elastic-plastic stress and strain can be determined by solving the modified Neuber rule in combination with the modified Ramberg-Osgood as given in Eq. (3.16) and (3.17).

$$\sigma_{eq}^{a}\varepsilon_{eq}^{a} = \sigma_{eq}^{e}\varepsilon_{eq}^{e} = \frac{(\sigma_{eq}^{e})^2}{E} \; and \; \varepsilon_{eq}^{a} = \frac{\sigma_{eq}^{a}}{E} + \left(\frac{\sigma_{eq}^{a}}{K'}\right)^{\frac{1}{n'}} \tag{3.16}$$

Give:

$$\frac{{\sigma_{eq}^{a}}^2}{E} + \sigma_{eq}^{a}\left(\frac{\sigma_{eq}^{a}}{K'}\right)^{\frac{1}{n'}} = \frac{(\sigma_{eq}^{e})^2}{E} \tag{3.17}$$

Using the equation above and the Ramberg-Osgood relation, Eq. (3.18) and (3.19) can be found.

$$\frac{\Delta\sigma^2}{E} + 2\Delta\sigma\left(\frac{\Delta\sigma}{2K'}\right)^{\frac{1}{n'}} = \frac{(K_t\Delta S)^2}{E} = \frac{(\Delta\sigma_{LE})^2}{E} \tag{3.18}$$

$$\frac{\sigma^2}{E} + \sigma\left(\frac{\sigma}{K'}\right)^{\frac{1}{n'}} = \frac{(K_t S)^2}{E} = \frac{(\sigma_{LE})^2}{E} \tag{3.19}$$

Now, this equivalent stress needs to be converted into the principal stresses. It is assumed that Hencky's flow rule holds, which means that the maximum principal strain ε_1 can be expressed as in Eq. (3.20).

$$\varepsilon_1 = \left(\frac{1}{E} + \frac{\varepsilon_{eq}^{p}}{\sigma_{eq}^{a}}\right)\sigma_1^a - \left(\frac{v}{E} + \frac{1}{2}\frac{\varepsilon_{eq}^{p}}{\sigma_{eq}^{a}}\right)\sigma_2^a \tag{3.20}$$

The terms on the right side of Eq. (3.20) can be rewritten as given in Eq. (3.21) and (3.22).

$$\left(\frac{1}{E} + \frac{\varepsilon_{eq}^{p}}{\sigma_{eq}^{a}}\right)\sigma_1^a = \left(\frac{\sigma_{eq}^{a}}{E\sigma_{eq}^{a}} + \frac{E\varepsilon_{eq}^{p}}{E\sigma_{eq}^{a}}\right)\sigma_1^a = \left(\frac{\sigma_{eq}^{a} + E\varepsilon_{eq}^{p}}{E}\frac{1}{\sigma_{eq}^{a}}\right)\sigma_1^a = \frac{\varepsilon_{eq}^{a}}{\sigma_{eq}^{a}}\sigma_1^a \tag{3.21}$$

$$\left(\frac{v}{E} + \frac{1}{2}\frac{\varepsilon_{eq}^{p}}{\sigma_{eq}^{a}}\right)\sigma_2^a = \left(\frac{2\sigma_{eq}^{a}v + E\varepsilon_{eq}^{p}}{2E\sigma_{eq}^{a}}\right)\sigma_2^a = \left(\frac{1}{2} - \frac{\left(\frac{1}{2} - v\right)\sigma_{eq}^{a}}{E\varepsilon_{eq}^{a}}\right)\sigma_2^a \tag{3.22}$$

This leads to Eq. (3.23).

$$\varepsilon_1 = \frac{\varepsilon_{eq}^{a}}{\sigma_{eq}^{a}}(\sigma_1^a - v' * \sigma_2^a) \tag{3.23}$$

Where:

$$v' = \frac{1}{2} - \left(\frac{1}{2} - v\right)\frac{\sigma_{eq}^a}{E\varepsilon_{eq}^a} \tag{3.24}$$

In a similar way, the strain in the other principal direction can be determined. This yields Eq. (3.25).

$$\varepsilon_2 = \frac{\varepsilon_{eq}^a}{\sigma_{eq}^a}(\sigma_2^a - v' * \sigma_1^a) \tag{3.25}$$

The ratio between the stresses can then be determined as in Eq. (3.26).

$$a = \frac{\sigma_2^a}{\sigma_1^a} = \frac{\frac{\varepsilon_2}{\varepsilon_1} + v'}{1 + v'\frac{\varepsilon_2}{\varepsilon_1}} \tag{3.26}$$

The assumption of a constant surface strain ratio leads to Eq. (3.27).

$$\frac{\varepsilon_2}{\varepsilon_1} = \frac{\varepsilon_2^e}{\varepsilon_1^e} \rightarrow\ a = \frac{\sigma_2^a}{\sigma_1^a} = \frac{\frac{\varepsilon_2^e}{\varepsilon_1^e} + v'}{1 + v'\frac{\varepsilon_2^e}{\varepsilon_1^e}} \tag{3.27}$$

The principal stresses and strains can then be calculated from the equivalent stress as given in Eq. (3.28) and (3.29).

$$\sigma_1^a = \sigma_{eq}^a \frac{1}{\sqrt{1 - a + a^2}} \tag{3.28}$$

$$\sigma_2^a = a\sigma_1^a \tag{3.29}$$

Moftakhar method

Moftakhar et al [38] developed a method to determine the notch stresses and strains. The following assumptions have been made by the authors:

- **Hencky's flow rule holds**
- **Equivalent stress:** Von Mises equivalent stress is generally assumed to hold for steels.
- **Proportional loading:** This means that it is assumed that the ratio of in-plane principal strains is constant. This generally holds for notch strains [38], but not for other situations.
- **Principal stresses and strain axes are fixed in orientation:** It is assumed that the stresses and strains ahead of the crack tip are in the principal direction.
- **Masing behaviour:** It is implicitly assumed in this method that the material experiences Masing behaviour

The Moftakhar method use nearly the same assumptions as the Hoffman-Seeger method, but is also suitable for plane strain situations. Another difference is that the method is instead based on equating the plastic strain energy density to the elastic strain energy density of each direction, as given in Eq. (3.30) - (3.32).

$$\sigma_{11}^a\varepsilon_{11}^a = \sigma_{11}^e\varepsilon_{11}^e \tag{3.30}$$

$$\sigma_{22}^a\varepsilon_{22}^a = \sigma_{22}^e\varepsilon_{22}^e \tag{3.31}$$

$$\sigma_{33}^a\varepsilon_{33}^a = \sigma_{33}^e\varepsilon_{33}^e \tag{3.32}$$

Using Hencky's total deformational equations are then used to be able to define the strains in different directions. This yields Eq. (3.33).

$$\varepsilon_{ij} = \frac{1+v}{E}\sigma_{ij}^a - \frac{v}{E}\sigma_{kk}^a\delta_{ij} + \frac{3}{2}\frac{\varepsilon_{eq}^p}{\sigma_{eq}^a}S_{ij} \tag{3.33}$$

Where:

$$\sigma_{eq}^{a} = \frac{1}{\sqrt{2}}\sqrt{(\sigma_{11}^{a} - \sigma_{22}^{a})^2 + (\sigma_{22}^{a} - \sigma_{33}^{a})^2 + (\sigma_{33}^{a} - \sigma_{11}^{a})^2} \tag{3.34}$$

$$\sigma_{kk}^{a} = \sigma_{11}^{a} + \sigma_{22}^{a} + \sigma_{33}^{a} \tag{3.35}$$

$$S_{ij} = \sigma_{ij}^{a} - \frac{1}{3}\sigma_{kk}^{a}\delta_{ij} \tag{3.36}$$

$$\delta_{ij} = 1 \; for \; i = j \; and \; \delta_{ij} = 0 \; for \; i \neq j \tag{3.37}$$

$$\varepsilon_{eq}^{p} = f(\sigma_{eq}^{a}) \tag{3.38}$$

It is assumed that $f\left(\sigma_{eq}^{a}\right)$ is identical to the relationship between stress and plastic strain in a uniaxial tension or compression test. Which means that the equivalent plastic strain can be determined as given in Eq. (3.39).

$$\varepsilon_{eq}^{p} = \left(\frac{\sigma_{eq}^{a}}{K'}\right)^{\frac{1}{n'}} \tag{3.39}$$

Using the Hencky's total deformational equations and the Neuber, a set of six equations with six unknowns can be formed, given in Eq. (3.40). These equations hold for a general tri-axial stress state and can be reduced when e.g. plane stress is assumed. In that case ε_{33}^{a} becomes a function of σ_{11}^{a} and σ_{22}^{a}, making it a redundant variable. The last equation also reduces to zero, leaving four functions and four variables. By solving these equations, one can find the plastic stresses and strains at a given point ahead of the crack tip.

$$\begin{cases} \varepsilon_{11}^{a} = \frac{1}{E}\left(\sigma_{11}^{a} - \nu(\sigma_{22}^{a} + \sigma_{33}^{a})\right) + \frac{\left(\frac{\sigma_{eq}^{a}}{K'}\right)^{\frac{1}{n'}}}{\sigma_{eq}^{a}}\left(\sigma_{11}^{a} - \frac{1}{2}(\sigma_{22}^{a} + \sigma_{33}^{a})\right) \\ \varepsilon_{22}^{a} = \frac{1}{E}\left(\sigma_{22}^{a} - \nu(\sigma_{11}^{a} + \sigma_{33}^{a})\right) + \frac{\left(\frac{\sigma_{eq}^{a}}{K'}\right)^{\frac{1}{n'}}}{\sigma_{eq}^{a}}\left(\sigma_{22}^{a} - \frac{1}{2}(\sigma_{11}^{a} + \sigma_{33}^{a})\right) \\ \varepsilon_{33}^{a} = \frac{1}{E}\left(\sigma_{33}^{a} - \nu(\sigma_{22}^{a} + \sigma_{11}^{a})\right) + \frac{\left(\frac{\sigma_{eq}^{a}}{K'}\right)^{\frac{1}{n'}}}{\sigma_{eq}^{a}}\left(\sigma_{33}^{a} - \frac{1}{2}(\sigma_{22}^{a} + \sigma_{11}^{a})\right) \\ \sigma_{11}^{a}\varepsilon_{11}^{a} = \sigma_{11}^{e}\varepsilon_{11}^{e} \\ \sigma_{22}^{a}\varepsilon_{22}^{a} = \sigma_{22}^{e}\varepsilon_{22}^{e} \\ \sigma_{33}^{a}\varepsilon_{33}^{a} = \sigma_{33}^{e}\varepsilon_{33}^{e} \end{cases} \tag{3.40}$$

Determination of residual stress

Once the elastoplastic stresses ahead of the crack tip are determined, the plastic residual stress at a given point x_i ahead of the crack tip can be determined using Eq. (3.41).

$$\sigma_r(x_i) = \sigma_y^{a}(x_i) - \Delta\sigma_x^{a}(x_i) \tag{3.41}$$

It has been proposed by Noroozi et al [53], that only the compressive part of the residual stress ahead of the crack tip has to be mirrored onto the crack faces to mimic the crack opening. The compressive region, x_{int} in Figure 3.6, is also called the integration domain [33]. The conversion of the x-coordinate of the stress to the coordinate on the r-axis (starting at the crack end) is given by Eq. (3.42). The r-coordinate at which the compressive residual stress becomes tensile is denoted as r_{start}.

$$r_i = a - 2\rho^{*} - x_i \tag{3.42}$$

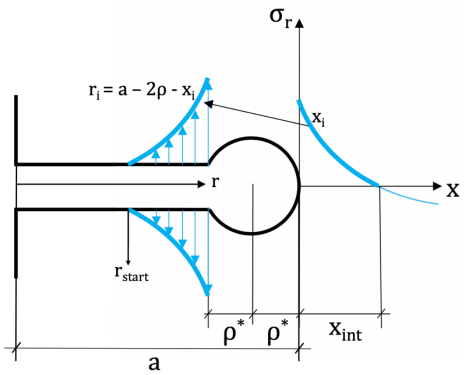

Figure 3.6 Depiction of mirroring of plastic residual stresses ahead of the crack tip onto crack face

Programming flowchart

The flowchart for this part of the UniGrow model is presented in Figure 3.7. It has been converted into a separate module that is part of the larger UniGrow model. The model consists of a loop starting at $x = 0$ and ending at $x = a - 2\rho^*$, since this denotes the length of the crack face. On each point, first, the elastic stresses are determined and subsequently converted to elastoplastic stresses. With these stresses, the residual stress can be determined. If the residual stress is compressive, the stress is added to the stress on the crack face. Once the residual stress is tensile, the loop stops and a starting point (r_{start}) is defined.

At the same time, a checking parameter (x_{check}) is defined. This parameter is used to check whether the data consists of more than one point. If this is not the case, no integration can be performed and thus the $K_{res} = 0$. If the data consists of more than one point, integration can be done and the residual stress values and corresponding r-values will be used to create the function $\sigma_{res}(x)$. This function is created by means of linear interpolation of the values.

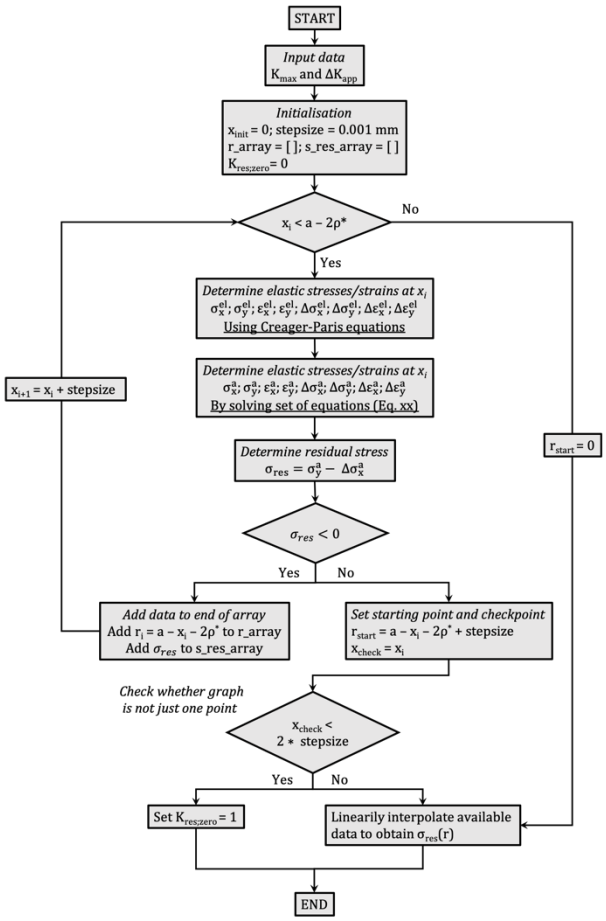

Figure 3.7 Flowchart for the Stress Module

3.1.3.3 Determination of plastic residual stress intensity factor

The determination of the plastic residual stress intensity factor has to be done using the weight function method, as recommended by Noroozi et al [53]. The basis for the determination of K_{res} is the integral given by Eq. (3.43). The residual stress ($\sigma_{res}(x)$) from the previous section will be used together with the weight functions (m(x, a)) that will be discussed below.

$$K_{res} = \int_{r_{start}}^{(a-2\rho^*)} \sigma_{res}(x) m(x,a) dx \tag{3.43}$$

Weight Function

It is common practice to use the weight function related to the geometry and crack type in question. In the case of a CT specimen, this would be the weight function by Fett and Munz [14], given in Eq. (3.44). Its validity is $0 < \alpha = \frac{a}{W} < 0.85$.

$$m(x,a) = \sqrt{\frac{2}{\pi a}} \frac{1}{\sqrt{1-\rho}} \left\{ 1 + \sum_{\eta=1}^{4} \sum_{\mu=1}^{5} \frac{A_{\eta\mu} \alpha^{\mu-1}}{(1-\alpha)^{\frac{3}{2}}} (1-\rho)^{\eta} \right\} \tag{3.44}$$

η	$\mu = 1$	2	3	4	5
1	2.673	-8.604	20.621	-14.635	0.477
2	-3.557	24.9726	-53.398	50.707	-11.837
3	1.230	-8.411	16.957	-12.157	-0.940
4	-0.157	0.954	-1.284	-0.393	1.655

Table 3.2 Values of η and μ used in Fett and Munz weight function

However, it was proposed by Mikheevskiy [33] that the universal one-dimensional weight function can be used to make the determination of the plastic residual stress intensity factor geometrically independent. The universal weight function, given in Eq. (3.45), has been shown to provide good estimations for weight functions of one- and two-dimensional cracks [16].

$$m(x,a) = \frac{2}{\sqrt{2\pi(a-x)}} \left[1 + M_1 \left(1 - \frac{x}{a}\right) + M_2 \left(1 - \frac{x}{a}\right)^2 + \ldots + M_n \left(1 - \frac{x}{a}\right)^n \right] \tag{3.45}$$

Mikheevskiy [33] argues that, if the integration domain (x_{int} in Figure 3.6) is relatively small, the term $(1 - x/a)$ in Eq. (3.45) tends to zero. Since $(1 - x/a)$ is multiplied with the geometry-related terms $M_1 \ldots M_n$, these terms will fall away. This leaves a geometrically independent weight function as given in Eq. (3.46). Both the geometrically independent and geometry-specific weight function will be tested to see the difference between the application of the two.

$$m(x,a) = \frac{2}{\sqrt{2\pi(a-x)}} \tag{3.46}$$

Integration

The plastic residual SIF, K_{res}, can be determined by evaluating the integral given in Eq. (3.47. However, since the residual stress isn't definable by an equation, evaluation of this integral has to be done numerically. To do this, both curves are split up into a number of intervals on which they are assumed to be linear. The intervals are 0.001 mm wide, meaning that this assumption approximately holds. The following assumption is then used [39]:

$$K_{res} = \int_{a_0}^{a} m(x,a)\sigma_{res}(x) dx = \sum_{j=1}^{i} \sigma_{avg} * S \tag{3.47}$$

If $m(x,a)$ and $\sigma_{res}(x)$ depend on variable x only, then the integral in Eq. (3.47)can be replaced by a summation given in Eq. (3.47)*. Here S represents the area under the curve $m(x,a)$ and σ_{avg} represents the value of the function $\sigma_{res}(X_i)$ corresponding to the coordinate X_i of the centroid of the area S.*

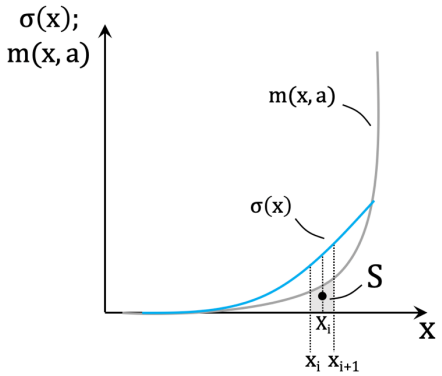

Figure 3.8 Integration of a multiplication two functions

An overview of the statement above is given in Figure 3.8. The curves are both linearized on the intervals to assure easy determination of the centroid of the area S, when making the interval very small, this approximation holds. The residual stress at the centroid of area S can be determined with Eq. (3.48).

$$\sigma_{avg} = \frac{\sigma_{res}(x_i) + \sigma_{res}(x_{i+1})}{2} \tag{3.48}$$

As recommended by [60], the value of the integral of the weight function, will be determined using Gaussian Quadrature. This will be done due to the singularity at $x = a$ of the weight function. [60] recommends using Gaussian Quadrature with 50 points on the singular intervals to assure proper convergence.

Programming flowchart

The flowchart for this part of the UniGrow model is presented in Figure 3.9. It has been converted into a separate module that is part of the larger UniGrow model. The model consists of a loop starting at $r = 0$ or $r = r_{start}$ (depending on the previous step) and ending at $r = a - 2\rho^*$, since this denotes the length of the crack face. On each interval, first, the average residual stress is determined. Subsequently, the area S, or integral of the weight function on the interval is determined. These two values are then multiplied and added to the plastic residual SIF.

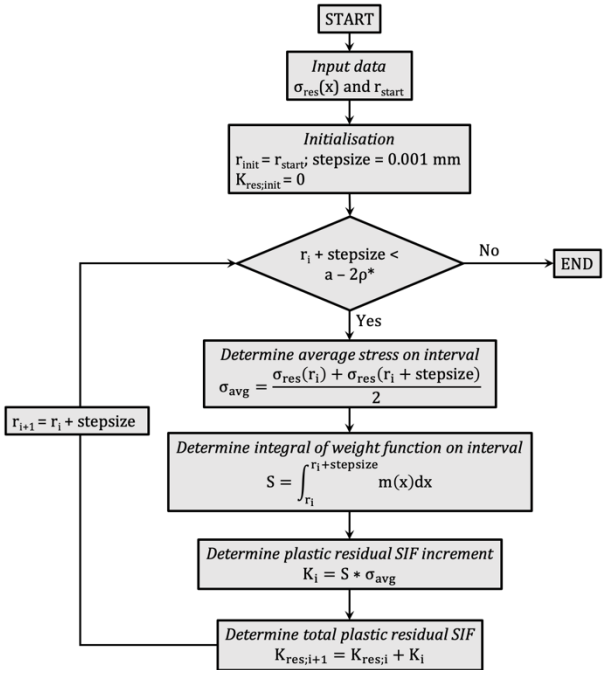

Figure 3.9 Flowchart for Residual Weight Function module

3.1.3.4 Determination of elastoplastic stress and strain on first block ahead of crack tip

The elastoplastic stresses ahead of the crack tip will be determined using the Creager-Paris equations with Neuber uniaxial plasticity correction. Instead of first determining the elastoplastic stress distribution ahead of the crack tip, first the average elastic stress on the first elementary block ahead of the crack tip is determined according to Eq. (3.49) and (3.50)[53].

$$\tilde{\sigma}_y^e = \frac{1.633 K_{max,tot}}{\sqrt{2\pi\rho^*}} \tag{3.49}$$

$$\Delta\tilde{\sigma}_y^e = \frac{1.633 \Delta K_{app,tot}}{\sqrt{2\pi\rho^*}} \tag{3.50}$$

This average elastic stress ahead of the crack tip will then be corrected to the average elastoplastic stress on the first elementary block ahead of the crack tip. This is done using the uniaxial Neuber method, the use of which is justified by the fact that the stress in x-direction at the crack tip has to be zero. The average elastoplastic stress on the first elementary block ahead of the crack tip can be determined by solving Eq. (3.51) and (3.52).

$$\frac{\tilde{\sigma}_y^{a\,2}}{E} + \tilde{\sigma}_y^a \left(\frac{\tilde{\sigma}_y^a}{K'}\right)^{\frac{1}{n'}} = \frac{\tilde{\sigma}_y^{e\,2}}{E} \tag{3.51}$$

$$\frac{\Delta\tilde{\sigma}_y^{a\,2}}{E} + 2\Delta\tilde{\sigma}_y^a \left(\frac{\Delta\tilde{\sigma}_y^a}{2K'}\right)^{\frac{1}{n'}} = \frac{\Delta\tilde{\sigma}_y^{e\,2}}{E} \tag{3.52}$$

Using the elastoplastic stress range ($\Delta\tilde{\sigma}_y^a$), the strain amplitude can be determined by using the Ramberg-Osgood relationship, as is shown in Eq. (3.53).

$$\tilde{\varepsilon}_y^a = \frac{\Delta\tilde{\sigma}_y^a}{2E} + \left(\frac{\Delta\tilde{\sigma}_y^a}{2K'}\right)^{\frac{1}{n'}} \tag{3.53}$$

3.1.3.5 Determination of the initiation life of the elementary block ahead of the crack tip

Using the strain amplitude $\tilde{\varepsilon}_y^a$, combined with $\tilde{\sigma}_y^a$ and the Smith-Watson-Topper damage parameter, the initiation life of the first elementary block ahead of the crack tip can be calculated. This can be determined by solving Eq. (3.54)for N_f.

$$\sqrt{\tilde{\sigma}_y^a \tilde{\varepsilon}_y^a E} = \sqrt{\sigma_f'^2 (2N_f)^{2b} + \sigma_f' \varepsilon_f' E (2N_f)^{b+c}} \tag{3.54}$$

Programming flowchart

In Figure 3.10 the flowchart for the implementation of this section in Python can be found. The determination of the stress on the first elementary block ahead of the crack tip and the determination of the initiation life of the first elementary block have been combined into one module. It has been converted into a separate module that is part of the larger UniGrow model. The model starts by the determination of the elastic and subsequently the elastoplastic stresses on the first block. Then the strain range and fatigue life can be determined.

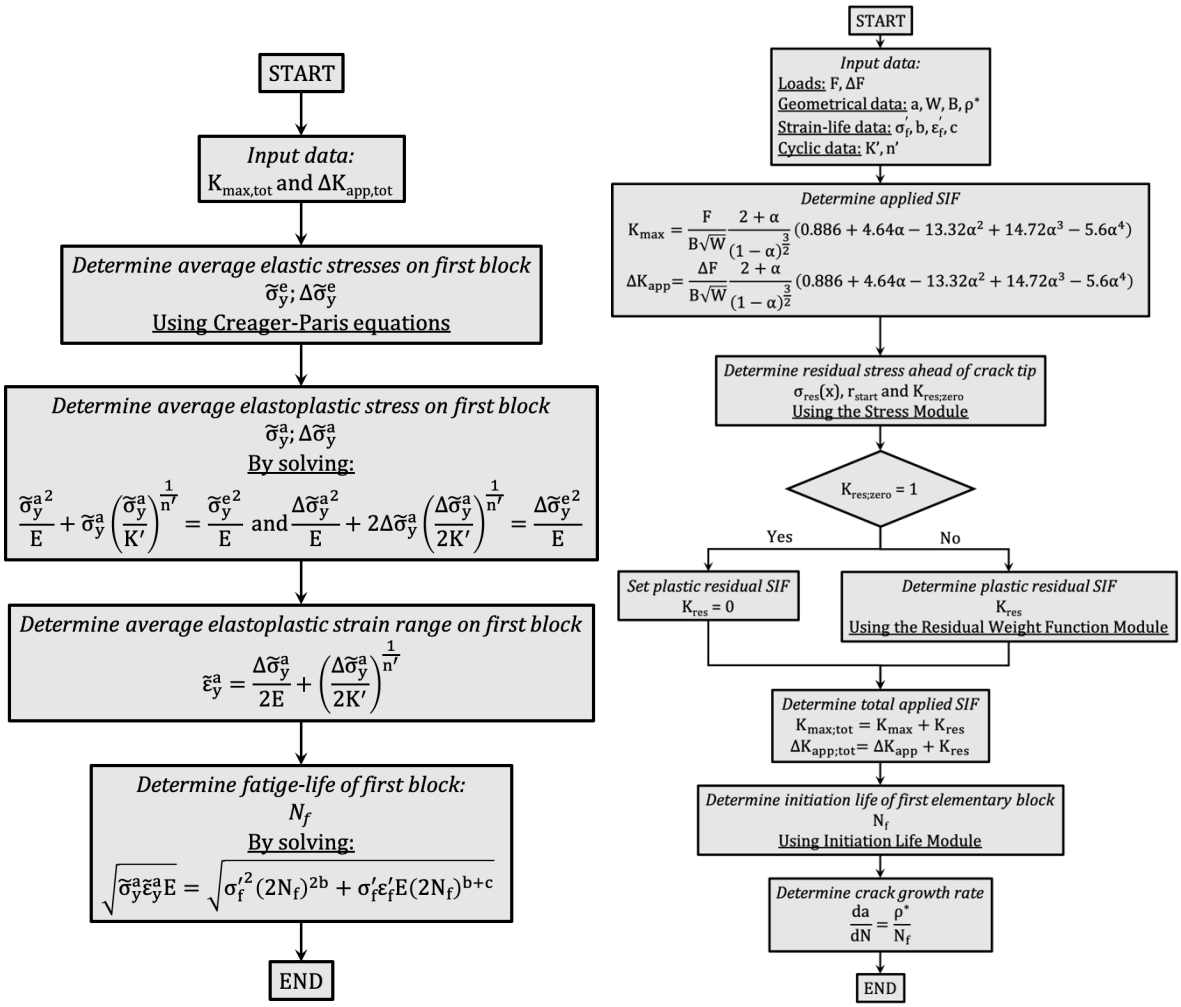

Figure 3.10 Flowchart for the Initiation Life module (left) and total implemented analytical UniGrow method (right)

3.1.3.6 Implementation of the total UniGrow method in Python

Implementation of the UniGrow model has been performed in Python, the flowchart of which is given in Figure 3.10. It consists of a linear program that calls separate modules for determination of variables. The steps largely match those given in the previous section and Figure 3.2. The mode starts off with some input definition, such as loads, geometrical data etc. Then the applied SIF is determined using the Newman-Srawley equations. Using the Stress Module, the residual stress ahead of the crack tip is calculated.

If the parameter $K_{res;zero}$ is set to 1 in the Stress Module, it means that no compressive residual stress is observed in the model and thus K_{res} is set to zero. If this is not the case, then the Residual Weight Function Module is used to determine K_{res}. After this, the total SIFs are determined which are then used to determine the fatigue life of the first elementary block ahead of the crack tip. The crack growth rate can then simply be calculated. The model will be run multiple times for the same geometry, each time varying the crack length to generate data for the da/dN curves.

3.1.3.7 Modelling input

The crack growth rate and K_{res} results are generated by applying maximum force of 2000 N, the minimum force depending on the stress ratio. This is kept constant and the crack length is increased from its initial length of 8 mm using crack increments of 1 mm. For the verification of the elastoplastic stresses, the same load values have been used as De Jesus et al [10]. These are a maximum force of 1614 N and a crack length of 8 mm or 25 mm.

3.1.4 Results and discussion

In this section the results from the verification of the analytical UniGrow are presented and discussed. The section will start by discussing the elastic, elastoplastic and residual stresses produced by the implemented UniGrow method. This is followed by a discussion of the calculated plastic residual SIFs. The section is closed off by a discussion of the determined crack growth rates.

3.1.4.1 Determination of elastoplastic stress ahead of crack tip

Firstly, the implementation of the Creager-Paris equations has been verified. This has been done for a crack length of 8 and 25 mm and a force of 1614 N (definition of local x- and y-direction is presented in Figure 3.4). The results, given in Figure 3.11, match exactly with the curves provided by Jesus et al [10], meaning correct implementation.

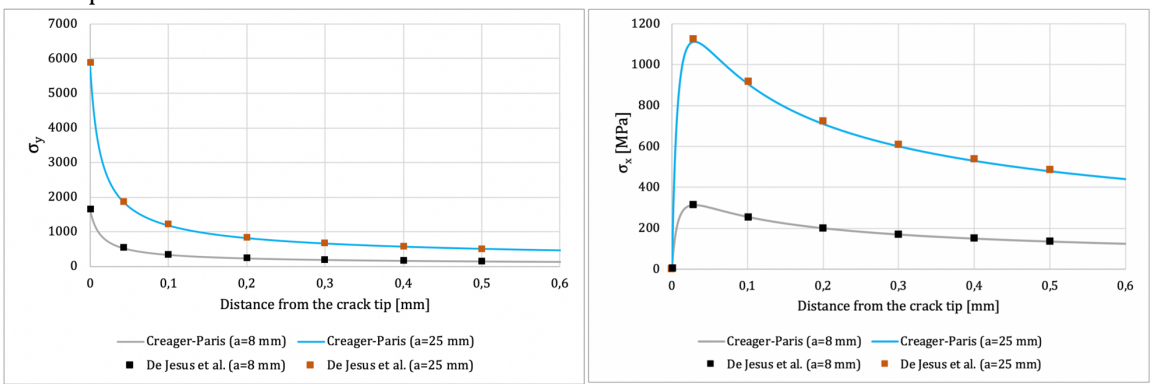

Figure 3.11 Elastic stress distribution ahead of the crack tip: comparison of Creager-Paris results and results from De Jesus et al [10]

Once the elastic stress distribution has been determined, a correction needs to be done to obtain the elastoplastic stresses. De Jesus et al [10] corrected the elastic stresses by using a multiaxial Neuber correction, it has not been specified explicitly which procedure has been used. Elastoplastic FEA was also used to obtain elastoplastic stresses. In Figure 3.12 and Figure 3.13, the resulting elastoplastic stresses from both the Hoffmann-Seeger and Moftakhar correction method are presented in comparison to values from De Jesus et al [10].

In y-direction, the results are in quite good agreement with the results calculated by De Jesus et al [10]. The stress predicted by both Hoffman-Seeger and Moftakhar methods, is slightly too high at the crack tip and too low further away from the crack tip. This is mainly caused by the fact that analytical correction methods are unable to account for the redistribution of the stresses due to plasticity. Both of the elastoplastic correction models use a form of the Neuber method and therefore are upper bound methods. This also plays a part in the overestimation of the stresses at the crack tip. Directly at the crack tip, the stress in the Moftakhar method makes a sudden drop. This will be discussed in the next paragraph. The difference between the Neuber method used by De Jesus et al [10] and the generated results could result from a different specification of the correction method. Despite these differences, the overall results are very similar.

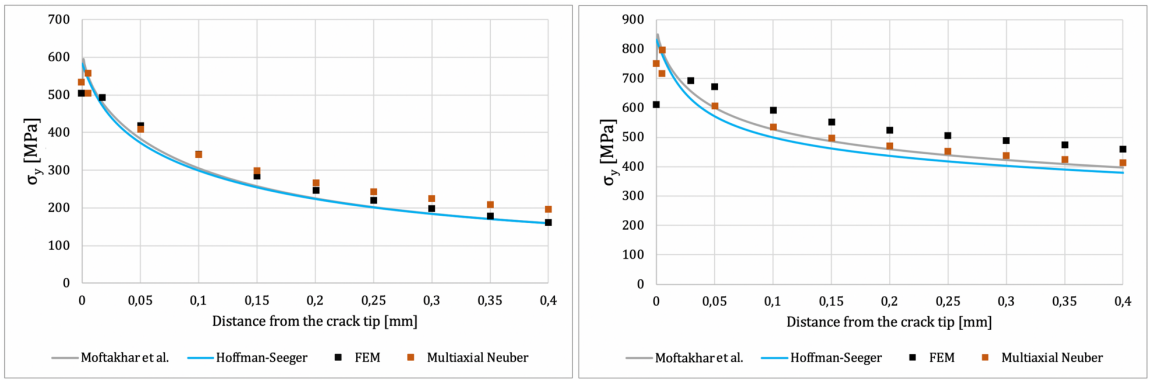

Figure 3.12 Elastoplastic stress distribution in y-direction ahead of the crack tip: comparison of analytical results and results by De Jesus et al [10] for crack lengths of 8 mm (left) and 25 mm (right) (F = 1614 N)

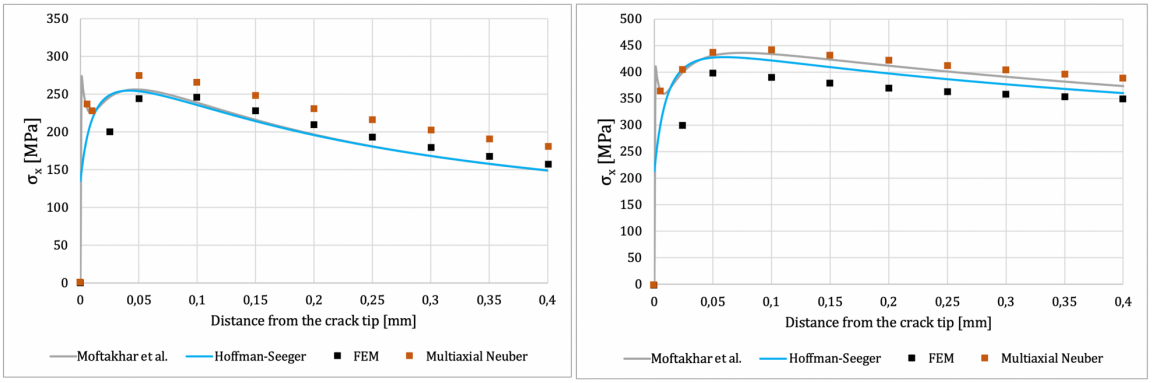

Figure 3.13 Elastoplastic stress distribution in x-direction ahead of the crack tip: comparison of analytical results and results by De Jesus et al [10] for crack lengths of 8 mm (left) and 25 mm (right) (F = 1614 N)

In x-direction, several interesting things can be observed. The most noteworthy being an inexplicable spike in the stress in the Moftakhar method near the crack tip. The same phenomena, however less pronounced, is also observed in the Neuber results from De Jesus et al [10] but is not present in FEA results. The spike in x-direction allows the stress in y-direction to get higher (as hydrostatic stress doesn't cause yielding). The sudden decrease in stress from the spike to zero stress in x-direction, also forces the stress in y-direction to drop.

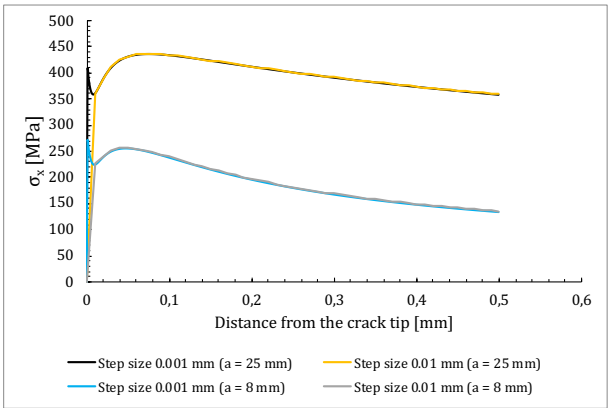

Figure 3.14 Influence of step size on stress in x-direction

The spike is an inaccuracy in the analytical method and the magnitude of it depends on how refined the elastoplastic analysis is. The results in Figure 3.13 have been determined by determining the stress at intervals of 0.001 mm. In Figure 3.14 it is demonstrated that when the step size is increased to 0.01 mm, the spike nearly completely disappears. This leaves a curve that is more representative of the physical reality and resembles the Hoffman-Seeger curve quite well. Therefore, it has been decided to henceforth use a step size of 0.01 mm.

In the Hoffman-Seeger method, another type of anomaly is present. In this method, the stress in x-direction doesn't reduce to zero at the crack tip. Since the crack tip is a free surface, the stress should reduce to zero. This means that the Hoffman-Seeger method produces less physically accurate results. According to Moftakhar et al [38], this is caused by the Hoffman-Seeger equations becoming too rigid for the uniaxial case. An overestimation of the stresses in x-direction at the crack tip, allows for higher stresses in y-direction to occur and therefore will most likely lead to an overestimation of the plastic residual stresses at the crack tip.

3.1.4.2 Determination of plastic residual stress ahead of crack tip

Using the elastoplastic stresses, one can determined the plastic residual stress ahead of the crack tip. The results for a crack length of 8 mm and 25 mm and R = 0 have been given in Figure 3.15. The general trend is that, compared to FEA results from De Jesus et al [10], the residual stress is overestimated. The Hoffman-Seeger method procures slightly higher results than the Moftakhar et al method. At the crack tip, the same drop is observed as in the elastoplastic results for the Moftakhar et al method.

Further away from the crack tip, the stress asymptotically decreases to zero. This is caused by the fact that here, both stress range and maximum stress are in the elastic regime. Therefore, at R = 0, $\sigma_y^a \approx \Delta\sigma_x^a$ and thus the residual stress reduces to zero. However, this is not physically accurate because the cross section as a whole would be out of balance due to there only being compressive stresses. This is caused by the fact that the analytical methods are unable of redistributing the stresses.

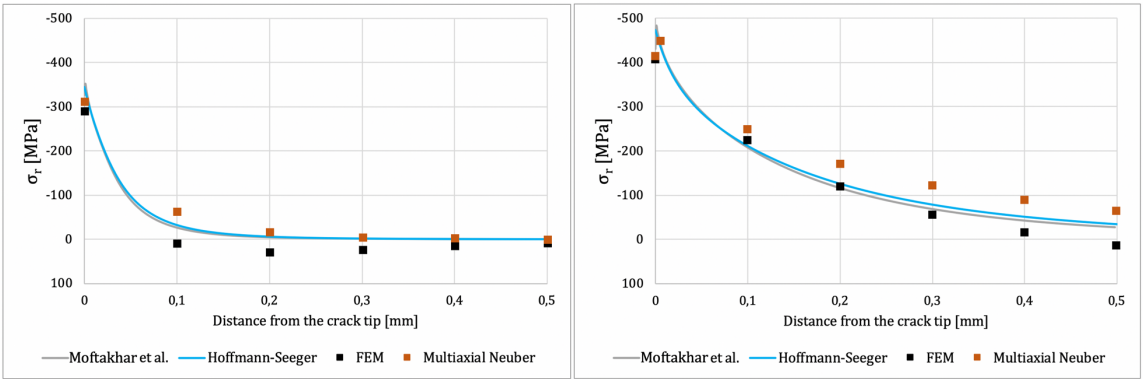

Figure 3.15 Plastic residual stress ahead of the crack tip: comparison of analytical results and results by De Jesus et al [10] for crack lengths of 8 mm (left) and 25 mm (right) (F = 1614 N)

3.1.4.3 Determination of plastic residual stress intensity factor

Using the previously obtained residual stress distributions and the weight function, one can determine the plastic residual SIF. According to Noroozi et al [53], this relationship should be linear. De Jesus et al calculated the plastic residual stress intensity factor based upon the residual stress results from FEA, as they deemed it to be more physically accurate than the analytical method.

The weight functions have been determined using both the plasticity corrections by Hoffmann-Seeger and Moftakhar et al. Furthermore, both the weight function for the CT specimen and the geometrically independent weight function have been applied. The results of these calculations are given in Figure 3.16, Figure 3.17 and Figure 3.18. Overall, it can be said that the Hoffmann-Seeger and Moftakhar et al yield very similar results, with the Hoffman-Seeger method predicting slightly higher K_{res} values (due to prediction of higher residual stress).

When using the CT weight function the, results match quite well for low applied SIF ranges for R = 0 and R = 0.5. For higher applied SIF ranges, the results start to deviate, and both the analytical method predict higher K_{res}-values than De Jesus et al [10]. This difference is mainly caused by the inability of the methods to redistribute the stresses away from the crack tip, causing an overestimation of the stresses at the crack tip. This overestimation is more pronounced for higher applied SIFs as can be seen in Figure 3.15, explaining the deviation of the analytical results from De Jesus et al [10].

At R = 0, another effect causes additional deviation from the results by De Jesus et al [10]. This is caused by the residual stress asymptotically decreasing to zero when using analytical results. As ΔK_{app} increases, the residual stress further away from the crack tip keep increasing, never becoming tensile. This adds to the overestimation of K_{res}.

The universal weight function has a more singular character and therefore, most of its weight is attributed to the part of the residual stress distribution closest to the crack tip. The residual stress close to the crack tip is quite similar to the one predicted by FEA (still observing some overestimation). The expectation is that the K_{res} at R = 0 will be overestimated to a lesser extent than when using the CT weight function. This means that the WF corrects the physically inaccurate solution provided by the analytical elastoplastic correction method. Furthermore, De Jesus et al [10] have also used the universal weight function, which would explain better correspondence.

The predicted plastic residual SIF seems to be nonlinear for low ΔK_{app}, slowly decreasing to zero. This could be caused by the fact that the relationships determined by De Jesus et al [10] have been sampled at specific points, away from this low limit. Also, K_{res} is severely underestimated for R = 0.7. However, the relative different might be large, but the absolute difference is fairly limited.

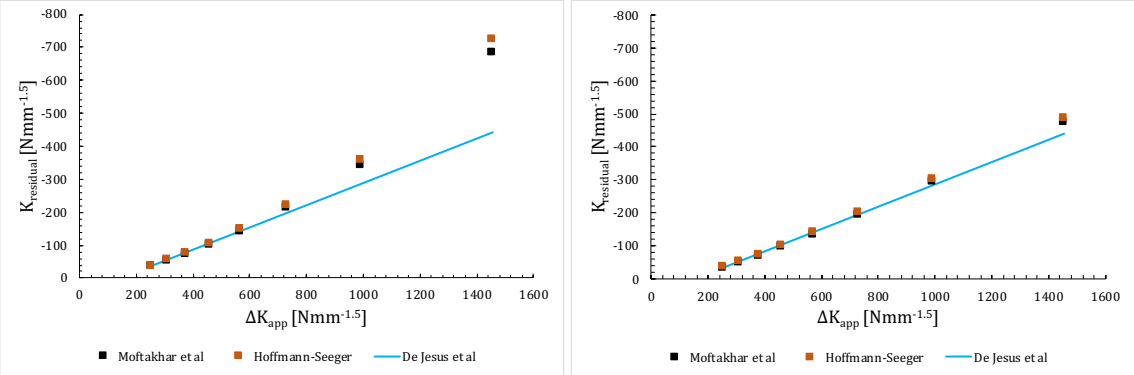

Figure 3.16 Plastic residual SIF as a function of the applied SIF range (R=0) for CT WF (left) and universal WF (right) compared to results predicted by De Jesus et al [10]

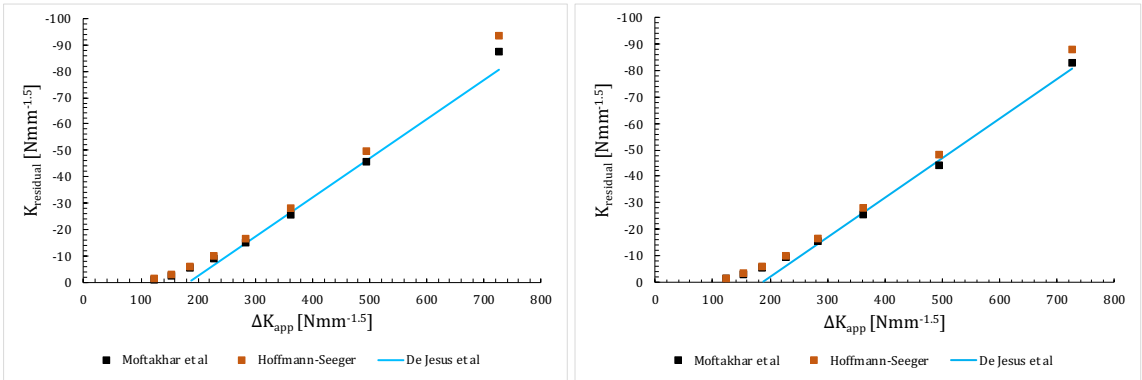

Figure 3.17 Plastic residual SIF as a function of the applied SIF range (R=0.5) for CT WF (left) and universal WF (right) compared to results predicted by De Jesus et al [10]

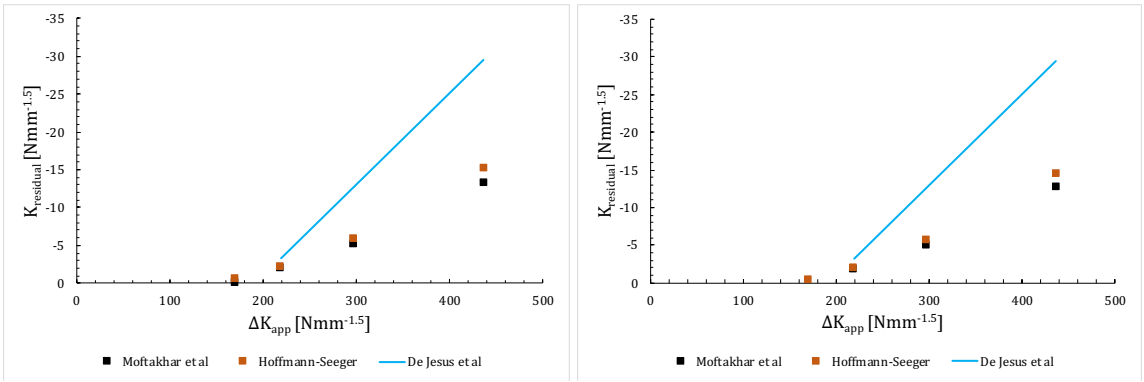

Figure 3.18 Plastic residual SIF as a function of the applied SIF range (R=0.75) for CT WF (left) and universal WF (right) compared to results predicted by De Jesus et al [10]

3.1.4.4 Determination of the crack growth rate

The crack growth as predicted by the UniGrow method has then be determined for each stress ratio. Also, here, the effect of the plasticity correction method and the weight function method has been considered. The results are given in Figure 3.19, Figure 3.20 and Figure 3.21.

Overall, good correspondence is found between the results from the analytical UniGrow implementation and the UniGrow method by De Jesus et al [10]. For R = 0, deviation from results by De Jesus et al [10] can be found, especially when using the CT weight function. This is due to overestimation of the plastic residual SIF, as was presented in the previous section. The SIF that is "felt" by the material at the crack tip is less than expected and therefore crack growth rates are underestimated. This difference is especially present for higher values of ΔK_{app}. Results for R = 0 when using the universal weight function are much better, as the plastic residual SIF values match the ones from De Jesus et al [10]. This, again, signifies the importance of proper determination of this variable.

In the previous section, it was also noted that, for R = 0.7 and R = 0.5, there were relatively large differences between the ΔK_{app} - K_{res} relationship predicted by current research and De Jesus et al [10]. However, as was postulated before, the absolute value of the plastic residual SIF is low and therefore the impact of this difference on the crack growth rate is limited. This confirms the prediction of Noroozi et al [53] that for high stress ratios (R > 0.5), one could leave out the residual stress, since this would have an insignificant effect on the crack growth rate.

Moftakhar et al and Hoffman-Seeger correction methods yield nearly the same results, as K_{res} predictions were also similar for both methods. For the same K_{res} predictions, the implemented UniGrow method in this study and the one by De Jesus et al yield the same result. It can thus be concluded that the determination of the fatigue life of the elementary material block ahead of the crack tip has been properly implemented.

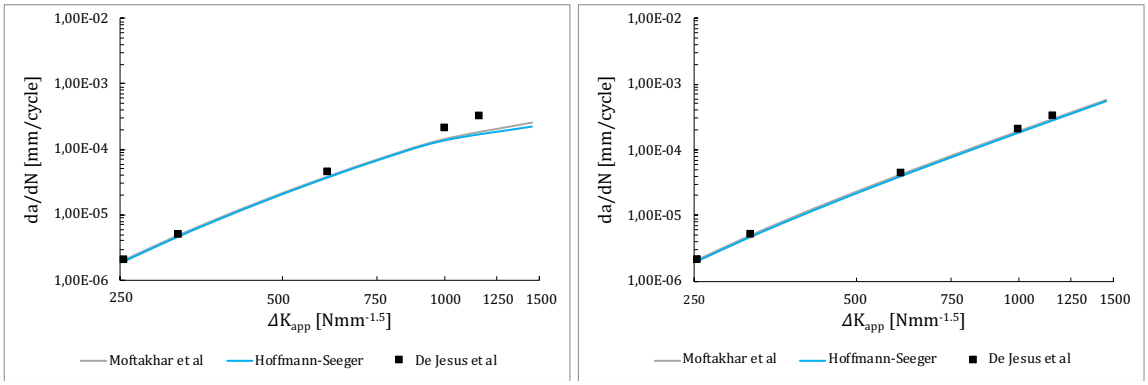

Figure 3.19 Crack growth speed as a function of the applied SIF range (R=0) for CT WF (left) and universal WF (right)

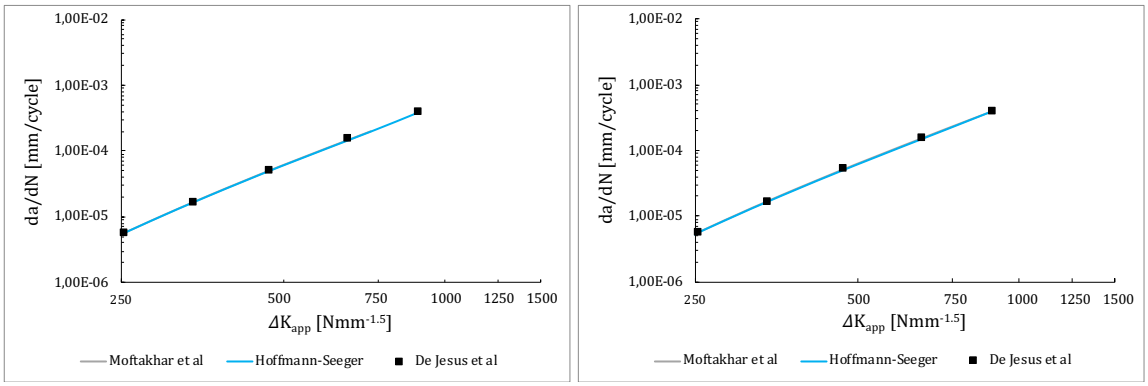

Figure 3.20 Crack growth speed as a function of the applied SIF range (R=0.5) for CT WF (left) and universal WF (right)

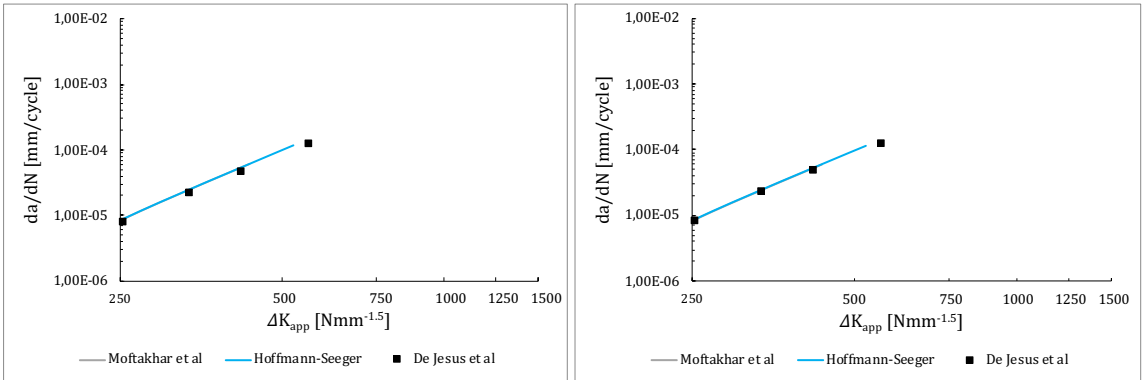

Figure 3.21 Crack growth speed as a function of the applied SIF range (R=0.75) for CT WF (left) and universal WF (right)

3.1.4.5 Discussion

As was discussed in the previous sections, the analytical UniGrow implementation has been completely verified with the model by De Jesus et al [10]. Even though the model is verified, still some limitations can be found when comparing it to the more advanced implementation by De Jesus et al [10]. Especially the determination of one of the most vital parameters in the UniGrow method, K_{res}, lacks accuracy when using this method. This lack of accuracy is most important for lower stress ratios, where the effect of plastic residual stresses ahead of the crack tip on the crack growth rates can be significant.

The inaccurate predictions of K_{res} can be attributed to the inability of the elastoplastic stress correction methods to properly predict the elastoplastic stresses ahead of the crack tip. These are very often overestimated, especially near the crack tip. Since the residual stresses near the crack tip are the main contributors for slowing down the crack growth, overestimation of these stresses causes underprediction of crack growth rates. In the elastoplastic FEA model that was run by De Jesus et al [10], it is visible that stress is normally distributed away from the crack tip. The analytical model is incapable of doing this, leading to under prediction of the compressive residual stress further away from the crack tip. At R = 0, the stresses are even compressive along the entire cross section, asymptotically reducing to zero.

The elastoplastic correction methods itself also showed anomalous behaviour. The elastoplastic correction method by Moftakhar et al produced a spike at the crack tip in x-direction, which wasn't observed in elastoplastic FEA results by De Jesus et al [10]. This was corrected for using larger increments between the locations where the stresses were determined. The Hoffman-Seeger method, on the other hand, produced nonzero stress results of the stress in x-direction at the crack tip. This method therefore also yields physically inaccurate results, as the crack tip is a free surface and thus the stress should be zero.

When using the universal weight function, better results were obtained for K_{res}. Especially for R = 0, where the singular weight function acts as a scissor to "cut off" the inaccurate, asymptotically decreasing tail of the predicted plastic residual stress distribution. This, however, doesn't fix the underlying issue of improper determination of the plastic residual stresses, but simply corrects the consequence.

3.2 Verification of numerical UniGrow implementation

As could be seen in the previous chapter and what has also been observed by De Jesus et al [10], the analytical determination of the elastoplastic stresses ahead of the crack tip leaves some room for improvement. De Jesus et al [10] proposed to use elastoplastic FEA as a more appropriate alternative for the determination of the elastoplastic stresses. When using this method, the relationship between ΔK_{app} and K_{res} is determined first, after which this relationship serves as input for the UniGrow model.

In this section, the numerical method as proposed by De Jesus et al [10] will be implemented and verified. First, the verification data will be presented. Then the details of the numerical implementation will be discussed. Lastly, the crack growth results are presented and discussed.

3.2.1 Model description and model data

The data that was used in section is the same as used in section 5.1. The dimensions and parameters used in this section are presented in Table 3.3.

Dimensions		Material parameters		Strain-life parameters	
$\boldsymbol{W}$	40 mm	E	205.2 GPa	σ_f'	1005.5 MPa
$\boldsymbol{a_n}$	8 mm	v	0.275	b	-0.1033
$\boldsymbol{B}$	4.35 mm	K'	948.35 MPa	ε_f'	0.3678
$\boldsymbol{L}$	50 mm	n'	0.1533	c	-0.5475
$\boldsymbol{H}$	48 mm				
$\boldsymbol{h}$	22 mm				

Table 3.3 Material parameters and dimensions of the CT specimens [10]

3.2.2 Global UniGrow implementation

The calculation method, globally, consists of about 5 steps, of which a summary is given in Figure 3.22. The implemented method is similar to the one in chapter 5.1 and are given below:

1. **Determination of the applied stress intensity factor:** The applied stress intensity factor will be established using an analytical equation derived by Newman and Srawley [73]. This topic will not be further addressed, reference is made to section 3.1.3.1 for further background.
2. **Determination of the elastoplastic stress distribution ahead of the crack tip:** The elastic stresses ahead of the stress tip will be determined using elastoplastic FEA. The CT specimen will be modelled and loaded and unloaded once, after which the residual stress is recorded in the model. This will be used to determine the plastic residual stress intensity factor. This will be addressed further in section 3.2.3.1.
3. **Determination of the residual stress intensity factor:** Using the weight function method and the elastoplastic stresses from the previous step, the plastic residual SIF will be determined. These values will be used to determine the linear relationship between ΔK_{app} and K_{res}. Further background on this will be given in section 3.2.3.2.
4. **Determination of the elastoplastic stress and strain on first elementary block ahead of the crack tip:** This will be done using the Creager-Paris equations in combination with the Neuber uniaxial plasticity correction. This will not be further addressed; reference is made to section 3.1.3.4 for further background.
5. **Determination of the initiation life of the first elementary block ahead of crack tip:** The initiation life will be determined using both the Smith-Watson-Topper damage parameter as the Morrow damage method. This will be further addressed in section 3.2.3.3.

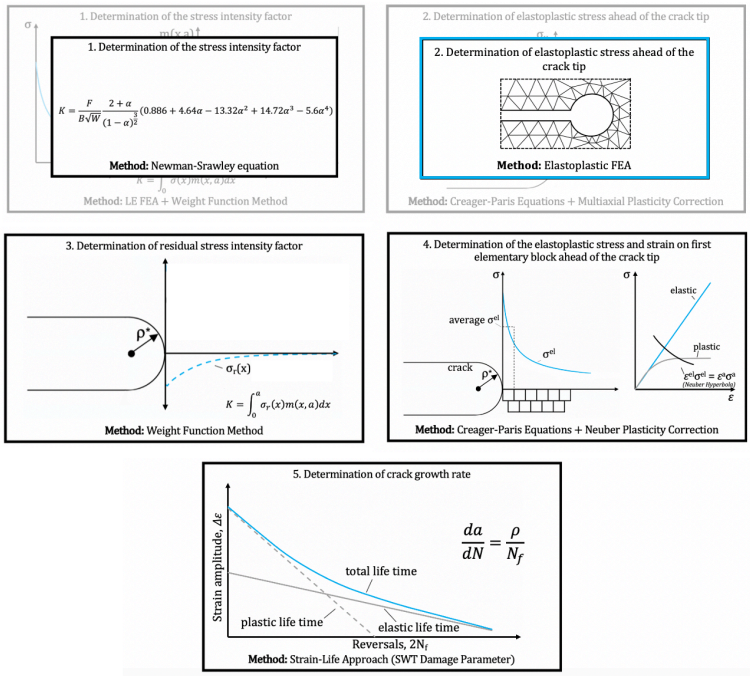

Figure 3.22 Global calculation procedure of the numerical UniGrow method

3.2.3 Implemented methods

Most of the implemented methods are similar to the ones used in section 3.1, therefore, solely the determination of K_{res} using elastoplastic FEA will be discussed in this section. Lastly, the flowchart for the implementation in Python is given.

3.2.3.1 Determination of K_{res} using elastoplastic FEA

The CT specimen is modelled similar to the one by De Jesus et al [10], a summary of the modelled geometry is given in Figure 3.23. Half of the CT specimen is modelled due to symmetry and to save computational time. The geometry is simplified, removing the initial notch that is present in a CT specimen, since the sole interest is the effect of the crack length and the notch. This is similar to the model proposed by De Jesus et al [10]. The crack tip is modelled as a quarter circle.

The pin that is used to load the CT specimen is modelled as a rigid body that is controlled by a remote point. The remote point is loaded by a force. The remote point is restrained in its sideways movement and angular rotation. The contact surface between the pin and the CT specimen is modelled as frictionless. The commercial software package ANSYS 18.2 was used to model the specimen. The CT specimen is modelled with the sizes specified in Table 3.3, with varying crack lengths and loads.

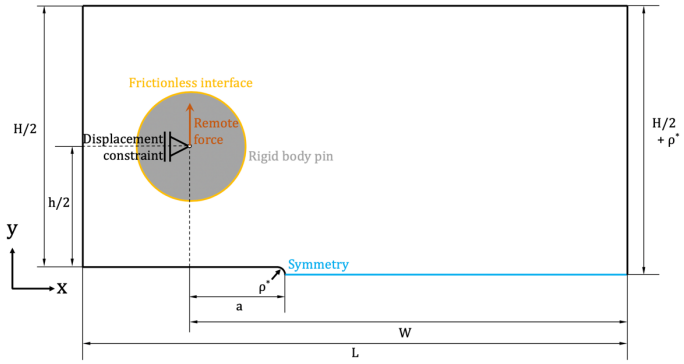

Figure 3.23 Boundary and load conditions for the modelled CT specimen in ANSYS

Plasticity

Plasticity has been accounted for using the built-in multi-linear kinematic hardening module in ANSYS 18.2 and Von-Mises yield theory. Kinematic hardening was used as it is deemed the most appropriate to describe the plasticity in steel. The Ramberg-Osgood relationship using the parameters determined by testing from De Jesus et al [10] served as input for the multi-linear kinematic hardening. In Figure 3.24 the input Ramberg-Osgood relationship and the stress-strain relationship that was found in FEA are presented.

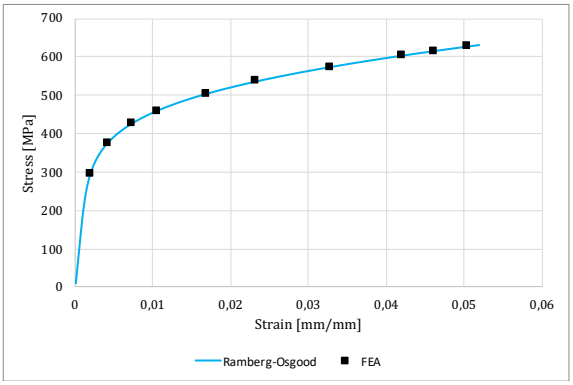

Figure 3.24 Comparison between stress-strain curves generated with Ramberg-Osgood relationship and FEA using multi-linear kinematic hardening

Mesh Convergence

Similar to De Jesus et al [10], triangular quadratic plane stress elements have been used (due to the limited thickness). The overall mesh size has been set to 1 mm and the meshing is done using an advancing front method to produce well-formed elements with less distortion. The mesh size near the crack tip is reduced using an edge sizing method that is refined to obtain convergence. 2 mm away from the crack tip on the crack plane, 0.5 mm edge sizing has been used. An overview of the mesh design is given in Figure 3.25.

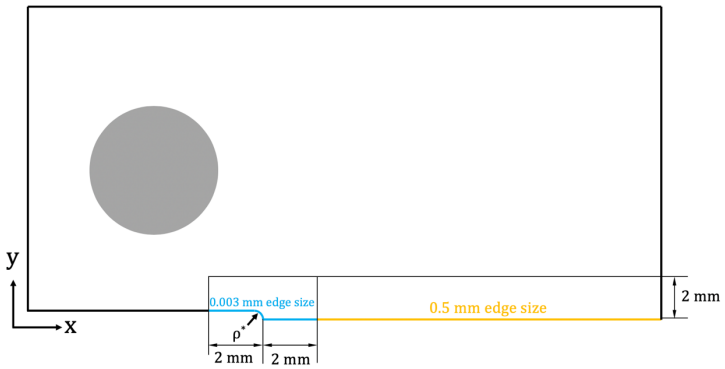

Figure 3.25 Mesh dimensioning of the CT specimen

Several mesh sizes near the crack tip were tried, starting from a mesh size equal to the elementary block size (0.03 mm) down to 0.003 mm, where convergence was found. Both for stresses in y and x direction, but also for the crack tip stress in x-direction which should be zero as this is a free surface. The results of the FEA are presented in Table 3.4. The refined mesh around the crack tip can be found in Figure 3.26 and Figure 3.27.

Element size	Maximum σ_y [MPa]	Maximum σ_x [MPa]	Crack tip σ_x [MPa]
0.03 mm	1603.7	420.8	188.3
0.01 mm	1760.1	400.9	31.6
0.005 mm	1791.8	398.7	3.3
0.003 mm	1790.4	398.2	1.7

Table 3.4 Maximum elastic stress for distinct mesh sizes (a = 8 mm, F = 1614 N)

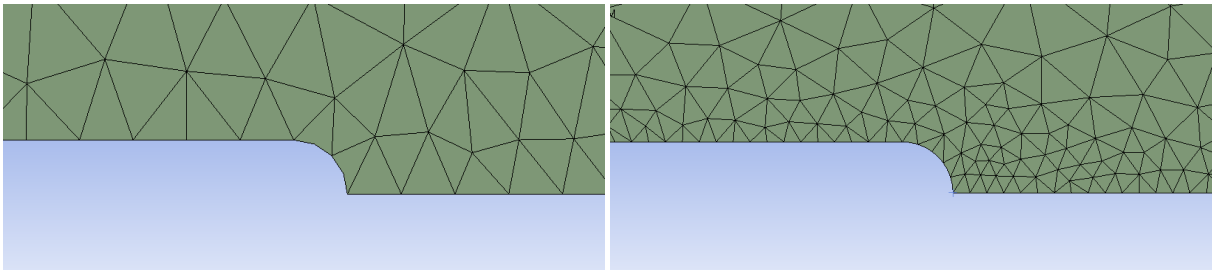

Figure 3.26 Mesh size at the crack tip for an edge size of 0.03 mm (left) and 0.01 mm (right)

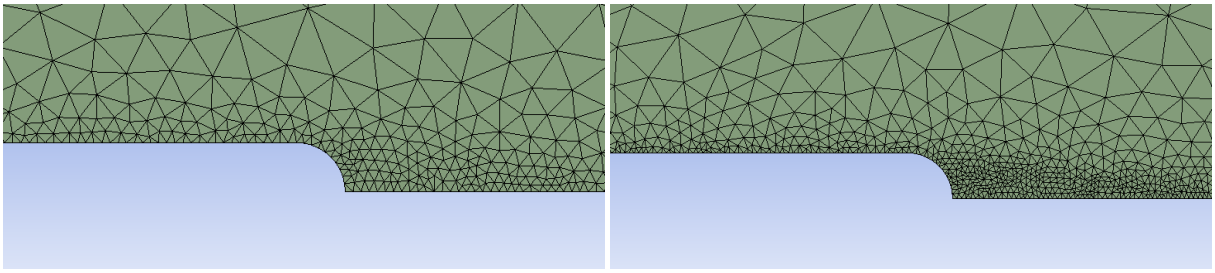

Figure 3.27 Mesh size at the crack tip for an edge size of 0.005 mm (left) and 0.003 mm (right)

3.2.3.2 Determination of ΔK_{app} vs. K_{res}

The (linear) relationship between ΔK_{app} and K_{res} has been determined by modelling the elastoplastic model of the CT specimen with various crack sizes and forces, as specified in Table 3.5. Using the Newman-Srawley equation, ΔK_{app} is determined for each of the variations.

Stress ratio	a = 8 mm	a = 14 mm	a = 20 mm
R = 0.0	F_{max} = 1614 N	F_{max} = 1614 N	F_{max} = 1614; 2000; 2500 N
R = 0.5	F_{max} = 1614 N	F_{max} = 1614 N	F_{max} = 1614; 2000; 2500 N
R = 0.7	F_{max} = 1614 N	F_{max} = 1614 N	F_{max} = 1614; 2000; 2500 N

Table 3.5 Modelled combinations of crack sizes and loads for the determination of K_{res}

From the model, the residual stress ahead of the crack tip can be determined. The model is loaded with the maximum load and then unloaded to the minimum load level. The stress at the end of the unloading step is defined as the plastic residual stress. Using both the CT weight function and the universal weight function, the plastic residual SIF can then be determined. The five data points, each representing one crack size-force combination, are then used to derive the ΔK_{app}-K_{res} relationship.

The implementation of this procedure in Python is given in Figure 3.28. The procedure is combination of the residual stress module and the weight function module presented in chapter 5.1. The procedure starts by exporting plastic residual stress data to Python, mirroring it and placing it on the r-axis. Again, only the compressive plastic residual stresses are considered in the model. Once the import is complete, a σ_{res} function is produced by linearly interpolating the stress between the data points from FEA. The same method for the determination of the plastic residual SIF as presented in chapter 5.1.3.3 is then used. At the same time, the Newman-Srawley equation is used to determine ΔK_{app}. The data will then be written to Excel, where the relationship between ΔK_{app} and K_{res} will be derived.

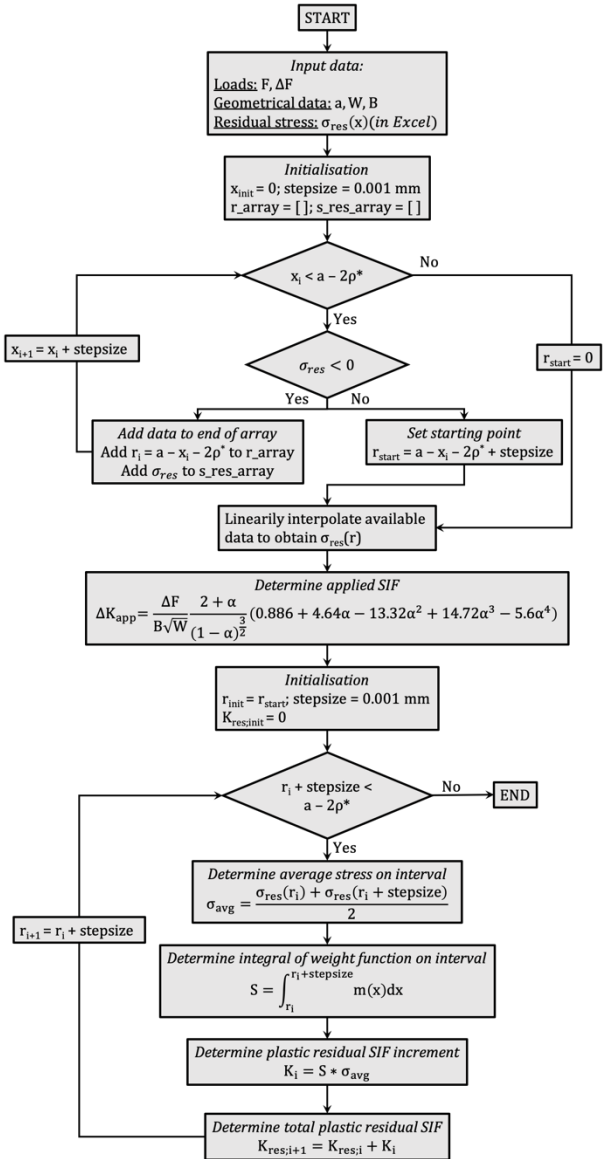

Figure 3.28 Flowchart used for the determination of the ΔK_{app}-K_{res} relation

3.2.3.3 Determination of the initiation life of the elementary block ahead of the crack tip

In previous chapter, the Smith-Watson-Topper (SWT) damage parameter has been used to determine the crack growth results. According to De Jesus et al [10], the use of the Smith-Watson-Topper damage parameter implicitly means that the influence of the mean stress is taken into account twice: once through the influence on the plastic residual stress intensity factor and once by the SWT damage parameter. De Jesus et al [10] argue that this could lead to overestimation of the stress ratio effect. They propose to use the method proposed by Morrow, given in Eq. (3.55), instead.

$$\frac{\Delta\varepsilon}{2} = \frac{\sigma_f'}{E}\left(2N_f\right)^b + \varepsilon_f'\left(2N_f\right)^c \tag{3.55}$$

Notice how here, no mean stress correction has been applied. De Jesus et al [10] argue that the number of cycles necessary to fail the elementary block ahead of the crack tip is in the Low Cycle Fatigue range (according to De Jesus et al [10] this is defined as $N_f < 5 * 10^4$). It was observed by Koh et al [23] and Lin et al [30] that in the LCF range, the mean stresses in specimens with large, constant strain amplitude tend to decrease quickly to zero mean stress. This is due to rapid cyclic stress relaxation caused by plastic strains in the specimen. This is the reason why no mean stress effect is considered in the calculations.

3.2.3.4 *Implementation of the total UniGrow method in Python*

The implementation of the numerical UniGrow method differs very slightly from the implementation of the analytical UniGrow method, as can be seen in Figure 3.29. The Stress Module and Residual Weight Function Module have been replaced by one function that determines the plastic residual SIF based on the applied SIF range. The rest of the model remains the same.

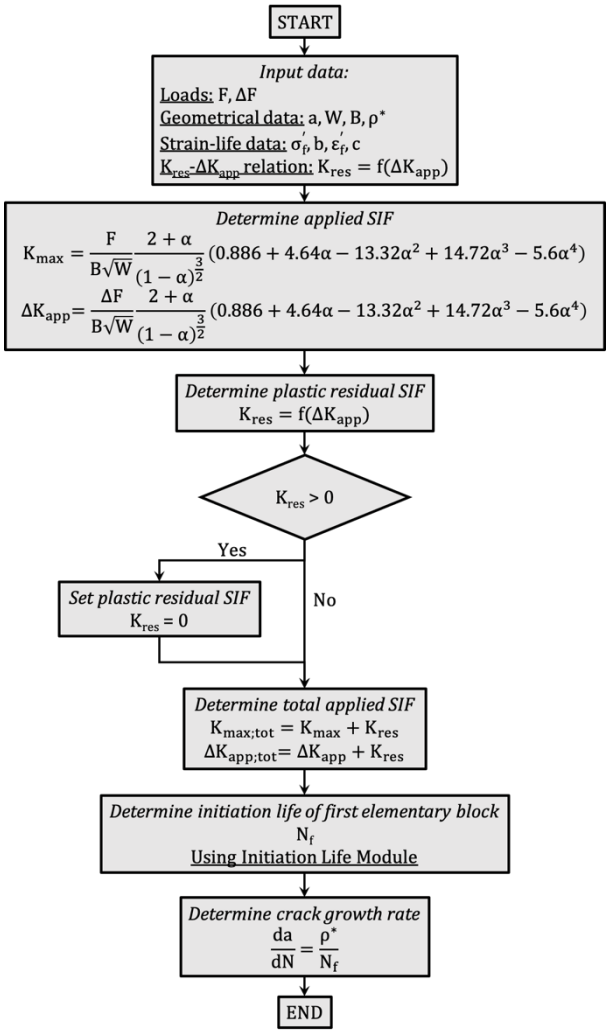

Figure 3.29 Flowchart for the numerical implementation of the UniGrow method

3.2.3.5 *Modelling input*

The crack growth rate results are generated by applying maximum force of 2000 N, the minimum force depending on the stress ratio. This is kept constant and the crack length is increased from its initial length of 8 mm using crack increments of 1 mm. For the verification of the elastoplastic stresses, the same load values have been used as De Jesus et al [10]. These are a maximum force of 1614 N and a crack length of 8 mm or 25 mm. K_{res} values have been determined at stresses and crack lengths specified in Table 3.5.

3.2.4 Results and discussion

In this section the results from the verification of the numerical UniGrow are presented and discussed. The section will start by discussing the elastic, elastoplastic and residual stresses produced by the implemented UniGrow method. This is followed by a discussion of the calculated plastic residual SIFs. The section is closed off by a discussion of the determined crack growth rates.

3.2.4.1 *Elastic results*

The first step of verifying the functioning of the FEA model is comparing the resulting elastic stresses to the Creager-Paris equations (presented in Figure 3.30) and the elastic results by De Jesus et al (presented in Figure 3.31). The elastic stress as determined by the FEA model is very similar to the Creager-Paris equations in y-direction, however a difference is found in x-direction. This difference was also found by De

Jesus et al [10], which means that it might possibly a limitation of the Creager-Paris equation. The results from the elastic FEA do match very closely with the results from De Jesus et al [10] albeit that the peak of the stresses in x-direction from FEA is slightly higher than predicted by De Jesus et al [10]. This could be due to slight difference between the two models.

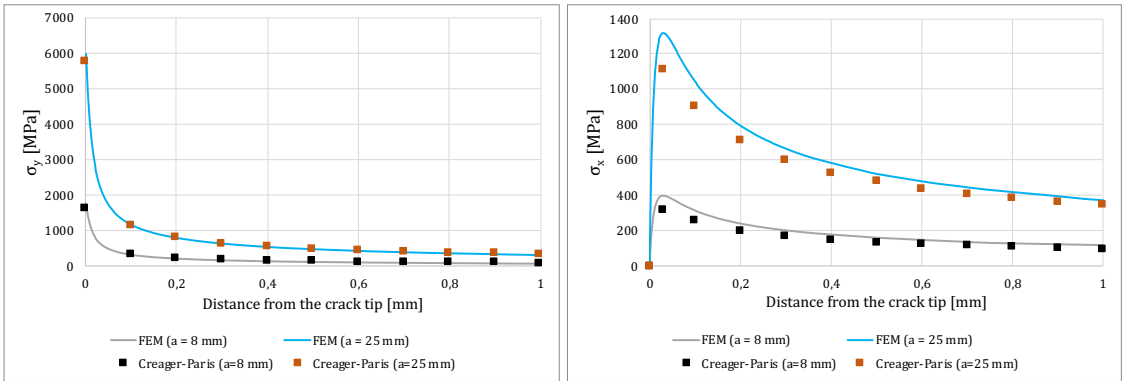

Figure 3.30 Elastic stress distribution ahead of the crack tip: comparison of Creager-Paris results to FEA (F = 1614 N)

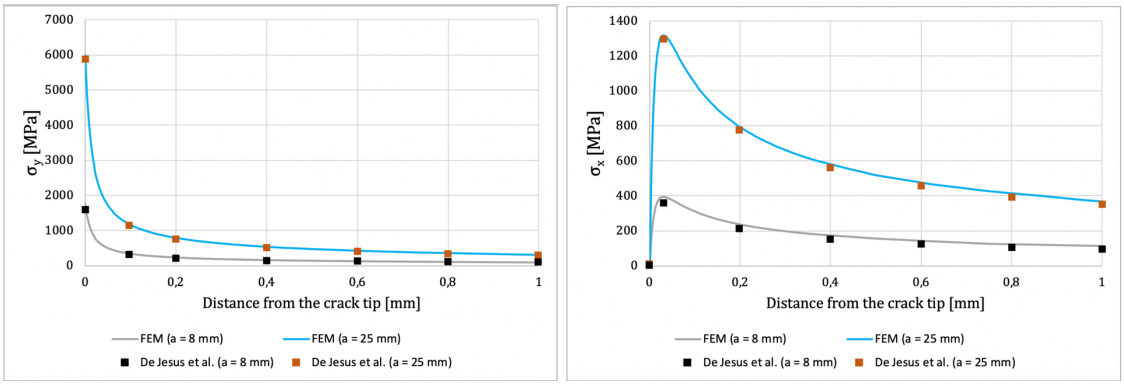

Figure 3.31 Elastic stress distribution ahead of the crack tip: comparison of Creager-Paris results and results from De Jesus et al [10] (F = 1614 N)

3.2.4.2 Elastoplastic stress results

The elastoplastic results have been calculated for a crack length of 8 mm and compared to the results by De Jesus et al [10], the results are presented in Figure 3.32. The plastic results from the FEA match the results from De Jesus et al [10] quite closely, however in x-direction the results from the FEA seems to be slightly higher compared to De Jesus et al. The same trend was also found for the elastic model. Higher stress in x-direction could possibly cause a deviation from results by De Jesus et al [10] when looking at the residual stress fields as the observed plastic strain will be higher at the maximum force. When unloading the model, this could then lead to an overestimation of the plastic residual stresses.

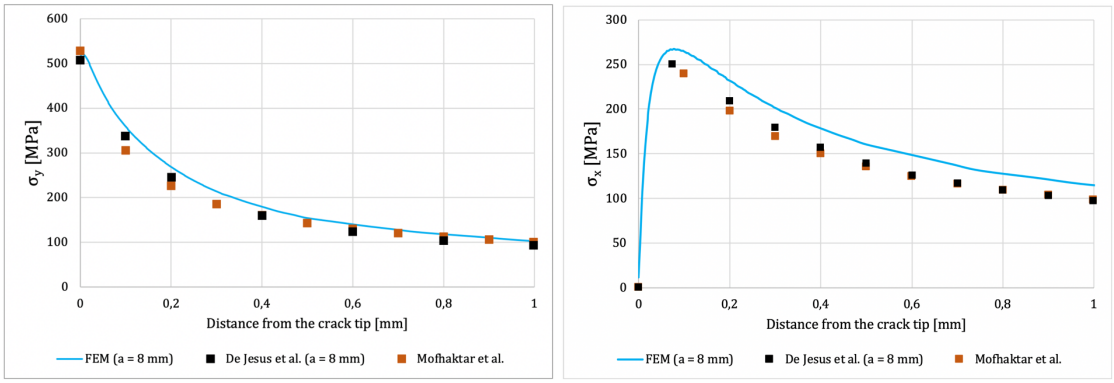

Figure 3.32 Elastoplastic stress distribution in y-direction (left) and x-direction (right) ahead of the crack tip: comparison of FEA results and results by De Jesus et al [10] (F = 1614 N)

As can be seen in Figure 3.33, the residual stresses closely match the results from De Jesus et al [10] for R = 0. The results being much better than the results from analytical UniGrow. What is especially clear, is that the residual stress doesn't asymptotically decrease to zero. Instead, the compressive residual stresses are balanced by tensile stresses. As expected, the residual stress predicted by the numerical UniGrow model is slightly too high, possibly due to aforementioned issue of the stresses in x-direction being overestimated.

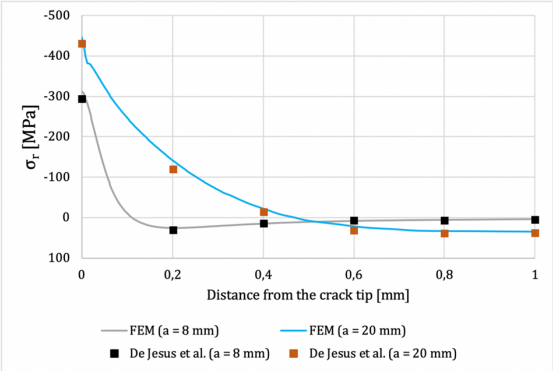

Figure 3.33 Plastic residual stress ahead of the crack tip: comparison of FEA results and results by De Jesus et al [10] (F = 1614 N)

3.2.4.3 Residual SIF results

The weight functions have been determined using both the weight function for the CT specimen and the geometrically independent (universal) weight function. The results of these calculations are given in Figure 3.34, Figure 3.35 and Figure 3.36. Generally, good correlation can be found between the results from the elastoplastic FEA and De Jesus et al [10] and very little difference can be seen between the two weight functions. Interesting is that also here, nonlinearity is observed for low values of ΔK_{app}, meaning that the assumption of linearity breaks down in this regime. Fortunately, the K_{res} values are relatively low in this region, indicating that assuming a linear relationship won't have a serious effect on the crack growth speeds.

The only difference between the two weight functions can be observed for R = 0, where the results for the CT weight function start to diverge for high ΔK_{app}. In the usage of the universal weight function, it is assumed that the integration domain (the size of the zone where compressive residual stress is found) is small. This assumption could start to break down at higher applied forces, therefore causing deviating results (as De Jesus et al [10] have also used the universal WF). By using the universal weight function, results match much better.

For R > 0, the plastic residual SIF is slightly overestimated. In terms of relative difference, this overestimation is quite large. However, the absolute difference is relatively small, and the plastic residual SIF is also relatively low compared to ΔK_{app}. It is therefore expected that this difference has little to no impact on the predicted crack growth rates. The predicted relations, however, do match the model from De Jesus et al much better than the ones predicted by the analytical UniGrow method.

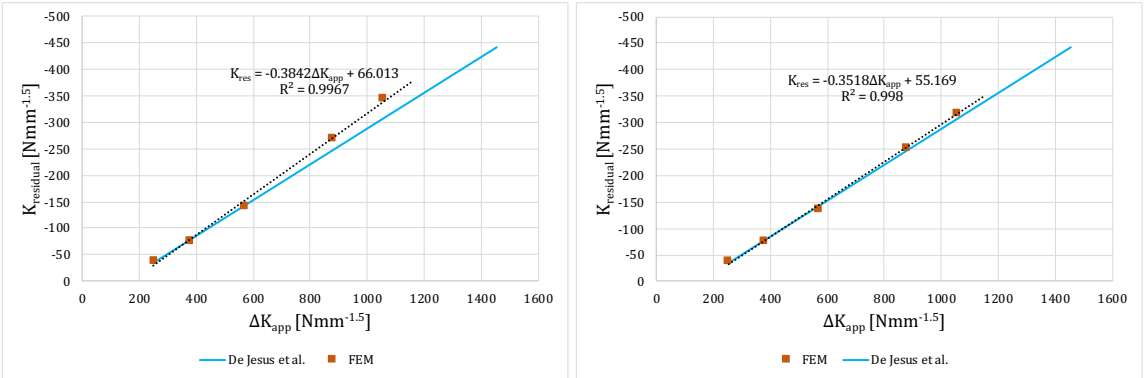

Figure 3.34 Plastic residual SIF as a function of the applied SIF range for CT WF (left) and universal WF (right) (R=0) compared to results from De Jesus et al [10]

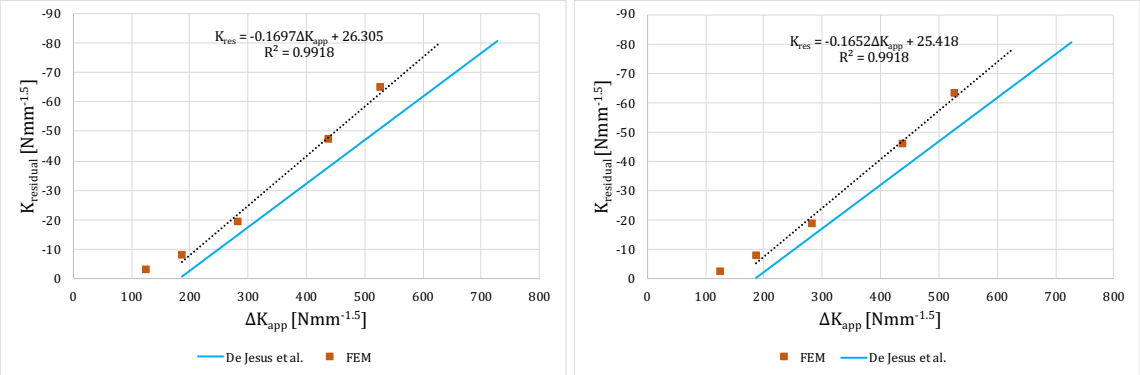

Figure 3.35 Plastic residual SIF as a function of the applied SIF range for CT WF (left) and universal WF (right) (R=0.5) compared to results from De Jesus et al [10]

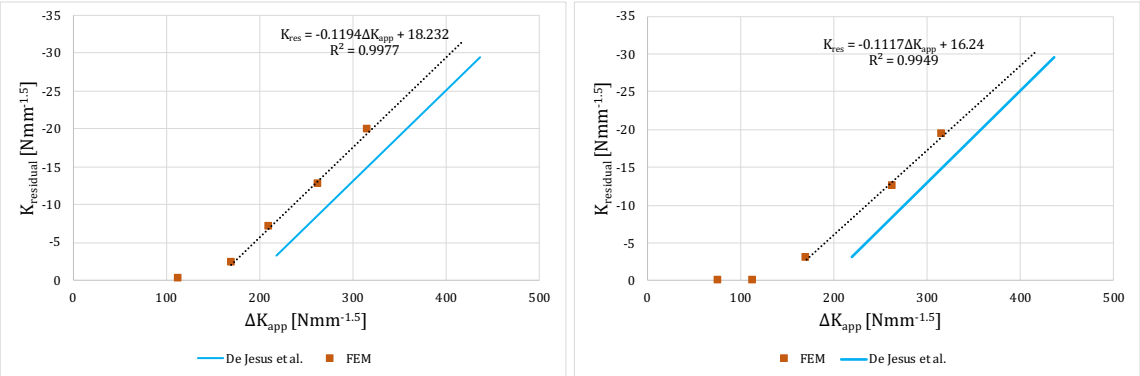

Figure 3.36 Plastic residual SIF as a function of the applied SIF range for CT WF (left) and universal WF (right) (R=0.7) compared to results from De Jesus et al [10]

3.2.4.4 Crack growth results

The crack growth as predicted by the UniGrow method was corrected. Since the weight function for the CT specimen and the universal weight function yielded similar results, solely the universal weight function has been used to determine the crack growth speed. The results of the calculations using both SWT and Morrow damage parameter are given in Figure 3.37, Figure 3.38 and Figure 3.39. Overall, very good correspondence is found between the results from the numerical UniGrow implementation and the UniGrow method by De Jesus et al [10], confirming proper implementation of the UniGrow method.

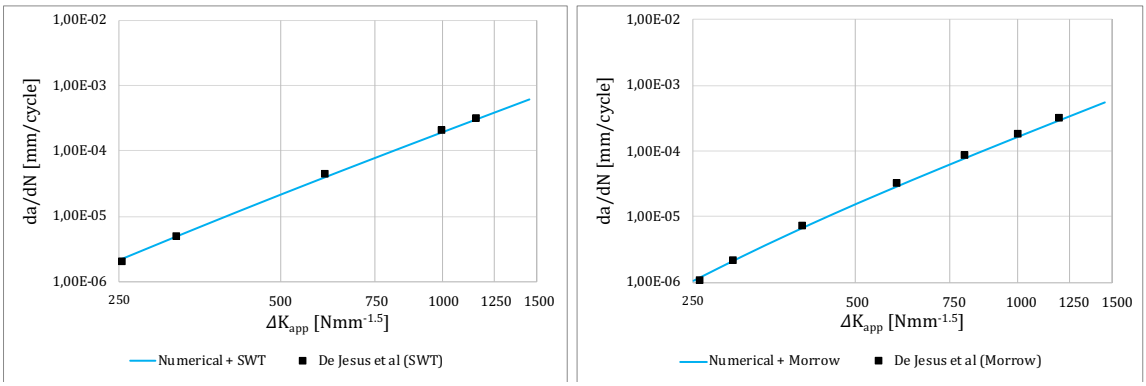

Figure 3.37 Crack growth speed as a function of the applied SIF range when using the SWT damage parameter (left) and Morrow damage (right) for R = 0 compared to the results by De Jesus et al [10]

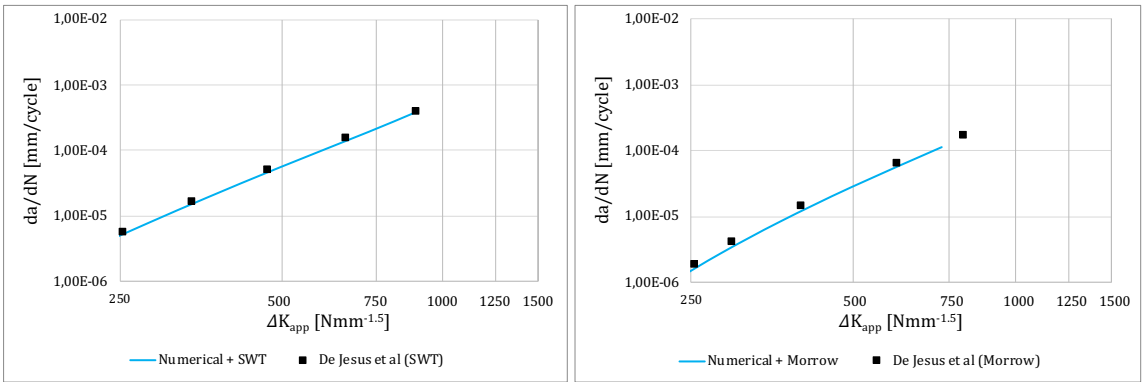

Figure 3.38 Crack growth speed as a function of the applied SIF range when using the SWT damage parameter (left) and Morrow damage (right) for R = 0.5 compared to the results by De Jesus et al [10]

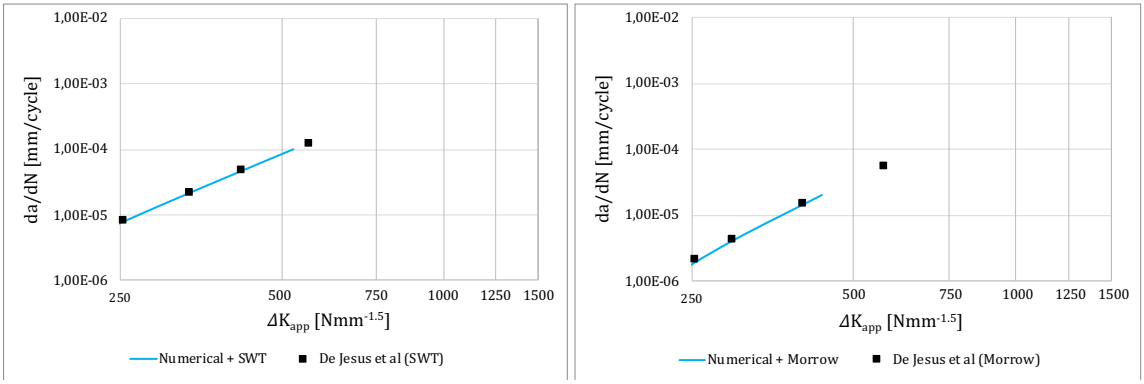

Figure 3.39 Crack growth speed as a function of the applied SIF range when using the SWT damage parameter (left) and Morrow damage (right) for R = 0.7 compared to the results by De Jesus et al [10]

3.2.4.5 Discussion

As was presented in the previous sections, the use of elastoplastic FEA yields much more physically accurate results in elastoplastic stress prediction. This yielded crack growth predictions that matched much better with the UniGrow model by De Jesus et al [10]. This, once again, confirms the need for accurate prediction of the plastic residual stress ahead of the crack tip.

In some cases, the use of analytical methods might lead to K_{res} results that are very similar to elastoplastic FEA. This was also observed in the previous sections, where crack growth speed predictions made with the analytical method, matched quite well with the numerical results. However, use of analytical functions doesn't guarantee this. When material parameters change, difference between these rather simplified analytical and more detailed numerical methods can change. It is therefore recommended to turn to elastoplastic FEA for the determination of the ΔK_{app} - K_{res} relation.

Concerning the ΔK_{app} - K_{res} results: both the CT weight function and the universal weight function yielded very similar results when using elastoplastic FEA. Usage of the universal WF in combination with elastoplastic FEA would be valid. This makes it possible to determine the relationship between ΔK_{app} and K_{res} from any geometry. For high values of ΔK_{app}, the CT weight function produced higher values of K_{res} than the universal weight function. This can be explained by the fact that the assumption of a small integration domain breaks down when the applied stress/force becomes rather large.

The current, numerical, implementation of the UniGrow method has been verified with the UniGrow method that was presented by De Jesus et al [10]. Predictions of crack growth speed and plastic residual SIF were accurate, whereas elastoplastic stresses in x-direction were overestimated to some extent. This is most likely due to slight differences in the specification of the FEA model, rather than actual differences in the implemented methods.

3.3 Validation of analytical and numerical UniGrow implementation

The UniGrow method has been previously implemented and verified. In this section, the previously implemented UniGrow method will be used to predict crack growth speeds in CT specimens made of S355 steel. This is to see how well the implemented UniGrow model performs. As a comparison of the performance of the numerical UniGrow method, the analytical model as presented in chapter 5.1 will be run as well.

Research by Carvalho et al [6] and De Jesus et al [11] will be used for the validation. They have performed crack growth tests on CT specimens made of S355 steel with very similar properties, which makes it suitable for analysis with one model. CT specimens are mainly suited for the determination of long crack growth speeds, limiting this validation to the LC region. In the next chapter, performance of the UniGrow model in the short crack region is evaluated. First the validation data will be presented, then the implemented UniGrow model is discussed and lastly the results are presented and discussed.

3.3.1 Experimental data

Experimental data has been taken from two different sources: De Jesus et al [11] and Carvalho et al [6]. Both researches have performed crack growth tests on CT specimens made of S355 steel and both have performed strain life tests on the steel used in the experiments. This makes the researches extremely useful for validation of the UniGrow method. This forthcoming section provides a summary of the performed researches and the data coming from the research.

3.3.1.1 De Jesus et al [11]

De Jesus et al [11] have done fatigue tests on CT specimens made of S355 steel. The material data is given in Table 1. The strain life parameters and the material properties were determined from 10 fatigue tests on smooth specimens under R = -1. The correlation between the fitted strain-life parameters and the experimental data was not very high for S355: $R^2 > 0.7634$ for the σ_f' and b and $R^2 = 0.8087$ for the other parameters. The correlation between the cyclic parameters K' and n' was poor for the S355 steel: $R^2 = 0.4881$. This is mainly due to the fact that no real Masing behaviour was observed in the S355 steel, which means that no clear unique cyclic stress-strain relation was observed. Furthermore, a higher-than-average ultimate stress of 732 MPa was observed.

Dimensions		Material parameters		Strain-life parameters	
$\boldsymbol{W}$	50 mm	E	210.5 GPa	σ_f'	952.2 MPa
$\boldsymbol{a_n}$	10 mm	v	0.3	b	-0.089
$\boldsymbol{B}$	8 mm	K'	595.85 MPa	ε_f'	0.7371
$\boldsymbol{L}$	62.5 mm	n'	0.0757	c	-0.664
$\boldsymbol{H}$	60 mm				
$\boldsymbol{h}$	27.5 mm				

Table 3.6 Material parameters and dimensions of the CT specimens tested by De Jesus et al [11]

The crack growth speed tests were obtained from tests on a total of nine CT specimens: two at R = 0, two at R = 0.25, two at R = 0.5 and one at R = 0.75.

3.3.1.2 Carvalho et al [6]

Carvalho et al [6] have done fatigue tests on CT specimens made of S355 steel. The strain life parameters and the material properties were determined from 13 fatigue tests on smooth specimens under R = -1. The correlation between the cyclic parameters K' and n' for the S355 steel was better than De Jesus et al found, but still poor: $R^2 = 0.6493$. The material tested by Carvalho et al [6] performs very similar as De Jesus et al in terms of strain-life and cyclic parameters, as can be seen in Figure 3.40. The curves for both properties of the material are very similar, justifying the assumption that the same material was used. No information on the ultimate strength of the material was provided by Carvalho et al [6].

Dimensions	
W	40 mm
a_n	8 mm
B	4 & 8 mm
L	50 mm
H	48 mm
h	22 mm

Table 3.7 Dimensions of the CT specimens tested by Carvalho et al [6]

The crack growth speed tests were obtained from tests on a total of eight CT specimens: four with a width of 4 mm and four with a width of 8 mm. Out of the four specimens for each width, two were tested at R = 0.01 and two at R = 0.5. The dimensions of the CT specimen are given in Table 3.7.

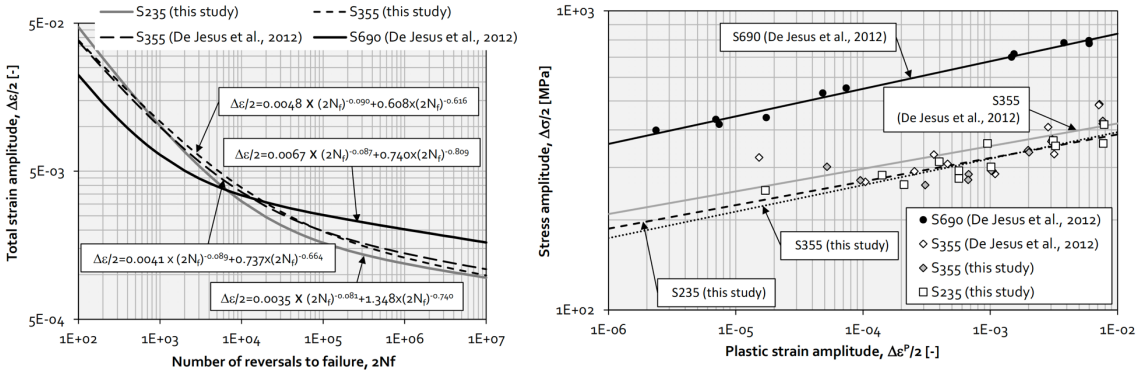

Figure 3.40 Strain life curves comparing the values measured by De Jesus et al [11] and Carvalho et al [6] for S355 steel (left) and the relationship between plastic strain amplitude and stress found by the two researchers for S355 (right) [6]

3.3.2 Global UniGrow implementation

Both the numerical and analytical UniGrow method will be implemented in this section. The global steps used in these models will be described below.

3.3.2.1 Numerical UniGrow method

In this validation step, the method as given in Figure 3.41 will be used. The method that is implemented in this section is the same method that was used for the verification of the numerical UniGrow method. In short, this entails:

1. **Determination of the applied stress intensity factor:** Will be done using the Newman-Srawley equation. This will not be further addressed in this chapter as this has been discussed before, reference is made to chapter 3.1.3.1 for background.
2. **Determination of the elastoplastic stress distribution ahead of the crack tip:** Will be done using a 2D elastoplastic FEA model of half the CT specimen. Chapter 3.3.3.1 will further address this topic.
3. **Determination of the residual stress intensity factor:** Using the residual stress from the previous step, $K_{res}$was determined using the universal weight function. To ease calculations, the relationship between K_{res} and ΔK_{app} is determined separately and used as input for the global calculation of the crack growth speed. Chapter 3.3.3.1 will further address this topic.
4. **Determination of the elastoplastic stress and strain on first elementary block ahead of the crack tip:** This will be done using the Creager-Paris equations in combination with the Neuber uniaxial plasticity correction. This will not be further addressed in this chapter as this has been discussed before, reference is made to chapter 3.1.3.4 for background.
5. **Determination of the initiation life of the first elementary block ahead of crack tip:** The initiation life was determined using the Smith-Watson-Topper damage parameter and the Morrow damage method. This will not be further addressed in this chapter as this has been discussed before, reference is made to chapter 3.1.3.5 for background.

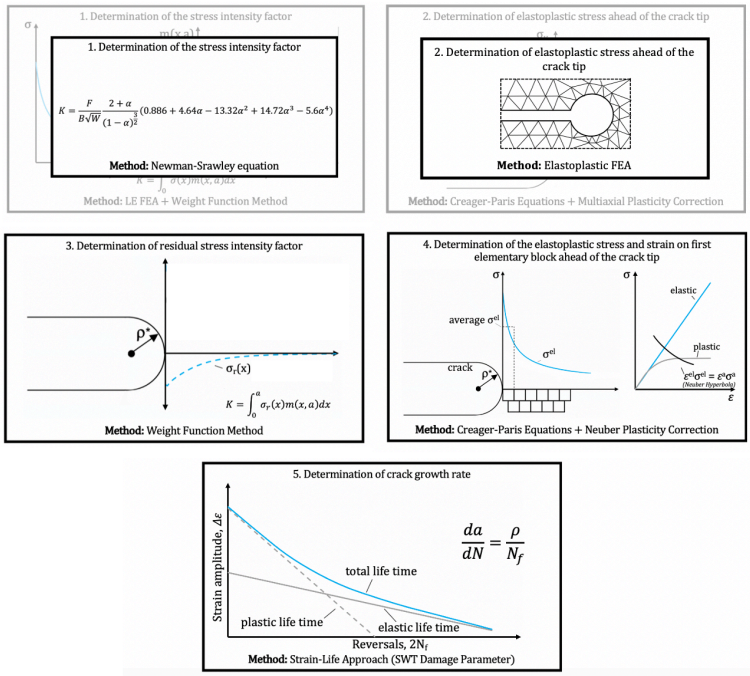

Figure 3.41 Global calculation procedure of the numerical UniGrow method used for validation

3.3.2.2 Analytical UniGrow method

The global steps of the analytical UniGrow method will be performed as follows:

1. **Determination of the applied stress intensity factor:** The applied stress intensity factor will be established using an analytical equation derived by Newman and Srawley [73]. This topic has been addressed in section 3.1.3.1.
2. **Determination of the elastoplastic stress distribution ahead of the crack tip:** The elastic stresses ahead of the stress tip will be determined using Creager-Paris equations. These will then be corrected for using analytical elastoplastic correction method. This topic has been addressed in section 3.1.3.2.
3. **Determination of the residual stress intensity factor:** Using the weight function method and the elastoplastic stresses from the previous step, the plastic residual SIF will be determined. In this case, the universal weight function will be used. This topic has been addressed in section 3.1.3.3.
4. **Determination of the elastoplastic stress and strain on first elementary block ahead of the crack tip:** This will be done using the Creager-Paris equations in combination with the Neuber uniaxial plasticity correction. This topic has been addressed in section 3.1.3.4.
5. **Determination of the initiation life of the first elementary block ahead of crack tip:** The initiation life will be determined using solely the Smith-Watson-Topper damage parameter. This topic has been addressed in section 3.1.3.5.

3.3.3 Implemented methods

Most of the implemented methods are similar to the ones used in section 3.2, therefore, solely the determination of K_{res} using elastoplastic FEA and the determination of the elementary block size will be discussed in this section. Lastly, the flowchart for the implementation in Python is given.

3.3.3.1 Determination of K_{res} using elastoplastic FEA

The modelled CT specimen is identical to the one used in the previous section; a summary of the modelled geometry is given in Figure 3.42. Half of the CT specimen is modelled due to symmetry and to save computational time. The geometry is simplified, removing the initial notch that is present in a CT specimen, since the sole interest is the effect of the crack length and the notch. The crack tip is modelled as a quarter circle. The pin that is used to load the CT specimen is modelled as a rigid body that is controlled by a remote point. The remote point is loaded by a force. The remote point is restrained in its sideways movement and angular rotation. The contact surface between the pin and the CT specimen is modelled as frictionless. The commercial software package ANSYS 18.2 was used to model the specimen. The CT specimen is modelled with the sizes specified in Table 3.6 and Table 3.7, with varying crack lengths and loads.

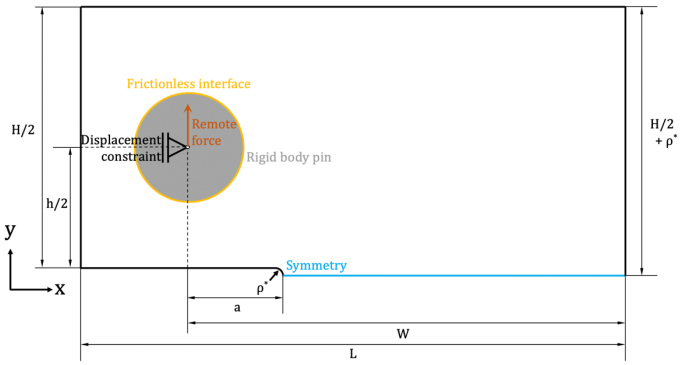

Figure 3.42 Boundary and load conditions for the modelled CT specimen in ANSYS

Plasticity

Plasticity has been accounted for using the built-in multi-linear kinematic hardening module in ANSYS 18.2 and Von-Mises yield theory. Kinematic hardening was used as it is deemed the most appropriate to describe the plasticity in steel. The Ramberg-Osgood relationship using the parameters determined by testing from De Jesus et al [10] served as input for the multi-linear kinematic hardening. In Figure 3.43 the input Ramberg-Osgood relationship and the stress-strain relationship from FEA are presented.

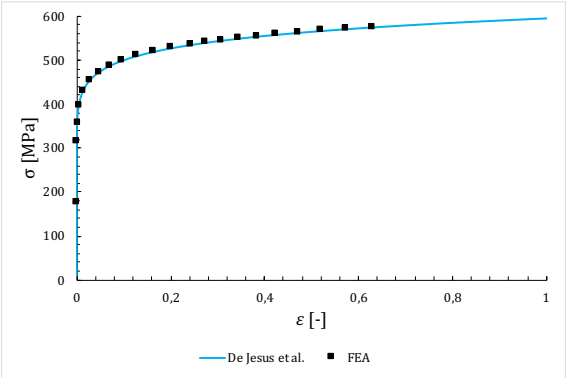

Figure 3.43 Comparison between stress-strain curves generated with Ramberg-Osgood relationship and FEA using multi-linear kinematic hardening

Mesh Convergence

Similar to the previous section, triangular quadratic plane stress elements have been used (due to the limited thickness). The overall mesh size has been set to 1 mm and the meshing is done using an advancing front method to produce well-formed elements with less distortion. The mesh size near the crack tip is reduced using an edge sizing method that is refined to obtain convergence. 2 mm away from the crack tip on the crack plane, 0.5 mm edge sizing criterion has been used. An overview of the mesh design is given in Figure 3.44.

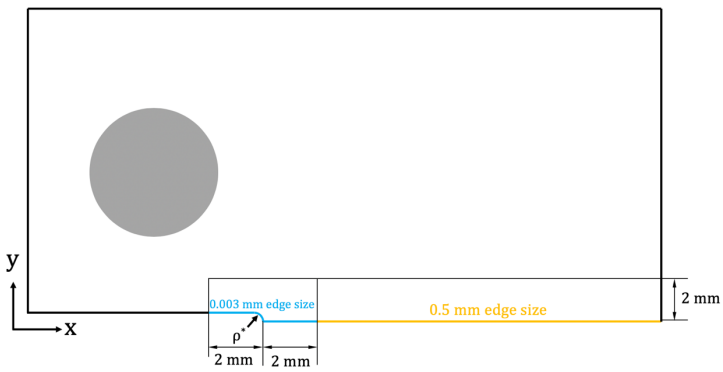

Figure 3.44 Mesh dimensioning of the CT specimen

Several mesh sizes near the crack tip were tried, starting from a mesh size of 0.01 refined to 0.0009 mm, where convergence was found. Both for stresses in y and x direction, but also for the crack tip stress in x-direction which should be zero. The results for various mesh sizes for a crack length of 10 mm and an applied force of 1000 N can be found in Table 3.8. The used elementary block size, and thus radius of the crack tip was 0.045 mm. This was found to yield the best crack growth results. The mesh around the crack tip is presented in Figure 3.45 and Figure 3.46.

Element size	Maximum $\boldsymbol{\sigma_y}$ [MPa]	Maximum $\boldsymbol{\sigma_x}$ [MPa]	Crack tip $\boldsymbol{\sigma_x}$ [MPa]
0.01 mm	471.2	103.3	1.98
0.005 mm	468.9	103.1	0.474
0.003 mm	463.5	102.7	0.212
0.0009 mm	465.7	102.7	0.02

Table 3.8 Maximum elastic stress for distinct mesh sizes (a = 10 mm, F = 1000 N)

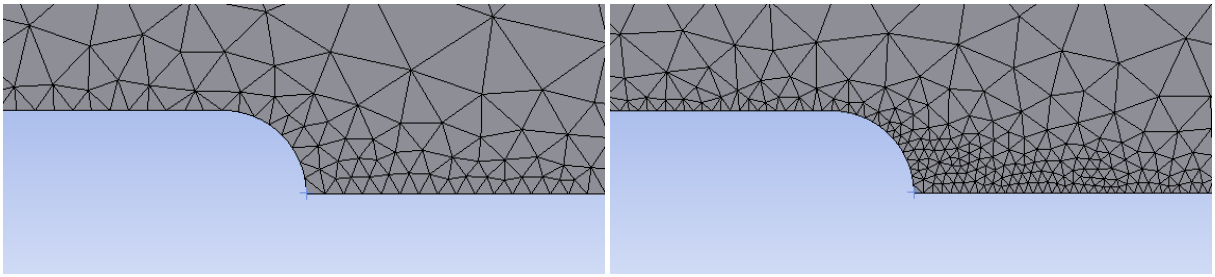

Figure 3.45 Mesh size at crack tip for an edge size of 0.01 mm (left) and 0.005 mm (right) (ρ^* = 0.045 mm)

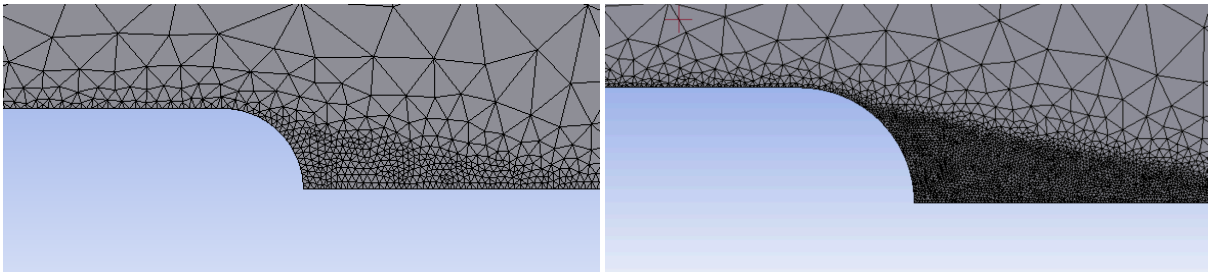

Figure 3.46 Mesh size at crack tip for an edge size of 0.003 mm (left) and 0.0009 mm (right) (ρ^* = 0.045 mm)

K_{app} *vs.* K_{res}

The (linear) relationship between ΔK_{app} and K_{res} has been determined by modelling the elastoplastic model of the CT specimen with various crack sizes and forces, as specified in Table 3.9. Using the Newman-Srawley equation, ΔK_{app} is determined for each of the variations.

Stress ratio	a = 20 mm
R = 0.0	F_{max} = 1000; 1500; 3000; 4000; 6000; 8000 N
R = 0.25	F_{max} = 1500; 3000; 4000; 6000; 8000 N
R = 0.5	F_{max} = 1500; 3000; 4000; 6000; 8000; 10000 N
R = 0.75	F_{max} = 4000; 6000; 8000; 10000; 12000 N

Table 3.9 Modelled combinations of crack sizes and loads for the determination of K_{res}

From the model, the residual stress ahead of the crack tip can be determined. The model is loaded with the maximum load and then unloaded to the minimum load level. The stress at the end of the unloading step is defined as the plastic residual stress. Using both the CT weight function and the universal weight function, the plastic residual SIF can then be determined. The five or six data points, each representing one crack size-force combination, are then used to derive the ΔK_{app} - K_{res} relationship. The implementation of this procedure in Python is given in Figure 3.28 in and for further background, reference is made to section 3.2.3.2.

3.3.3.2 Implementation of the total UniGrow method in Python

The implementation of the numerical UniGrow method is the same as used in chapter 3.2 and the analytical model that is used, is the same as implemented in chapter 3.1. The flowcharts for implementation can be found in Figure 3.10 and Figure 3.29

3.3.3.3 Determination of elementary block size

The elementary block size is a key parameter that has to be determined before the UniGrow method can be used. In this section, several methods that can be used to determine this block size are discussed.

Threshold Method

According to Noroozi et al [53], the elementary block size can be determined by using the threshold SIF ΔK_{th} and fatigue limit $\Delta\sigma_{th}$. The crack doesn't grow at the threshold SIF if the local stress at the crack tip is equal to the fatigue limit. This is given in Eq. (3.56). Since the fatigue limit is below the yield stress, elastic stress-strain analysis can be used.

$$\Delta\sigma_{th} = \frac{\Delta K_{th}\psi_{y,1}}{\sqrt{2\pi\rho^*}} \tag{3.56}$$

This can subsequently be rewritten to Eq. (3.57) to obtain the necessary elementary block size. The fatigue limit and the threshold SIF must be determined at the same stress ratio. Furthermore, care must be taken that the fatigue may not grow due to either K_{max} or ΔK being below their respective threshold values. To make sure that ΔK is governing, but to prevent plasticity, Noroozi et al [53] propose to use 0.2 < R < 0.3.

$$\rho^* = \frac{\left(\psi_{y,1}\right)^2}{2\pi}\left(\frac{\Delta K_{th}}{\Delta\sigma_{th}}\right)^2 \tag{3.57}$$

Fitting method

The other, more empirical method is the fitting method. In this method, data from crack growth tests is used to find the appropriate elementary block size. In this study, this is the preferred method since other data of the material is not available. To provide the UniGrow method with an extra challenge, the elementary block size will be fitted to the R = 0.0 case. It is then possible to see how well the UniGrow method will predict the crack growth rates for the other stress ratios.

3.3.4 Results and discussion

In this section the results from the validation of the analytical and numerical UniGrow are presented and discussed. The section will start by discussing the plastic residual stresses produced by the implemented UniGrow method. This is followed by a discussion of elementary block size. The section is closed off by a discussion of the determined crack growth rates.

3.3.4.1 Plastic Residual Stress Results

Plastic residual stresses have been determined for all stress ratios at a crack length of 20 mm and at various applied forces. This has been done using both the analytical and numerical methods. The results of the calculations are given in Figure 3.47 and Figure 3.48.

Near the crack tip, in the first 0.02 mm, the analytical and numerical UniGrow method match very well. However, the two methods start deviating from this point, the numerical method predicting higher residual stress values. This is due to the redistribution of stresses. Qualitatively, the difference between the two methods is similar as presented in section 3.1 and therefore it can be concluded that the elastoplastic FEA seems to function properly.

Integration lengths (i.e. the length of the compressive part of the plastic residual stress distribution) are very similar for both methods. Except for R = 0, where the analytical method predicts no tensile residual stress in the cross section and the plastic residual stress asymptotically decreases to zero. It is expected that, due to the slightly higher stress prediction, the plastic residual SIF of the numerical method will be slightly higher than the one predicted by the analytical method.

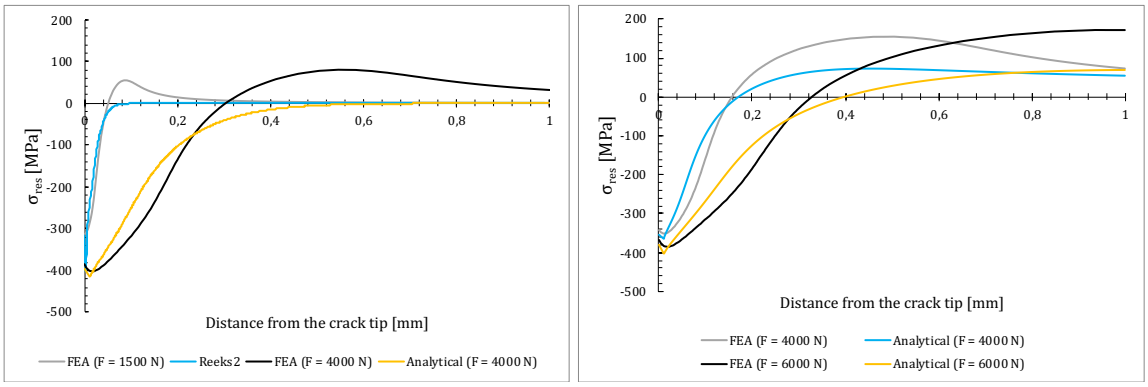

Figure 3.47 Plastic residual stress ahead of the crack tip: comparison of analytical results and FEA results for R = 0 (left) and R = 0.25 (right) (a = 20 mm)

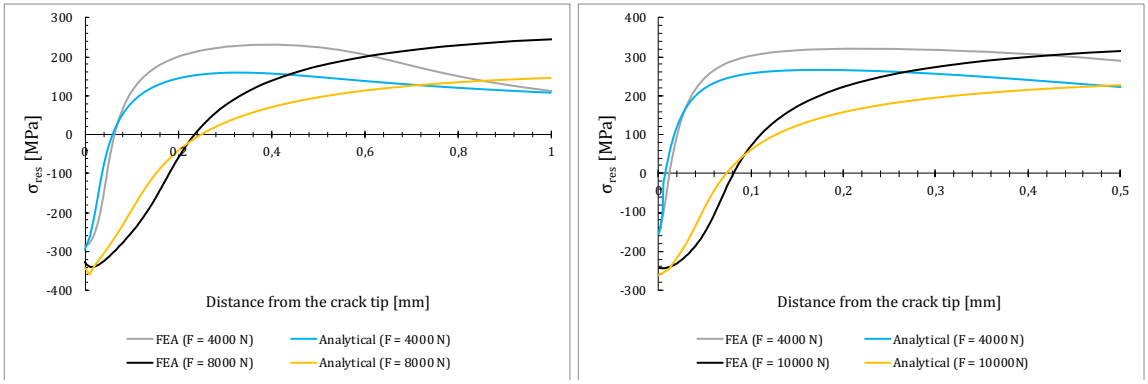

Figure 3.48 Plastic residual stress ahead of the crack tip: comparison of analytical results and FEA results for R = 0.5 (left) and R = 0.75 (right) (a = 20 mm)

3.3.4.2 Elementary Block Size

The elementary block size has been determined by fitting the crack growth curve for R = 0 to the found data. This meant that it was possible to analyse the effect of the elementary block size on two of the most important outcomes of the UniGrow method: K_{res} and the crack growth curve. The results for an elementary block size of 10, 30 and 50 µm and R = 0 and R = 0.5 can be found in Figure 3.49 and Figure 3.50.

As can be seen, a smaller elementary block size leads to higher values of the plastic residual SIF. This is most likely due to the assumption that the crack tip radius is equal to this elementary block size. Reducing the size leads to a higher stress concentration and thus more plasticity at the crack tip, which in turn causes the plastic residual stresses to increase. With increased plasticity ahead of the crack tip, one would expect the crack growth rate to be lower. However, from Figure 3.50, this seems to not be the case. The crack growth speed increases as the material block size decreases, this effect being especially present in the regions of lower ΔK_{app} or threshold region. This is because the average stress on the elementary block ahead of the crack tip increases as it gets smaller, this effect being dominant over the effect of increased plasticity.

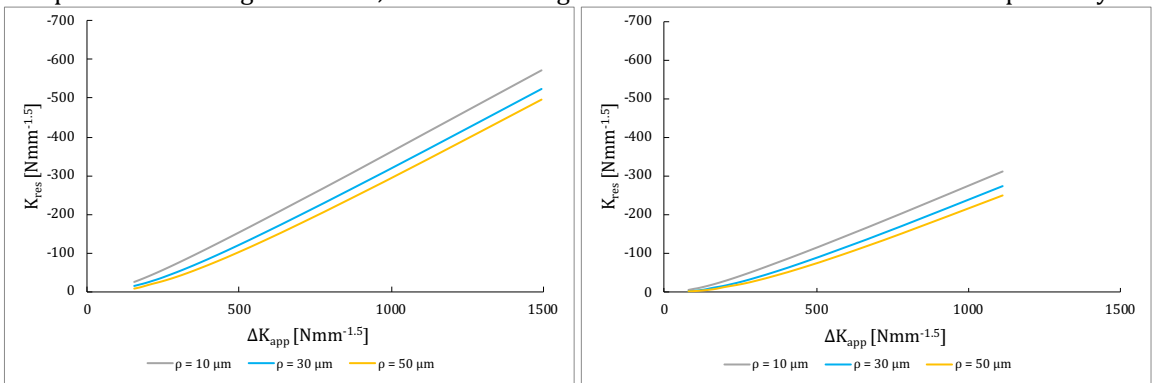

Figure 3.49 Influence of the elementary block size on the ΔK_{app}-K_{res} relation for R = 0 (left) and R = 0.5 (right)

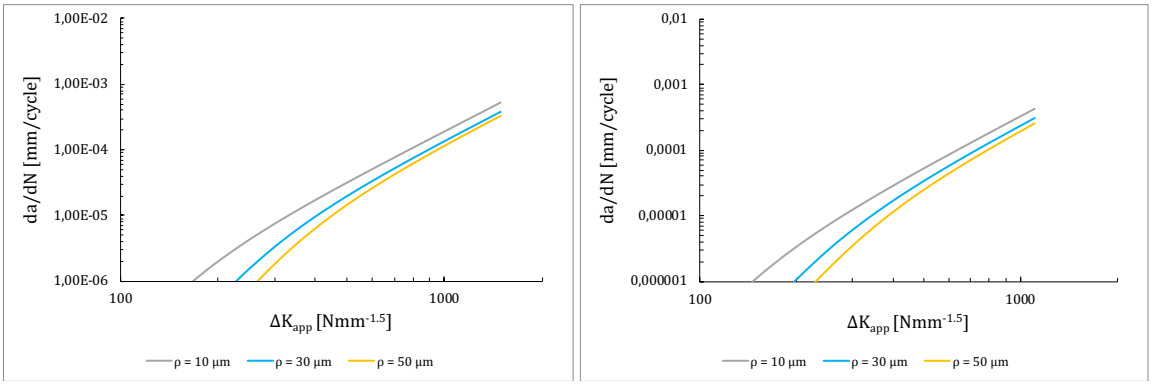

Figure 3.50 Influence of the elementary block size on the crack growth rate for R = 0 (left) and R = 0.5 (right)

The elementary block size was determined by fitting the UniGrow results for R = 0.0 to the experimental data. The found elementary block sizes is 45 μm for S355. The microstructure of the steel that was provided by De Jesus et al [11] is given in Figure 3.51. From this figure, it becomes clear that the determined elementary block size looks to be of the same order of magnitude as the grains of the material. This further strengthens the hypothesis that the elementary block size is related to the grain size of the material.

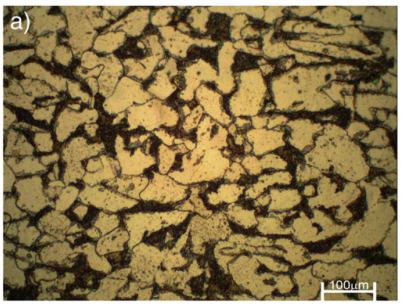

Figure 3.51 Measured grain size in the S355 material [11]

3.3.4.3 K_{res} vs. K_{app}

The weight functions have been determined using both the analytical and numerical UniGrow method. The results of these calculations are given in Figure 3.52 and Figure 3.53. The found relation between K_{res} and ΔK_{app} is linear in all cases, similar as predicted by [10], [53] and [54]. At all stress ratios except R = 0, the numerical UniGrow yields slightly higher K_{res} values than the analytical UniGrow. The difference is caused by the underestimation of the residual stress ahead of the crack tip by the analytical UniGrow. The small difference between the two methods R = 0 can be explained by the asymptotical decrease of the residual stress to zero when using the analytical method. This causes higher K_{res} values.

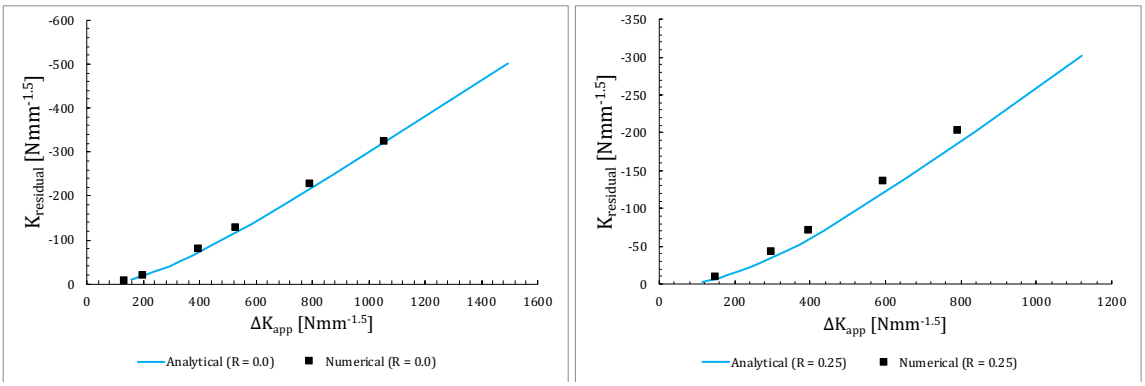

Figure 3.52 Plastic residual SIF as a function of the applied SIF range for R = 0 (left) and R = 0.25 (right)

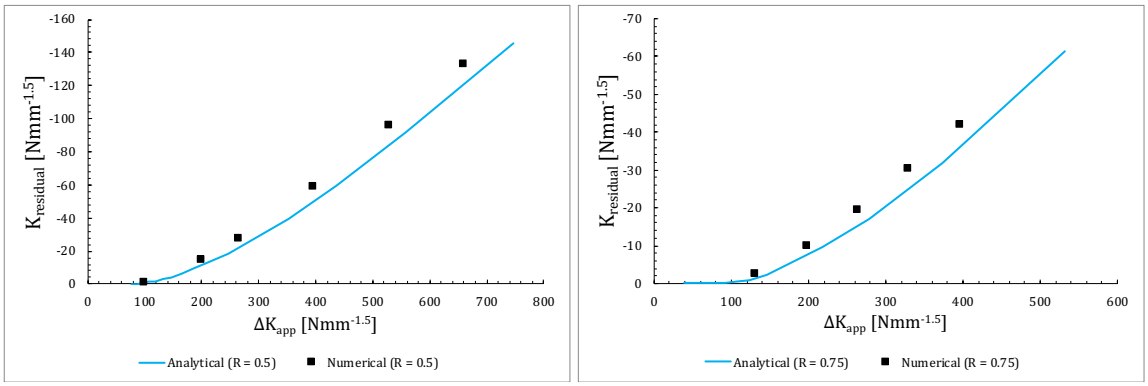

Figure 3.53 Plastic residual SIF as a function of the applied SIF range for R = 0.5 (left) and R = 0.75 (right)

In Figure 3.54 the fitted relationships for the numerical K_{res} – results are presented. All curves have high R^2 values, indicating good fit. For R = 0.5, the material still seems to experience quite significant plastic residual stresses ahead of the crack tip. This contradicts the prediction by Noroozi et al [53] who have proposed that for R ≥ 0.5, the plastic residual stresses are negligible. For 0.75, the plastic residual stresses have significantly decreased.

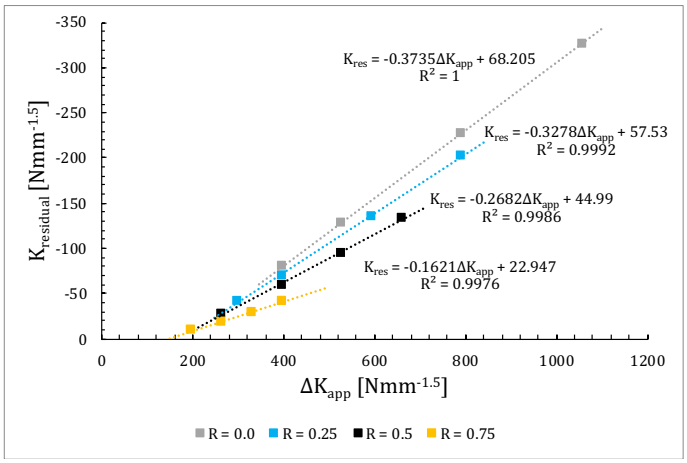

Figure 3.54 Plastic residual SIF as a function of the applied SIF range for S355 at various stress ranges

3.3.4.4 Crack Growth Results

The crack growth results using the analytical and numerical UniGrow method have been compared to the crack growth data obtained by De Jesus et al [11]. The results have been given in Figure 3.55 and Figure 3.56. Overall, the predicted crack growth rates match very well with the crack growth results. However, for R = 0.25, the crack growth rate is underestimated. Also, at higher applied SIFs, the crack growth rate seems to be underestimated slightly by the UniGrow method when compared to the experimental results.

The crack growth results using the numerical and analytical UniGrow implementation are very similar, the analytical crack growth curve being slightly higher than the numerical one. This is solely caused by the difference in estimation of plastic residual SIF by the two methods. In contrary to what was concluded in the previous chapter, this material seems to be modelled quite well by both methods. Still, it is advised to solely use the numerical method, as it provides more consistent results.

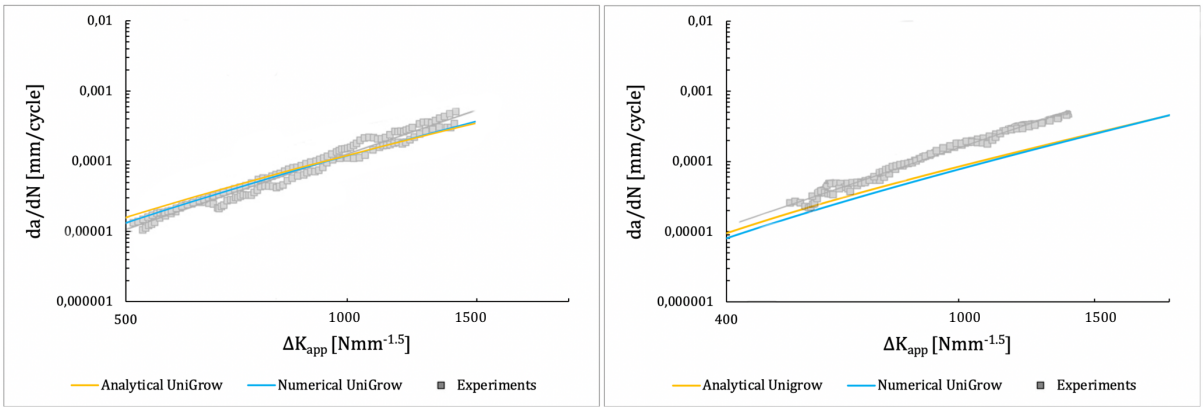

Figure 3.55 Crack growth speed predicted by the UniGrow model compared to experimental results by De Jesus et al [11] for R = 0 (left) and R = 0.25 (right)

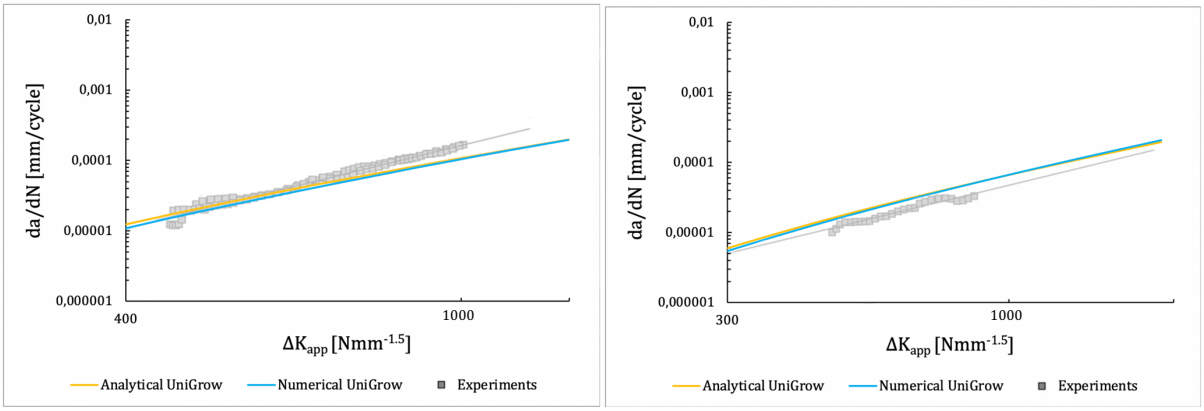

Figure 3.56 Crack growth speed predicted by the UniGrow model compared to experimental results by De Jesus et al [11] for R = 0.5 (left) and R = 0.75 (right)

Results comparing the numerical UniGrow model using the SWT damage parameter and the Morrow method to experiments from De Jesus et al [11] are given in Figure 3.57 and Figure 3.58. Results from the Morrow and SWT methods are very similar, the only significant deviation being at R = 0.75, where the UniGrow + Morrow method predicts better results than the UniGrow + SWT method. Apart from R = 0.75, no significant overestimation of the crack growth rates is observed when using the SWT parameter.

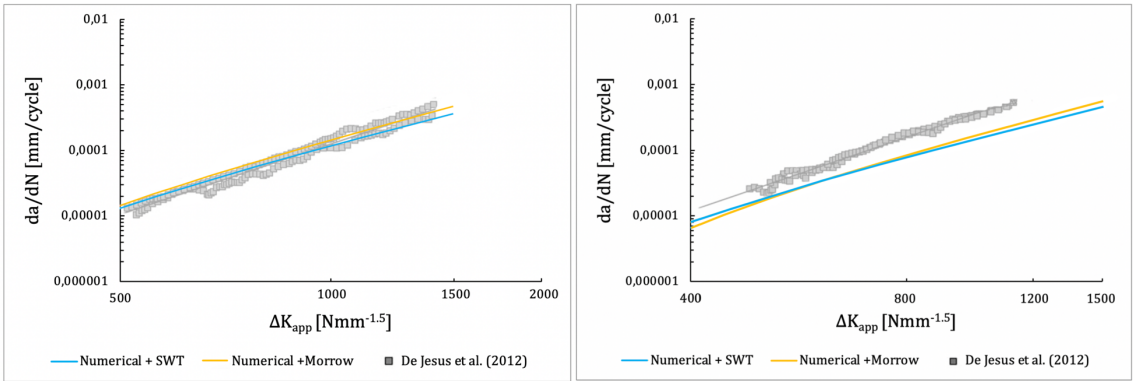

Figure 3.57 Crack growth speed predicted by the UniGrow model compared to experimental results by De Jesus et al [11] for R = 0 (left) and R = 0.25 (right)

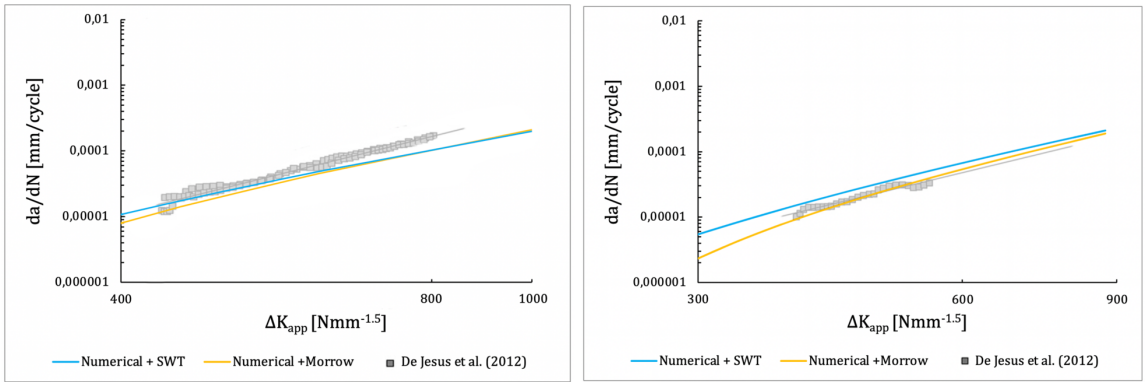

Figure 3.58 Crack growth speed predicted by the UniGrow model compared to experimental results by De Jesus et al [11] for R = 0.5 (left) and R = 0.75 (right)

For the calculated crack growth speeds in the validated ranges, it was found that for the failure of the elementary block ahead of the crack tip, N_f was always below 10^4. De Jesus et al [10] have defined the LCF range to be $N_f < 5 * 10^4$. Since all found fatigue lives are in the LCF range, rapid cyclic stress relaxation occurs and thus mean stress has a small effect on the fatigue life of the elementary block ahead of the crack tip. This justifies the use of the Morrow method without correction of mean stress.

Carvalho et al [6] have tested CT specimens made of different widths. The crack growth rate predictions together with the experimental results have been presented in Figure 3.60, solely the numerical results are provided. The results for R = 0.01 at high ΔK_{app} are slightly underestimated by the UniGrow model. However, here better results are obtained when the UniGrow + Morrow method has been used. The same effect can be observed for the R = 0 results from De Jesus et al [11] in Figure 3.57.

Crack growth predictions for R = 0.5 results match very well with the experimental results for specimens of 4 and 8 mm thickness. Furthermore, both the UniGrow + Morrow and UniGrow + SWT method seem to provide crack growth predictions that match the experimental results. Neither of the two performing significantly better than the other.

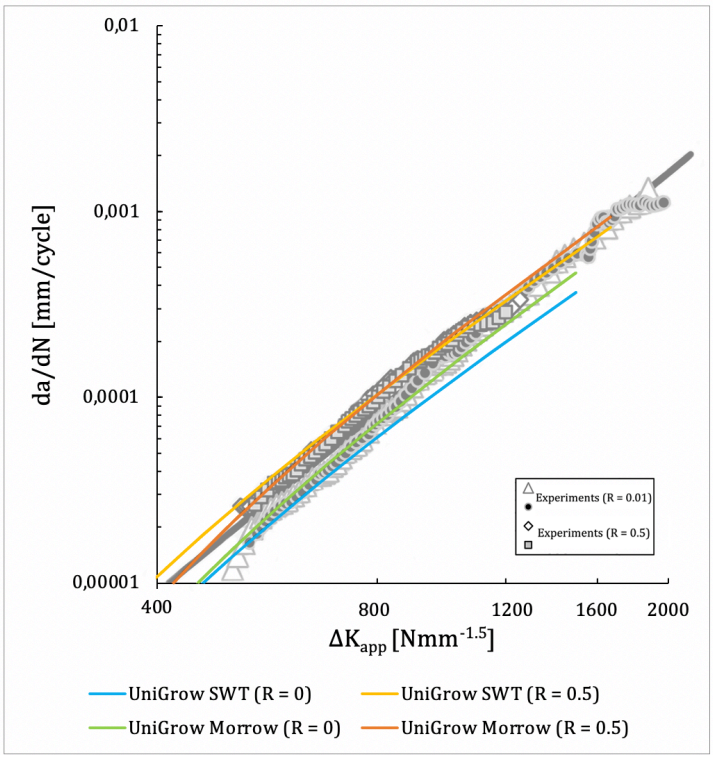

Figure 3.59 Crack growth speed as a function of the applied SIF range compared to experimental results by Carvalho et al [6] for B = 4 mm

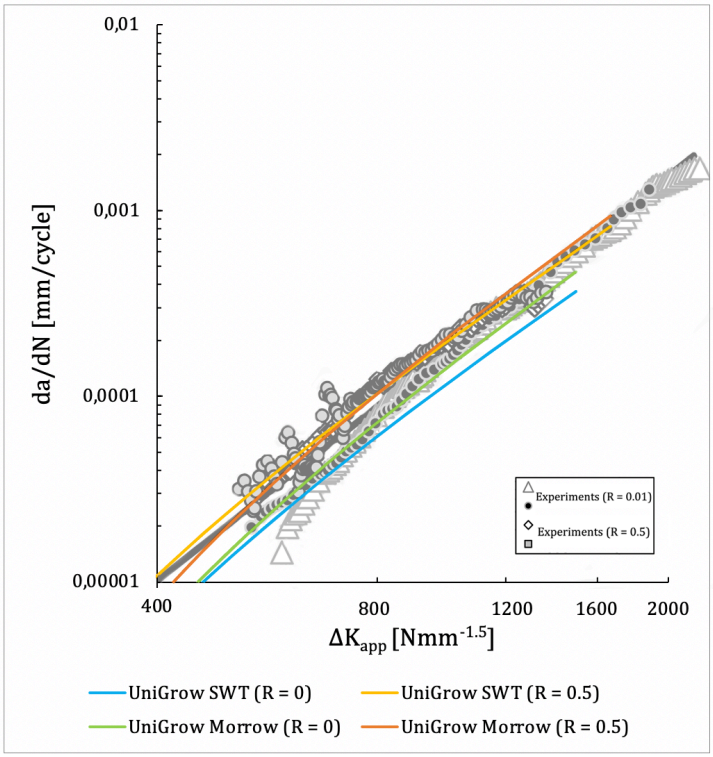

Figure 3.60 Crack growth speed as a function of the applied SIF range compared to experimental results by Carvalho et al [6] for B = 8 mm

3.3.4.5 Discussion

The results presented in the previous section show good correspondence between the UniGrow method and the experimental results by Carvalho et al [6] and De Jesus et al [11]. Matching results weren't only observed for the R = 0, which was used to determine the elementary block size, but also for other stress ratios. This is a good indication that the UniGrow model is able to predict the crack growth rates in mild steel CT specimens subject to Mode I crack growth.

Analytical UniGrow implementation

Even though some discrepancy has been found in the values of the plastic residual SIF, the analytical and numerical UniGrow method predict very similar crack growth speeds. However, the methods for determination of the elastoplastic stresses remains physically inaccurate and thus should be used with care. It is therefore recommended to solely use the analytical method to obtain an approximate value for the elementary block size. After an estimate has been found, the numerical UniGrow method can be used to obtain the exact residual stresses ahead of the crack tip. This prevents having to repeatedly do extensive elastoplastic FEA for different elementary block sizes.

Morrow vs. SWT

De Jesus et al [10] proposed to use the Morrow method instead of the SWT damage parameter to determine the fatigue life of the elementary block ahead of the crack tip. In section 3.3.4 it has been shown that both damage methods seem to perform equally well and predict a similar effect of the stress ratio on the crack growth speed. Except for R = 0.75, where usage of the Morrow method resulted in a significantly better determination of the crack growth speed.

These results contradict those found by De Jesus et al [10] where it was found that the Morrow method was better at accounting for the stress ratio effect than the SWT damage parameter. To investigate what might cause this difference, the fatigue lives of the elementary block ahead of the crack tip of P335NL1 and S355 were calculated. The materials were loaded with the same nominal stress ratio, elastoplastic stress and strain amplitude. The resulting strain-life curves for R = 0 and R = 0.5 have been displayed in Figure 3.61. The range applicable to crack growth ($N_f < 5 * 10^4$) is especially of interest. In Figure 3.62, the crack growth rate as a function of the applied SIF range for R = 0, R = 0.5 and R = 0.75 is given for both steels.

In Figure 3.61, it can be seen that for R = 0, Morrow and SWT results match quite closely for both S355 and P355NL1 steel. This effect can then also be observed in the calculated crack growth rates for R = 0 in Figure 3.62: for this stress ratio the SWT and Morrow method produce very similar results. For the P355NL1 steel, a larger discrepancy is observed in the strain life curve using SWT and Morrow at a stress ratio of R = 0.5. This then also results in large differences in the predict crack growth rate. For the S355, this is not the case and therefore crack growth rates match much better.

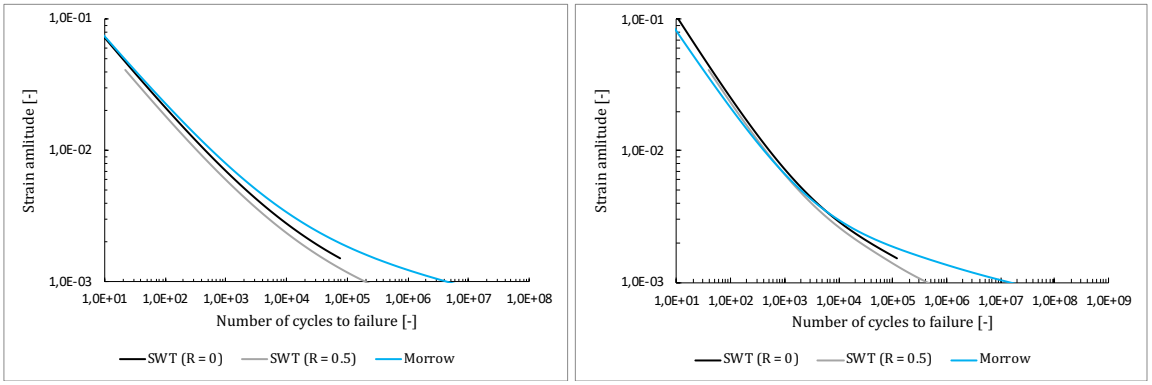

Figure 3.61 Number of cycles to failure as function of the applied strain amplitude for P355NL1 steel [10] (left) and S355 steel [11] (right)

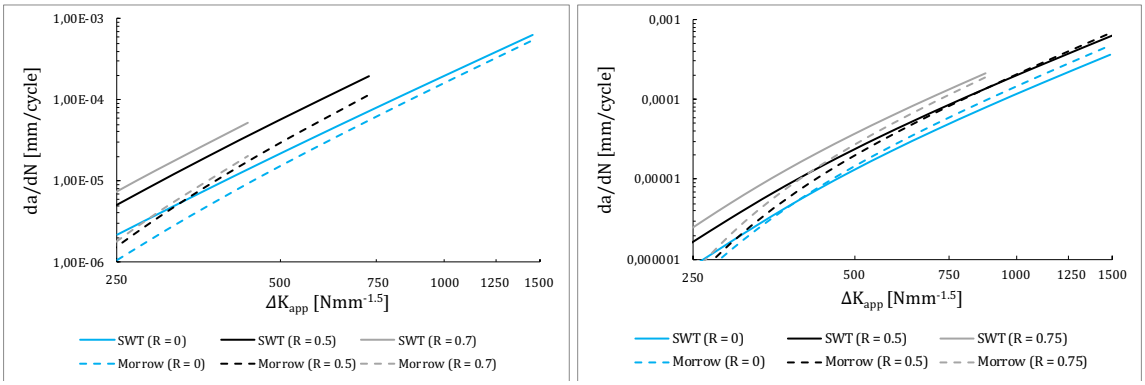

Figure 3.62 Crack growth rate as a function of the applied SIF range for P355NL1 steel [10] (left) and S355 steel [11] (right)

The root cause of the difference between the results by De Jesus et al [10] and the results of this study can thus be related to the fit between the SWT and Morrow strain life curves in the LCF range. This seems to be dependent on the material properties. However, as the Morrow approach has shown good results for both S355 and P355NL1 steel and its use is physically grounded, it seems to be the preferred approach for determining the crack growth rates. The applicability of the SWT method has to be determined on a case-by-case basis.

However, the validity of the application of the Morrow method without mean stress correction for applied SIF ranges in the HCF range is questionable. It was noted by Koh et al [23] and Lin et al [30] that in specimens subjected to strain ranges where no plasticity was observed, cyclic stress relaxation did not occur. In these specimens, significant influence of the mean stress on the fatigue life was found. Figure 3.61 seems to support these observations: for $N_f > 5 * 10^4$, deviation between SWT and Morrow method starts to occur.

Based on these considerations, it is recommended to only use the Morrow method when the number of cycles required to fail the elementary block ahead of the crack tip is in the LCF range. A limit of this range could be $N_f < 5 * 10^4$ as defined by De Jesus et al [10]. In practice this will come down to only using the Morrow method to predict crack propagation rates and thus makes it inapplicable for the crack initiation phase.

4 Total Fatigue Life

In the previous chapter, it has been shown that the UniGrow method is able to provide satisfactory predictions of crack growth speed in the long crack regime for different stress ratios. The fatigue life of steel specimens, however, also consists of short crack growth and the UniGrow model thus requires further validation before it can be used to predict fatigue lives. Validation of the UniGrow method for short crack growth is rarely discussed in literature. Instead, research often focusses on validating crack growth speeds of LC. Therefore, it needs to be made sure that the model also provides accurate SC growth rate predictions. Several studies have been done where the UniGrow method has been used to predict the fatigue life of specimens. The results from these studies form the basis for this chapter.

Additionally, the performance of the UniGrow as total fatigue model will be compared to the Two-Stage-Model, another total fatigue model first proposed by Röscher et al [64]. In this research, the fatigue life of different butt weld geometries was determined using the Two-Stage-Model, accounting solely for the geometry effect and neglecting the weld residual stresses. It is interesting to see how the UniGrow model performs compared to the Two-Stage-Model in the prediction of the fatigue lives of these butt-welded geometries. This will provide further insight into the performance of the UniGrow model as a total fatigue life model.

First, literature on fatigue life calculations using UniGrow will be discussed. Subsequently, the Two-Stage-Model and the data from the research by Röscher et al [64] will be discussed. Then the implementation of the UniGrow model that will be used for this part of the research will be described and lastly, the results will be presented and discussed.

4.1 Literature on fatigue life calculations using UniGrow

Whereas much of the literature on the UniGrow method focusses on validating crack growth rates with experimental results, some research has been done where the fatigue life of specimens is calculated. An overview and discussion of the literature that has used the UniGrow method to determine the fatigue life of Mode I cracks and their conclusions will be given in this section.

4.1.1 Mikheevskiy et al [35] (2012)

The first research attempting to use the UniGrow method to predict the fatigue life of a detail, in contrary to previous research that focused solely crack growth speeds, was done by Mikheevskiy et al [35] in 2012. The UniGrow model was used to predict the fatigue crack growth of a corner crack in an attachment lug made of Al 7050-T7451 loaded with a variable load. Two different spectra of variable load were applied. The crack introduced into the specimen was a corner crack with dimensions of 1 mm in both directions. The crack slowly transitioned into a through-thickness edge crack. An overview of the detail that was modelled is given in Figure 4.1.

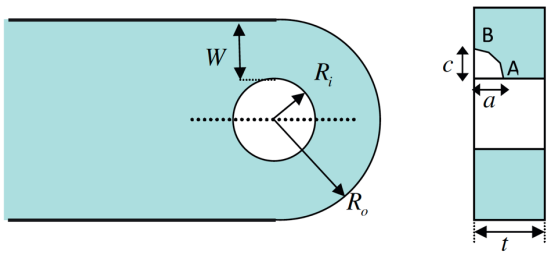

Figure 4.1 Attachment lug geometry with initial corner crack (W = 22 mm, R_i = 13 mm, R_o = 35 mm and t = 20 mm) [35]

The UniGrow model was first calibrated so that good crack growth results were obtained for different stress ratios. After this, the crack growth in the model using variable amplitude loading was modelled. The resulting crack growth curve, compared to experimental results, can be seen in Figure 4.2. The curve generated with the UniGrow model matches the experimental curve very well, especially in the early stages of fatigue crack growth. The main benefit of using the UniGrow model over a Paris Law-based method is that the different stress ratios and over and under loading can be accounted for by the same model. This is impossible when using LEFM. Unfortunately, this usage of the model only validates the crack growth prediction in the crack propagation stage, as the initial crack size was 1 mm.

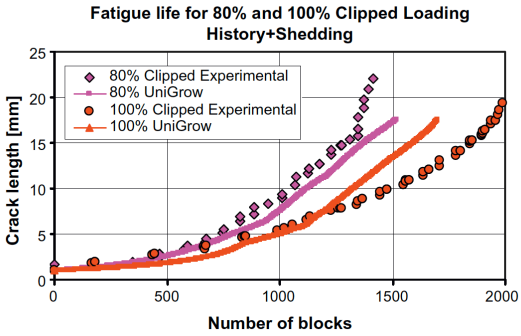

Figure 4.2 Fatigue growth prediction and experimental data for the two applied variable loading [35]

4.1.2 Mikheevskiy et al [36] (2015)

In 2015, Mikheevskiy et al [36], predicted the total fatigue life of a welded t-connection made of A36 (mild/low carbon) steel. The geometry that was used in experiments can be seen in Figure 4.3. As welding has been performed on the specimen, weld residual stresses will be present inside the structure. These were measured using x-ray diffraction technique. Both measured residual stress and a modified, assumed residual stress distribution were used in the determination of the fatigue life. The applied SIF has been calculated using the weight function method and the elastic stress in the critical cross section taken from FEA. Total fatigue life was determined assuming an initial semi-circular crack with a size equal to the elementary block size ρ^*.

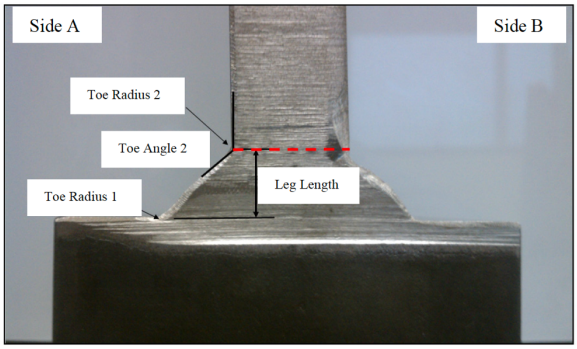

Figure 4.3 Geometry of welded specimen made of A36 steel [36]

Weld residual stresses were included by means superposition of the weld residual SIF on the applied SIF. The weld residual SIF was calculated by means of the weight function method and the given weld residual stress distributions. Very few experimental results were performed: six at R = 0.1, two at R = 0.3 and four at R = 0.5. For all the stress ratios, the experiments were done at two stress ranges. The S-N curves generated by the UniGrow calculations and the fatigue life results from experiments are given in Figure 4.4. Correspondence between UniGrow results and experiments is quite good for all stress ratios. Some difference was found between using the simplified and measures residual stresses, but both were more accurate then when no residual stress was used.

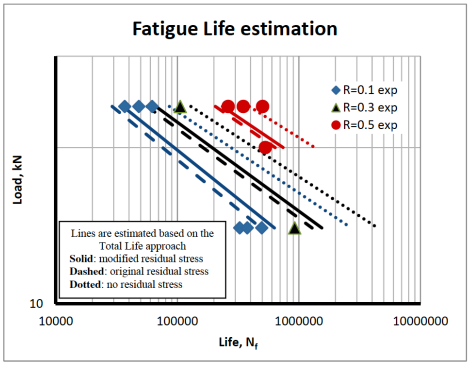

Figure 4.4 Fatigue life predicted by the UniGrow method and the experimental data [36]

4.1.3 Bogdanov et al [3] (2015)

In 2015, Bogdanov et al [3] predicted the fatigue life of a misaligned, welded cruciform joint made of 15G2ANb (low-alloy steel). A schematization of the geometry has been given in Figure 4.5. It has not been discussed by the authors whether weld residual stresses have been taken into account. The applied SIF has been calculated using the weight function method and the elastic stress in the critical cross section taken from FEA. Total fatigue life was determined assuming an initial semi-circular crack with a size equal to the elementary block size ρ^*.

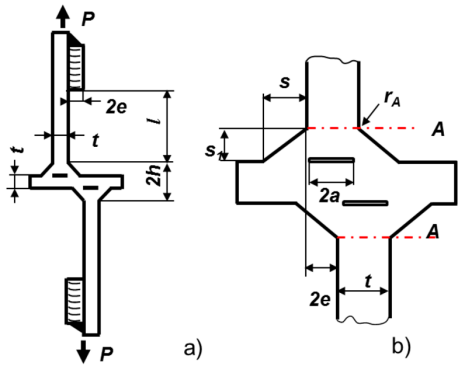

Figure 4.5 Geometry of the misaligned cruciform joint (t = 8 mm) [3]

This was also the first paper to account for effects of the crack being short. It has been proposed by Bogdanov et al [3] to correct the applied SIF for short cracks. This is method is loosely based on the Unified Approach. When a crack is short, the Creager-Paris equations predict stresses that are too low and start to deviate from the values for an elliptical notch. The correction will be done based on correcting the SIF so that the Creager-Paris equations (Eq. (4.1)) predict the same maximum stress values as for an elliptical notch (Eq. (4.2)).

$$\sigma_{CP} = \frac{2K}{\sqrt{\pi\rho^*}} = \frac{2S\sqrt{\pi a}}{\sqrt{\pi\rho^*}} \tag{4.1}$$

$$\sigma_{ellipse} = S\left(1 + 2\sqrt{\frac{a}{\rho^*}}\right) \tag{4.2}$$

The ratio between these two stresses is given in Eq. (4.3). It is suggested by Bogdanov et al [3] to increase the applied SIF with this factor.

$$\frac{\sigma_{ellipse}}{\sigma_{CP}} = 1 + \frac{1}{2}\sqrt{\frac{\rho^*}{a}} \tag{4.3}$$

Again, many similarities with the Unified Approach, as discussed in section 2.4.4. can be seen. Both methods propose the augmentation of the applied SIF with a factor that decreases as the crack grows longer. However, the UniGrow method does this by multiplying the values with a factor, whereas the Unified Approach adds a value to K_{max} and K_{min}. This increases the local stress ratio and with this, the crack growth speed.

Seven fatigue life tests have been performed at a constant amplitude range of quite low nominal stress $\sigma < 80MPa$. However, since the SCF of the welded detail is quite high (SCF ≈ 12), the stress at the crack is high and therefore fatigue lives are short and are spent mainly in the crack propagation phase. The S-N curve generated by the UniGrow calculations and the fatigue life results from experiments are given in Figure 4.6. There seems to be an excellent fit between UniGrow and the experimental results.

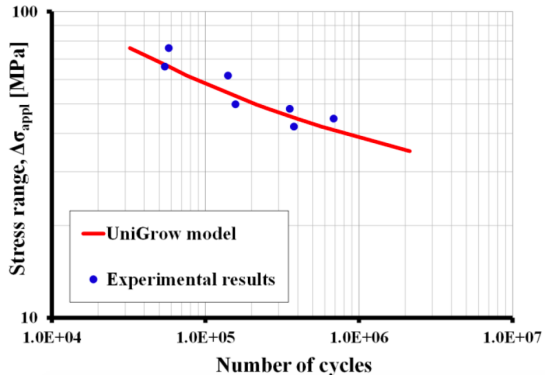

Figure 4.6 Results from fatigue model compared to experimental data [3]

4.1.4 Bang et al [1] (2018)

In 2018, Bang et al [1] predicted the fatigue life of 2024-T3 aluminium, 7075-T561 aluminium and Ti-6Al-4V titanium alloys. Fatigue tests from literature were used to assess the performance of the UniGrow model. These tests were done using smooth specimens, Single-Edge Notched Tension (SENT) specimens and Double-Edge Notched Tension (DENT) for 2024-T3 aluminium, 7075-T561 aluminium and Ti-6Al-4V titanium alloys respectively. A schematization of the geometries has been given in Figure 4.7. It has not been stated by Bang et al [1] which method has been used for the determination of the applied SIF.

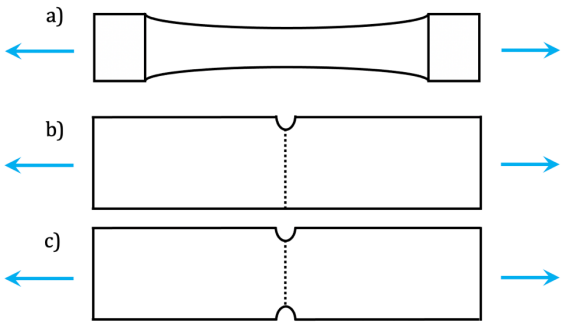

Figure 4.7 Typical geometry of a smooth specimen (a), SENT specimen (b) and DENT specimen (c)

In the literature from which the experimental data was taken, fatigue calculations have also been done and thus initial crack sizes were proposed. These initial sizes have also been used by Bang et al [1] in the determination of the fatigue life of the specimens. For the 7075-T561 Al alloy, the initial crack sizes were based on the initial flaws often detected in the structure [48]. The initial crack sizes for the other two alloys were based trial-and-error fitting [46], [45].

Additionally, Bang et al [1] proposed criteria for the UniGrow method for distinguishing between long and short crack growth. Three parameters were used as threshold parameters, if the crack at any point has values lower than the threshold values, the crack is considered to be a short crack. The three threshold criteria are:

- **Threshold crack size (a_{cr}):** The threshold crack size is the size where the physically short crack transitions to a physically long crack. This is usually assumed to be somewhere between 0.5 – 1 mm [37], where Bang et al [1] use 0.5 mm.
- **Threshold SIF (ΔK_{cr}):** Differs per material and stress-ratio and is related to the cut-off limit used in the Paris-Law.
- **Threshold crack growth (da/dN_{cr}):** Bang et al [1] have not clearly defined this parameter. However, it is expected that this is the crack growth rate at the threshold SIF.

Bang et al [1] investigated the use of using the short crack correction factor introduced by Bogdanov et al [1]. Also, a method based on using short crack growth data was used. This consists of making two separate UniGrow models: one fitted to the long crack growth data, the other to short crack growth data. The short crack model is then used to determine crack growth rates when the crack is in the short crack regime, as soon as it enters the long crack regime, the long crack model is used.

Results of these calculations are shown in the form of S-N curves in Figure 4.8. It was found that the UniGrow model predicted good total fatigue lives for cracks under high stress range. However, when the predicted fatigue life gets in the range of 10^5 – 10^6 cycles, the results start to deviate. For predictions of fatigue life >10^5 – 10^6, underprediction of the total fatigue life is observed when using the UniGrow method. Bang et al [1] attributed this to poor prediction of short crack growth speeds. The correction method showed better results than the curve fitting method. This is most likely due to the fact that the fitting method was defined as an average over the short crack growth experimental results. However, the crack growth speed of short cracks should depend on maximum applied stress.

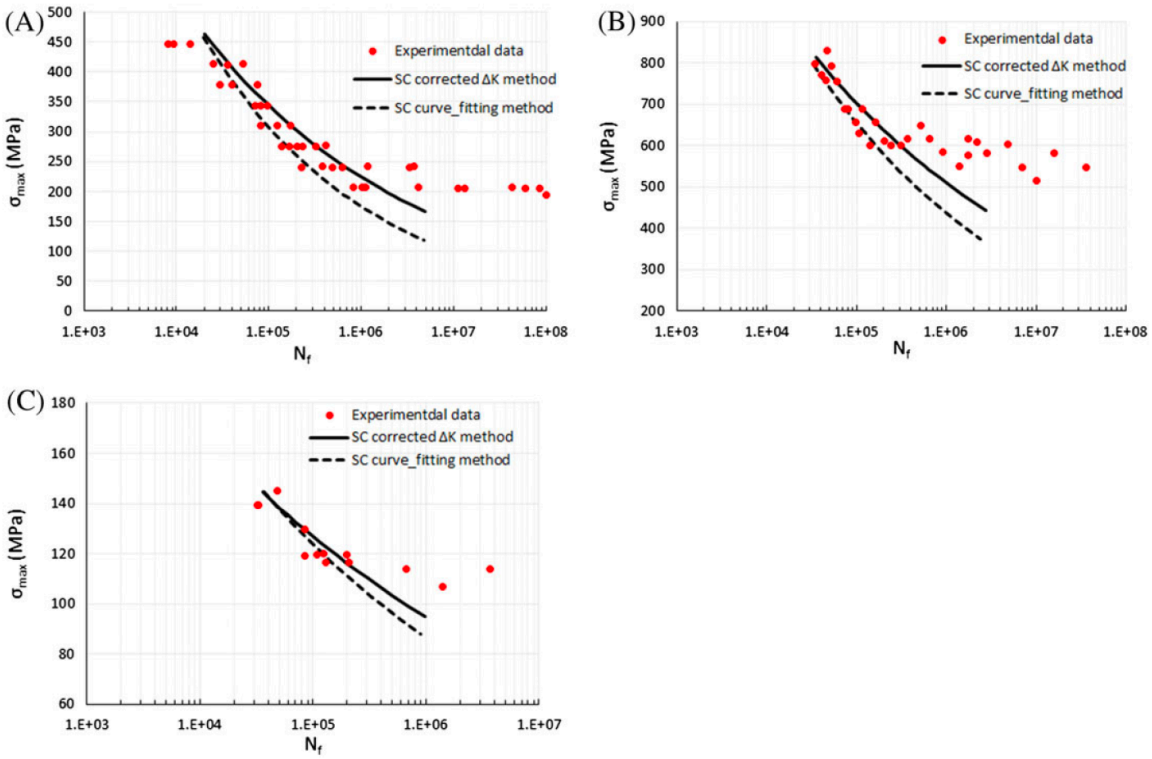

Figure 4.8 S-N curves for 2024-T3 aluminium, Ti-6Al-4V titanium, and 7075-T561 aluminium alloys compared to analytical results [1]

4.1.5 Discussion

From the previous section, it can be noted that good fatigue life predictions were done using the UniGrow model for crack propagation regime [35], welded specimens [3], [36] and the LCF fatigue regime for notched and unnotched specimens [1]. Poor results were obtained for fatigue lives >10^5 in the (un)notched specimens studied by Bang et al [1]. In this range, the UniGrow method showed underestimation of the fatigue life compared to experiments.

The cases where decent predictions of the UniGrow model were found have one common denominator: the predicted fatigue lives are all in a range that is dominated by fatigue crack propagation. Welded specimens usually spent a significant portion of their total fatigue life in propagating the crack due to initial weld defects and high stress concentrations at the weld toe [61]. Furthermore, the model also predicted reasonably good results in LCF range. In LCF, the stress ranges are relatively high, in which case most of its life is spent in fatigue crack propagation [20].

4.2 The Two-Stage-Model

It is often proposed by researchers that fatigue consists of two stages: crack initiation and crack propagation. This phenomenological model is at the basis of the Two-Stage-Model, a total life fatigue model, that was first introduced by Röscher et al [64] in 2019. First, a description of the model will be given, after which the data that will be used to compare the UniGrow method against is presented.

4.2.1 Model description

As described before, the Two-Stage-Model consists of two main steps: crack initiation and crack propagation. Each stage is described by a separate model, yielding an initiation life (N_i) and propagation life (N_p). These two are then added to obtain the total fatigue life (N_f). The two steps are modelled with the following models and assumptions:

- **Crack initiation:** This fatigue stage is modelled using the strain-life method. As stated before, this method is often assumed to be able to model fatigue crack initiation. It is thus implicitly assumed that the fatigue life of a smooth specimen represents the number of cycles it takes for the crack to grow 0.5 mm.

  First, a linear elastic FEA model is made of the weld, from which the stress concentration factor (K_t) can be obtained. K_t is defined as in Eq. (4.4), where $\sigma_{1,max}$ is the maximum principal stress and σ_{nom} is the nominally applied stress. The FEA model uses linear plane stress elements with a size of 0.167 to 0.25 mm as defined by IIW recommendation.

  $$K_t = \frac{\sigma_{1,max}}{\sigma_{nom}} \tag{4.4}$$

  A modified Neuber approach, that is valid for mild notches such as the weld toe, where the cross section could show yielding has been applied. After the elastic stresses/strains are converted to elastoplastic stresses/strains, the Smith-Watson-Topper damage parameter is used to predict the fatigue life of the initiation stage.

  An important note to make here is that the initiation life results by Röscher et al [64] have been calculated on the basis of a linear elastic FEA model that was based on linear elements of 0.17 – 0.25 mm. This means that some underestimation of the stress could also be present in the model by Röscher et al [64], which in turn could cause overestimation of the initiation life.
- **Crack propagation:** This fatigue stage is modelled using a LEFM-based method using the eXtended Finite Element Method (XFEM). XFEM allows for modelling a crack in FEA separate from the mesh of the model, which prevents the need for extensive remeshing. It also allowed Röscher et al [64] to let the crack grow on a non-predefined path, i.e. the crack can grow freely. The FEA model is slightly refined to elements of 0.1 mm in the expected crack area.

  An energy-based method (Virtual Crack Closure Technique) was used to determine the energy-release rate. The energy-release rate was used to determine the crack growth speed using the Paris-law. A crack increment of 0.1 mm is used. The initial location of the crack is the location where the highest principal stresses were observed. The initial crack direction is set as perpendicular to the direction of the highest principal stress, with an initial crack length of 0.5 mm.

What becomes clear from the model description is that the two methods are completely separate from each other, the only thing linking them is the location of crack initiation. The end of the fatigue life is defined as the point where the critical energy release rate is reached or when the crack length has reached 5 mm. This was done to save on computation time [64].

4.2.2 Model data

The Two-Stage-Model has been applied to several weld geometries, where the following fundamental assumptions have been made by Röscher et al [64]:

- **Weld residual stresses:** Weld residual stresses have been neglected in the calculations. Solely the influence of geometry is of consideration in this research.
- **Material parameters:** The base material, weld material and heat affected zone are assumed to made from the same material and thus have the same material parameters. This is a simplification, as it has often been shown that the material structure is altered by welding and that the weld

material and HAZ show considerable different behaviour. The material parameters are derived from the UML (Uniform Material Law) and are given in Table 4.1.

- **Crack type:** The crack type that is considered in this model is a through thickness edge crack. The plate is considered to be 0.1 mm wide. A 2D model has been used.

Material parameters		Strain-life parameters		Paris-Law parameters	
f_y	355 MPa	σ_f'	735 MPa	C	$3.39 * 10^{-14}$
f_u	490 MPa	b	-0.087	m	3.18
E	210000 MPa	ε_f'	0.59	K_{Ic}	2000 N/mm$^{3/2}$
v	0.3	c	-0.58	ΔK_0	180 N/mm$^{3/2}$
K'	808.5 MPa				
n'	0.15				

Table 4.1 Material, strain-life and Paris-Law parameter for the modelled S355 steel by Röscher et al [64]

Röscher et al [64] have defined 4 different weld qualities, ranging from A to D, in decreasing quality. Weld quality A is a high weld quality and has been based upon weld quality B from EN ISO 5817:2014. The weld will be modelled as an arc defined by a weld excess (e). Furthermore, weld quality B, C and D experience misalignment (v_o) between the two plates. The assumed weld geometry can be seen in Figure 4.9. Both weld excess and misalignment have been defined relative to the thickness (t) of the plate, the exact definitions are given in Table 4.2. The weld toe is modelled with a fictitious radius of 1 mm and the weld length is assumed equal to the thickness of the specimen.

Weld	Misalignment (v_o)	Weld Excess (e)
A	0	1 + 0.1t
B	0.05t	0.5 + 0.05t
C	0.1t	1 + 0.1t
D	0.15t	1 + 0.15t

Table 4.2 Various weld qualities modelled by Röscher et al [64] and their misalignment and weld excess

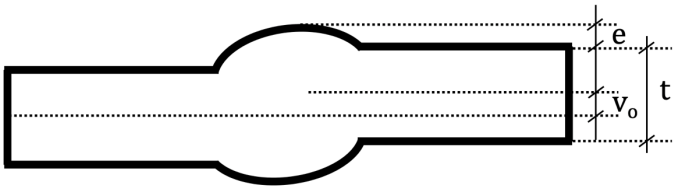

Figure 4.9 Assumed geometry used by Röscher et al [64] in the modelling of the welds

For each weld quality, Röscher et al [64] have analysed five different weld thicknesses for each weld quality, ranging from 10 to 30 mm. More detailed results were available for welds of a thickness of 20 mm; therefore, it has been chosen to model the weld quality A20, B20, C20 and D20. For A and C quality welds, plate thicknesses of 10 mm and 30 mm will also be modelled. This will be done to investigate whether the UniGrow model can account for the effect of the thickness. The modelled geometries with their misalignment, weld excess and SCF can be found in Table 4.3. The specimens are loaded with a stress ratio of R = 0.

Weld	Thickness (t)	Misalignment (v_o)	Weld Excess (e)	Stress Concentration Factor (K_t)
A10	10 mm	0 mm	2 mm	1.69
A20	20 mm	0 mm	3 mm	1.93
A30	30 mm	0 mm	4 mm	2.13
B20	20 mm	1 mm	1.5 mm	2.33
C10	10 mm	1 mm	2 mm	2.71
C20	20 mm	2 mm	3 mm	3.37
C30	30 mm	3 mm	4 mm	3.78
D20	20 mm	3 mm	4 mm	4.17

Table 4.3 Weld geometries modelled in this study [64]

4.3 Global UniGrow implementation

To match the model by Röscher et al [64], the following assumptions have been done:

- **Crack type:** It is assumed that an edge crack is present in the weld. The crack initiates from the point where the principal stresses are the highest and grows straight down (at right angles to the applied stress direction). It is assumed that pure Mode I crack growth is applicable here, even though shear stresses might be present. A comparison of the crack growth predicted by the UniGrow model and the Two-Stage-Model is presented in Figure 4.10.
- **Weld residual stresses:** Weld residual stresses will be neglected in the calculations. Solely the influence of geometry is of consideration in this research.
- **Material parameters:** The base material, weld material and heat affected zone are assumed to made from the same material and thus have the same material parameters.

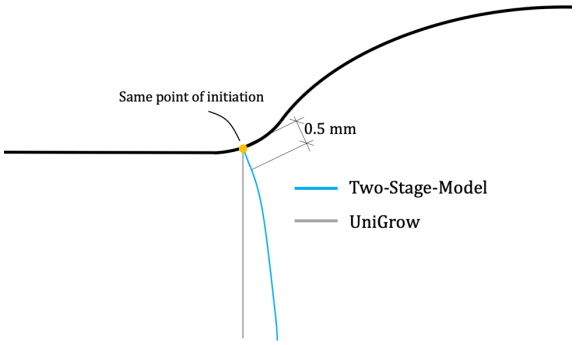

Figure 4.10 Schematic of assumed crack growth in UniGrow method and Two-Stage-Model

In this validation step, the method as given in Figure 4.11 will be used. The calculation procedure is largely the same as the one used in section 3.3, the largest difference being that the model will be looped. This will be discussed in further detail in section 4.4. The global steps of the UniGrow method will be performed as follows:

1. **Determination of the applied stress intensity factor:** The applied stress intensity factor will be established using the weight function method. A linear elastic FEA model will be made to determine the normal stresses (stresses perpendicular to crack direction) in the critical crack cross section. This is the cross section where the principal stress was found to be the highest. Since the use of the weight function method to determine SIFs in welded geometries has not been validated, the applied SIF at discrete intervals will also be determined using FEA. This topic will be addressed further in section 4.4.1.
2. **Determination of the elastoplastic stress distribution ahead of the crack tip:** It has been established that the relation between K_{res} and ΔK_{app} can be considered to be independent of geometry. For this reason, this relationship is established by modelling a flat plate with a crack, since accurate analytical formulas for the determination of ΔK_{app} are available. The elastoplastic stresses will be determined using a 2D elastoplastic FEA model. No analytical method will be used, since it is unable to account for the redistribution of the stress. Section 4.4.2 will further address this topic.
3. **Determination of the residual stress intensity factor:** Using the residual stress from the previous step, K_{res} was determined using the universal weight function. To ease calculations, the relationship between K_{res} and ΔK_{app} is determined separately and used as input for the global calculation of the crack growth speed. This will not be further addressed in this chapter as this has been discussed before, reference is made to section 3.2.3.2 for background.
4. **Determination of the elastoplastic stress and strain on first elementary block ahead of the crack tip:** This will be done using the Creager-Paris equations in combination with the Neuber uniaxial plasticity correction. This will not be further addressed in this chapter as this has been discussed before, reference is made to section 3.1.3.4 for background.
5. **Determination of the initiation life of the first elementary block ahead of crack tip:** The initiation life was determined using the Smith-Watson-Topper damage parameter. No use will be made of the Morrow method as this is not valid for SC. This will not be further addressed in this chapter as this has been discussed before, reference is made to section 3.1.3.5 for background.

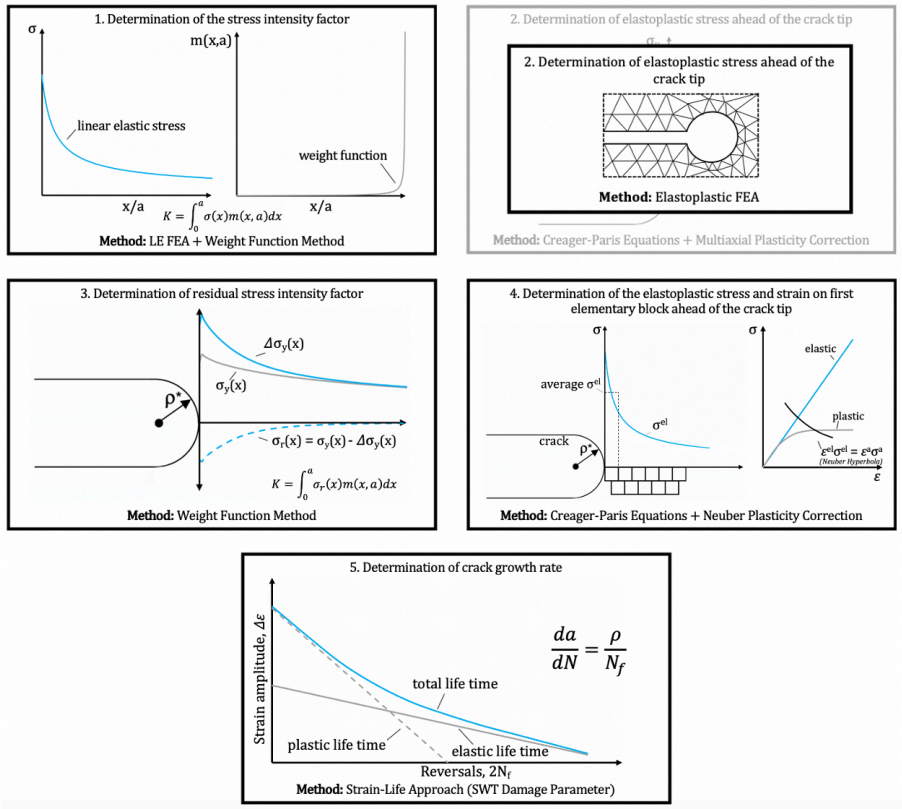

Figure 4.11 Global calculation procedure of the numerical UniGrow method

4.4 Calculation methods

In this section, attention will be given to some methods that are specific to this implementation of the UniGrow method. First, the determination of the applied SIFs will be discussed, after which the determination of the plastic residual SIF will be discussed. Finally, the full implementation of the UniGrow model will be presented.

4.4.1 Determination of the applied stress intensity factor

As discussed before, two methods will be used for the determination of the applied SIF: the weight function method and FEA. The advantage of the weight function method over FEA are the low calculation times and the use of relatively simple methods (it solely requires linear elastic FEA and Python). The weight function is, however, usually defined for use in a flat plate. Bogdanov et al [3] and Mikheevskiy et al [36] have used the weight function to determine the applied SIFs in welded geometries. They argue that the weight function for a flat plate can be used for a welded specimen and that the effect of the weld is accounted for through an altered stress distribution (due to the effect of the notch).

This method has been applied by the authors without showing whether the use of the method is valid. To investigate whether the use of the weight function method for welded geometries is valid, also FEA software is employed to determine the SIF. These results will then be used to justify the use of the weight function method.

4.4.1.1 Weight Function

In order to determine the stress intensity factor using the weight function method (given in Eq. (4.5)), two elements are required: the proper weight function ($m(x,a)$) and an elastic stress distribution ($\sigma(x)$). These two elements will be discussed after which the method for integration and implementation in Python will be discussed.

$$K_{app} = \int_0^a \sigma(x)m(x,a)dx \tag{4.5}$$

Weight Function

The weight function for an edge crack in a finite width plate has been analytically derived by Kaya and Erdogan [22] and is given in Eq. (4.6). The full formula for G can be found in Appendix A.2. No clear validation of the use of this weight function have been found, however, the use of it has been proposed by many authors.

$$m_{EC}(x,a) = \frac{2}{\sqrt{\pi a}} \frac{G\left(\frac{x}{a},\frac{a}{t}\right)}{\left(1-\frac{a}{t}\right)^{3/2}\sqrt{\left(1-\left(\frac{x}{a}\right)^2\right)}} \tag{4.6}$$

Determination of stress in cross section

To determine the stress in the critical cross section (i.e. the cross-section perpendicular to the applied stress where the highest principal stress is found), a linear elastic FEA model has been made. The model follows the sizes specified by Röscher et al [64]. The model is relatively simple and consists of a modelled weld with fixed boundary conditions on one side and a uniform stress on the other side. The length of the plate on either side of the model is equal to twice the thickness to ensure proper introduction of the stresses. A summary of the model can be found in Figure 4.12.

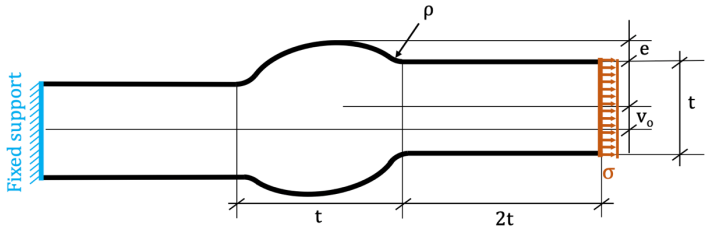

Figure 4.12 Constraints and loads on the linear elastic FEA model of the weld

The overall mesh size used in the model is 0.5 mm with a more refined mesh around points where stress concentrations might occur; the weld toes in this case. In the radius of the weld toe, edge sizing will be applied with various sizes until the model is converged. Quadratic, triangular plane stress elements will be used due to the limited thickness of the model. Advancing front method will be used to limit distortion in the elements. A summary of the mesh sizing is given in Figure 4.13.

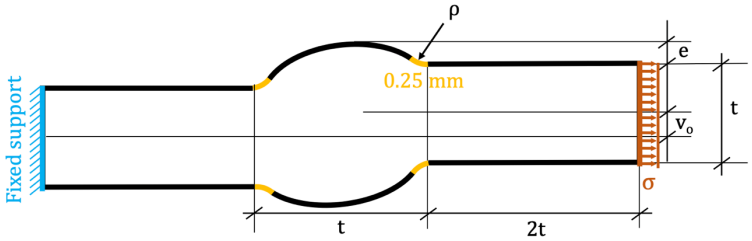

Figure 4.13 Mesh controls for the FEA model of the weld

Mesh sensitivity was studied using the B20 geometry. The weld was loaded with a uniform stress of 100 MPa and the element size was varied from 0.25 to 0.025 mm. An overview of the mesh is given in Figure 4.14, here, the aforementioned mesh controls can be seen.

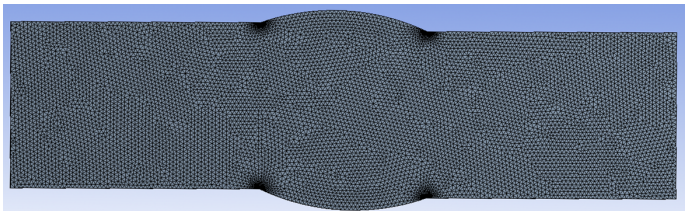

Figure 4.14 Overview of the mesh for the FEA model of the weld

A more detailed picture of the mesh at the crack tip can be viewed in Figure 4.15 and Figure 4.16. The maximum principal stress reported in each model is reported in Table 4.4. From this, it can be seen that the mesh can be considered to converge at an element size of 0.05 mm.

Element size	σ_1 [MPa]	% change
0.25 mm	260.4	-
0.1 mm	267.8	2,84
0.05 mm	269.4	0,60
0.025 mm	269.9	0,19

Table 4.4 Maximum elastic principal stress for distinct mesh sizes for B20 geometry (σ = 100 MPa)

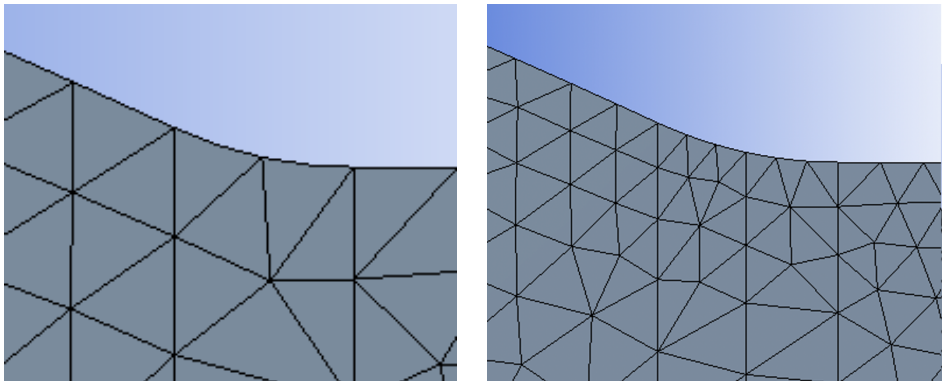

Figure 4.15 Mesh size at weld toe for an edge size of 0.25 mm (left) and 0.1 mm (right)

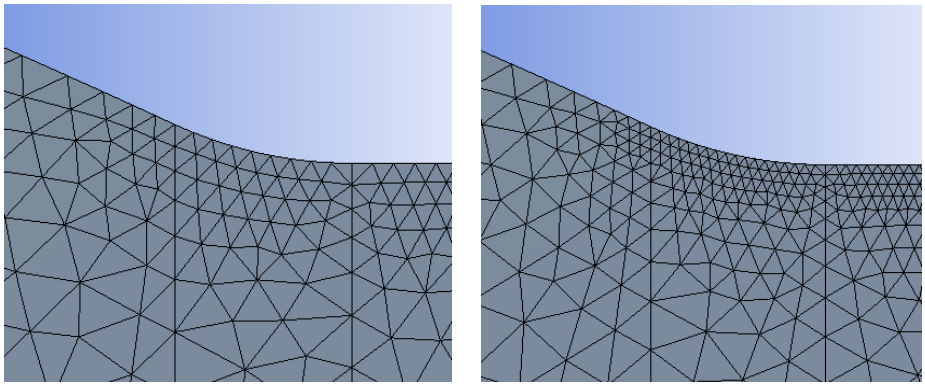

Figure 4.16 Mesh size at weld toe for an edge size of 0.05 mm (left) and 0.025 mm (right)

To verify that the modelled geometries match the ones that have been used by Röscher et al [64], all weld geometries have been re-modelled with linear plane stress elements of 0.25 mm. The SCF-value of a specimen was defined as in Eq. (4.7). The observed SCF-values can be found in Table 4.5. Here, it can be seen that they almost exactly match the ones found by Röscher et al [64], confirming that the modelled geometries are identical.

$$K_t = \frac{maximum\ principal\ stress}{applied\ stress} \tag{4.7}$$

Weld	K_t (Röscher et al)	K_t FEA
A10	1.69	1.70
A20	1.93	1.92
A30	2.13	2.13
B20	2.33	2.34
C10	2.71	2.74
C20	3.37	3.33
C30	3.78	3.72
D20	4.17	4.22

Table 4.5 SCF found by Röscher et al [64] and current study for the weld geometries

Integration

The plastic residual stress intensity factor is determined in a similar fashion as in section 3.2.3.2. The integral in Eq. (4.8) can be replaced with a summation simplified to allow for easy integration into Python. Here, S is the area under the curve $m(x,a)$ and σ_{avg} is the value of the function σ_r at the x-value of the centroid of the area under the curve $\sigma_r(x)$ [39].

$$K_{res} = \int_{a_0}^{a} m(x,a)\sigma_r(x)dx = \sum_{j=1}^{i}(\sigma_{avg} * S) \tag{4.8}$$

To assure easy calculation of the centroid of the stress curve, one can linearly approximate the curve on each interval x_i to x_{i+1}, by which σ_{avg} can be found as given in Eq. (4.9).

$$\sigma_{avg} = \frac{\sigma_r(x_i) + \sigma_r(x_{i+1})}{2} \tag{4.9}$$

As recommended by Prime [60], the value of the integral of the weight function, will be determined using Gaussian Quadrature. This will be done due to the singularity at $x = a$ of the weight function. Prime [60] recommends using Gaussian Quadrature with 50 points on the singular intervals to assure proper convergence.

Programming flowchart

The programming flowchart of this part of the program is given in Figure 4.17. It has been separated from the main UniGrow model as a separate module. The module consists of a loop that starts at x = 0 and runs until x = a. The model is relatively simple and follows the exact steps that have been introduced above. First, for each interval, the average stress will be determined. Then the integral of the weight function on this interval is determined and multiplied with the average stress. This is then added to the total stress. A step size of 0.001 mm is used to make sure that accurate SIFs are determined.

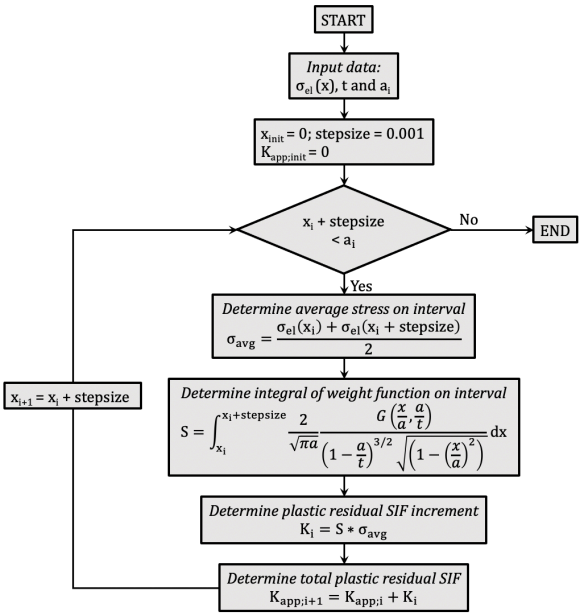

Figure 4.17 Flowchart for the determination of the applied SIF range

4.4.1.2 Finite Element Method

To justify the use of the weight function method for welded geometries, SIFs have also been determined with FEA. The Fracture Tool in ANSYS 18.2 has been used for this. This tool is used to define a pre-meshed crack in the model. The SIF is evaluated at the crack front through contour integration (J-integral method). The model is linear elastic and split in two sections on either side of the crack. The two bodies are connected through a bonded connection. The meshes of the two sections are connected as well through the Mesh Edit method.

An overall mesh size of 0.5 mm has been used and in the region of the crack, a region of 1 mm around the crack tip, the mesh size was reduced to 0.05 mm. Quadratic, triangular plane stress elements have been employed in the model. The model is loaded in the same way as the linear elastic model used for the weight function method. The crack is also in the same location as the critical cross section used by the weight function method. A summary of the model can be found in Figure 4.18, an example of the mesh is given in Figure 4.19.

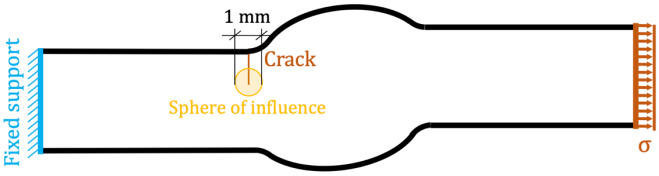

Figure 4.18 FEA model used for the determination of the SIF with mesh controls for a welded geometry

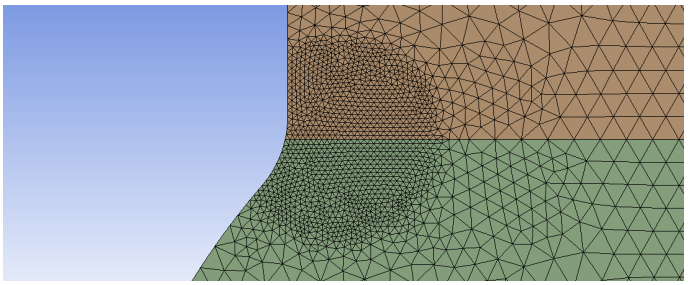

Figure 4.19 Example of mesh used near the crack tip for a welded geometry

4.4.1.3 Flat Plate Verification

As a baseline measurement of the performance of both the weight function method and the ANSYS Fracture Tool, first SIFs in a flat plate will be derived. Both methods will be compared to results from the Newman-Raju equations. These equations for semi-elliptical surface cracks can also be used to determine the SIF in an edge crack by setting a/c = 0. The calculations have been performed for a flat plate of 10 mm and 30 mm with crack lengths of 0.5, 1, 2, 3, 4 and 5 mm.

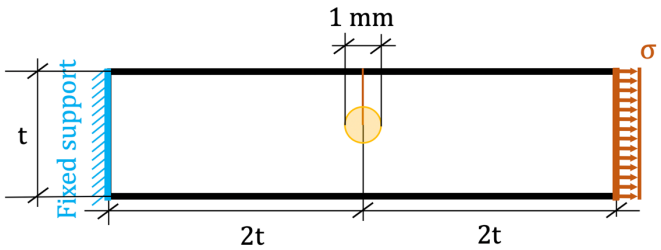

Figure 4.20 FEA model used for the determination of the SIF with mesh controls for a flat plate

No FEA model is required for the weight function method, as the stress is uniform. For the Fracture Tool, a similar model as for the welds has been made. The model is fixed on one end and loaded by a uniform stress on the other end. A summary of the model is given in Figure 4.20. An overall mesh size of 0.5 mm has been used and in the region of the crack, a region of 1 mm around the crack tip, the mesh size was reduced to 0.05 mm. Quadratic, triangular plane stress elements have been used in the model. An example of the mesh used is provided in Figure 4.21. The model is linear elastic and split in two sections on either side of the crack. The two bodies are connected through a bonded connection. The meshes of the two sections are also connected using a mesh edit.

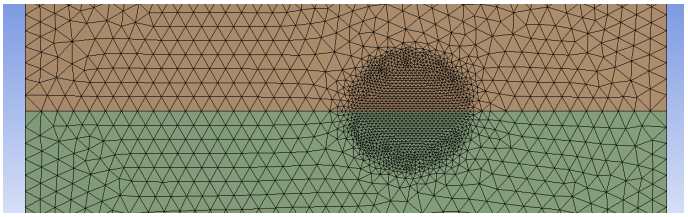

Figure 4.21 Example of mesh used near the crack tip for a flat plate

4.4.1.4 *Short crack correction*

Bogdanov et al [3] proposed a correction of the applied SIF for short fatigue cracks to account for the higher stresses. Bang et al [1] then proposed another method that entailed curve fitting a separate UniGrow model to short crack fatigue data. Considering the fact that the curve fitting method performed rather poorly as it couldn't account for effects of maximum stress and the fact that no experimental short crack data is available for this case an, the option of correcting the SIFs will be used.

This means that one UniGrow model will be used in which K_{max} and K_{min} will be augmented for short cracks. This means that for R = 0, K_{max} and ΔK_{app} will change as the K_{min} will remain zero. This can be seen in Eq. (4.10) and (4.11).

$$K^* = \left(1 + \frac{1}{2}\sqrt{\frac{\rho^*}{a}}\right) K \tag{4.10}$$

$$\Delta K^*_{app} = \left(1 + \frac{1}{2}\sqrt{\frac{\rho^*}{a}}\right) \Delta K_{app} \tag{4.11}$$

The criteria from Bang et al [1] for separating the short and long crack growth regime will be used in the calculations. The three separating criteria are:

- **Threshold crack size (a_{cr}):** This is usually assumed to be somewhere between 0.5 – 1 mm, where Bang et al [1] use 0.5 mm. As Röscher et al [64] also use 0.5 mm as the starting point for the crack propagation calculation, the threshold crack size is set to 0.5 mm.
- **Threshold SIF (ΔK_{cr}):** In this case, the value is taken from Table 4.1: $\Delta K_{cr} = 180$ N/mm$^{3/2}$.
- **Threshold crack growth (da/dN_{cr}):** As the definition of this parameter was not described by Bang et al [1], this parameter has not been used in this study.

Beside the issues with short crack growth speed prediction, some other assumptions in the UniGrow method require further attention when discussing short crack growth:

- **Creager-Paris equations:** In the formulation of the Creager-Paris equations it was assumed that the origin of the equations lies at $\rho/2$ from the crack tip. This assumption is only valid if $\rho \ll a$, so for long cracks. This could cause deviation in the results.
- **LEFM:** For SC, the size of the plastic zone might be in the same order of magnitude as the crack length and therefore conventional LEFM approaches might not be applicable [75]. The higher order terms in the elastic singularity that is used to characterize the local stresses based on K_I might have an appreciable effect on the stresses.

4.4.2 Determination of K_{res} using elastoplastic FEA

In this section the determination of the plastic residual stress intensity factor using elastoplastic FEA will be discussed. First, the used elastoplastic model will be presented and subsequently the method for the determination of the ΔK_{app} - K_{res} relation will be discussed.

4.4.2.1 *Basis of the model*

Considering the near-geometrical independency of the relationship between K_{res} and ΔK_{app}, the model of a flat plate was used to determine this relationship. The plate is 10 mm thick and 1 mm in width. It has been modelled with a crack length of 4 mm and has been loaded with various stresses. A summary of the model is given in Figure 4.22. The model consists of half a plate with the crack on the left side, symmetry is considered here to reduce calculation times. The crack has been modelled as a quarter circle, similar to the model used in chapter 5.3. The right-hand side of the plate is loaded with a uniform stress. The length of the plate is twice the thickness to ensure proper introduction of the stresses into the geometry. The CT specimen has been modelled with the software package ANSYS 18.2.

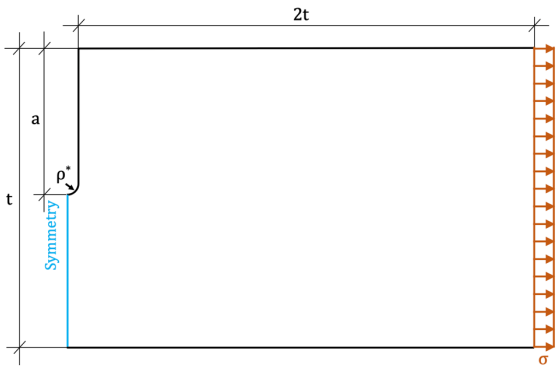

Figure 4.22 Boundary and load conditions for the elastoplastic flat plate model in ANSYS

4.4.2.2 Plasticity

Plasticity was accounted for using the built-in multi-linear kinematic hardening module in Ansys and Von-Mises yield theory. This was chosen as it is the most accurate to describe plasticity in steel. The Ramberg-Osgood relationship using the parameters determined by Röscher et al [64] served as input for the multi-linear kinematic hardening. In Figure 4.23 the input Ramberg-Osgood relationship and the stress-strain relationship from FEA are presented.

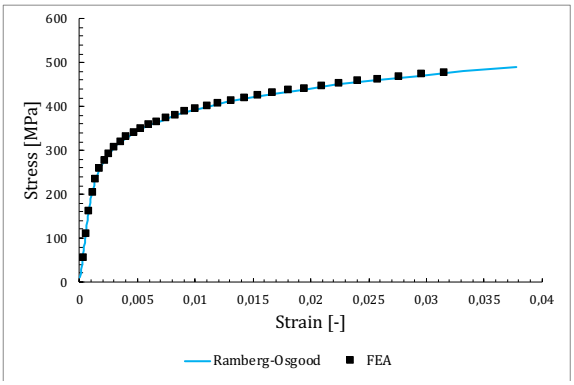

Figure 4.23 Comparison between stress-strain curves generated with Ramberg-Osgood relationship and FEA using multi-linear kinematic hardening for S355 steel

4.4.2.3 Mesh Convergence

Meshing of the model has been done using 1 mm size elements, using an advancing front method to decrease distortions in the mesh. The mesh close to the crack tip has been refined with an edge sizing method with various size in the 2 mm around the crack tip. Further along the crack front, 0.5 mm edge sizing criterion has been used. Quadratic, triangular plane stress elements have been used due to the limited thickness of the specimen. An overview of the mesh parameters is given in Figure 4.24.

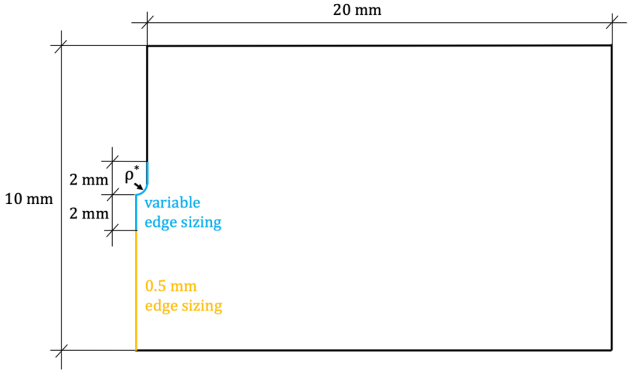

Figure 4.24 Mesh dimensioning of the elastoplastic of the flat plate

Several mesh sizes near the crack tip were tried, starting from a mesh size of 0.01 mm down to 0.001 mm. In Figure 4.25, a detailed overview of the mesh around the crack tip is given. As can be seen here, the mesh

is well-structured and refined near the crack tip. The used elementary block size, and thus radius of the crack tip was 0.09 mm. This was found to yield the best crack growth results.

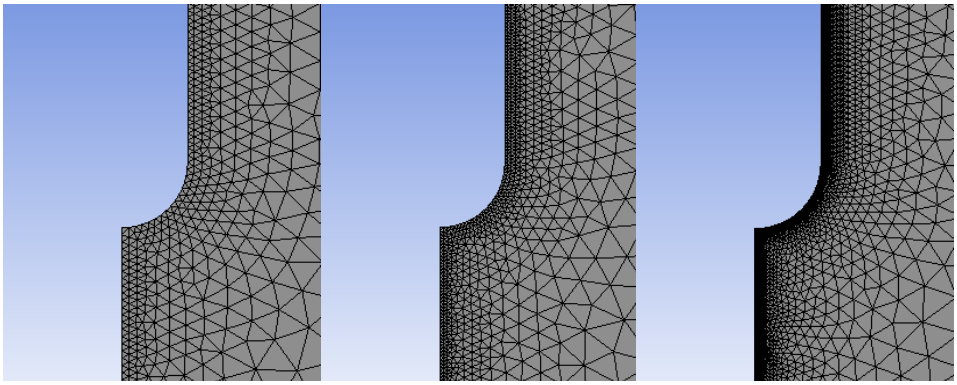

Figure 4.25 Mesh size at crack tip for an edge size of 0.01 mm (left), 0.005 mm (centre) and 0.001 mm (right)

In Table 4.6 the maximum stress in y- and x-direction found in each model have been given. Also, the stress in x-direction at the crack tip has been measured as this is supposed to be equal to zero. As can be seen in the table, the mesh is sufficiently converged at 0.005 mm.

Element size	Maximum $\boldsymbol{\sigma_y}$ [MPa]	Maximum $\boldsymbol{\sigma_x}$ [MPa]	Crack tip $\boldsymbol{\sigma_x}$ [MPa]
0.01 mm	2083.9	419.26	2.753
0.005 mm	2082.5	419.24	0.699
0.001 mm	2082	419.12	0.029

Table 4.6 Maximum elastic principal stress for distinct mesh sizes for B20 geometry (σ = 100 MPa)

4.4.2.4 Determination of ΔK_{app} vs. K_{res}

In this implementation of the UniGrow model, the relationship between K_{res} and ΔK_{app} will be input for the crack growth model. This decreases computation time. Several stress ranges ($\Delta\sigma = 10,\ 25,\ 50,\ 100,\ 150,\ 200$ MPa) are applied to the model and the residual stress after one loading and unloading cycle is subsequently exported to Excel. This serves as input for the residual SIF module, of which a summary has been given in Figure 4.26.

The module starts with importing the data from Excel and mirroring the stresses ahead of the crack tip to the axis behind the crack tip. Once the residual stress becomes positive or the end of the crack face is reached, this loop stops and a $\sigma_{res}(x)$ curve is generated by linearly interpolating the data from Excel. After this, ΔK_{app} is determined using the Newman-Raju equations. The final part of the model consists of determining the K_{res}. This is done in a similar fashion as the determination of the applied SIF. Once the model is done, K_{res} and ΔK_{app} are written to an Excel file. When all the results have been obtained, a linear trendline is drawn through the data to obtain the relationship between K_{res} and ΔK_{app}.

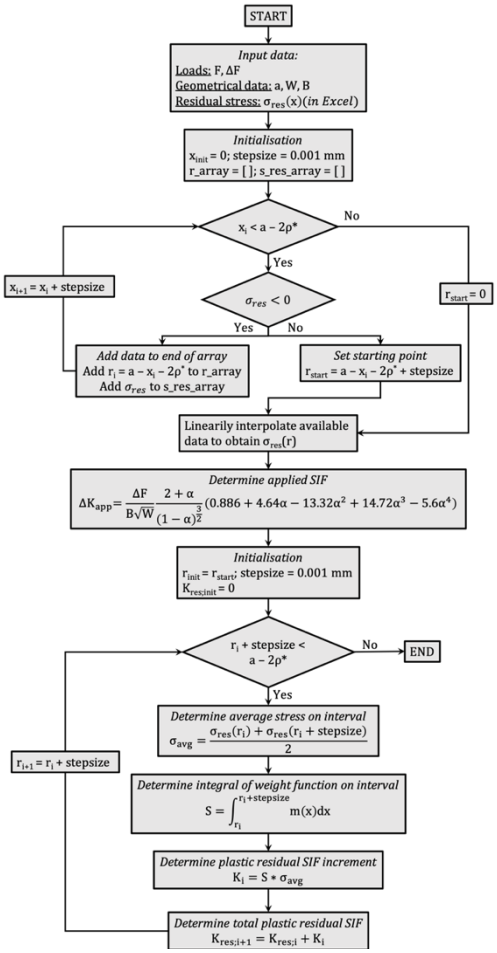

Figure 4.26 Flowchart for the determination of the plastic residual SIF from elastoplastic FEA results and the corresponding applied SIF range

4.4.3 Implementation in Python

The full implementation of the UniGrow method in Python is very similar to the implementation used in section 3.3. The major difference is the fact that the current implementation consists of a loop in which the crack grows with a certain crack increment (Δa). The flowchart of the model is given in Figure 4.27 and matches with the proposed methods in the previous sections.

First, the K_{res} - ΔK_{app} relation and the stress distribution is loaded in. The UniGrow model then starts growing the crack from an initial crack size that is equal to the elementary block size. The loop starts off by determining the applied SIFs, checking whether K_{max} is smaller than the rupture SIF and determining whether the crack can be considered as short. Then follows the determination of K_{res} after which the total SIFs and thus the initiation life of the first elementary block can be determined. With this, the instantaneous crack growth rate can be determined which can be used to determine the number of cycles needed to grow the crack by the crack increment Δa.

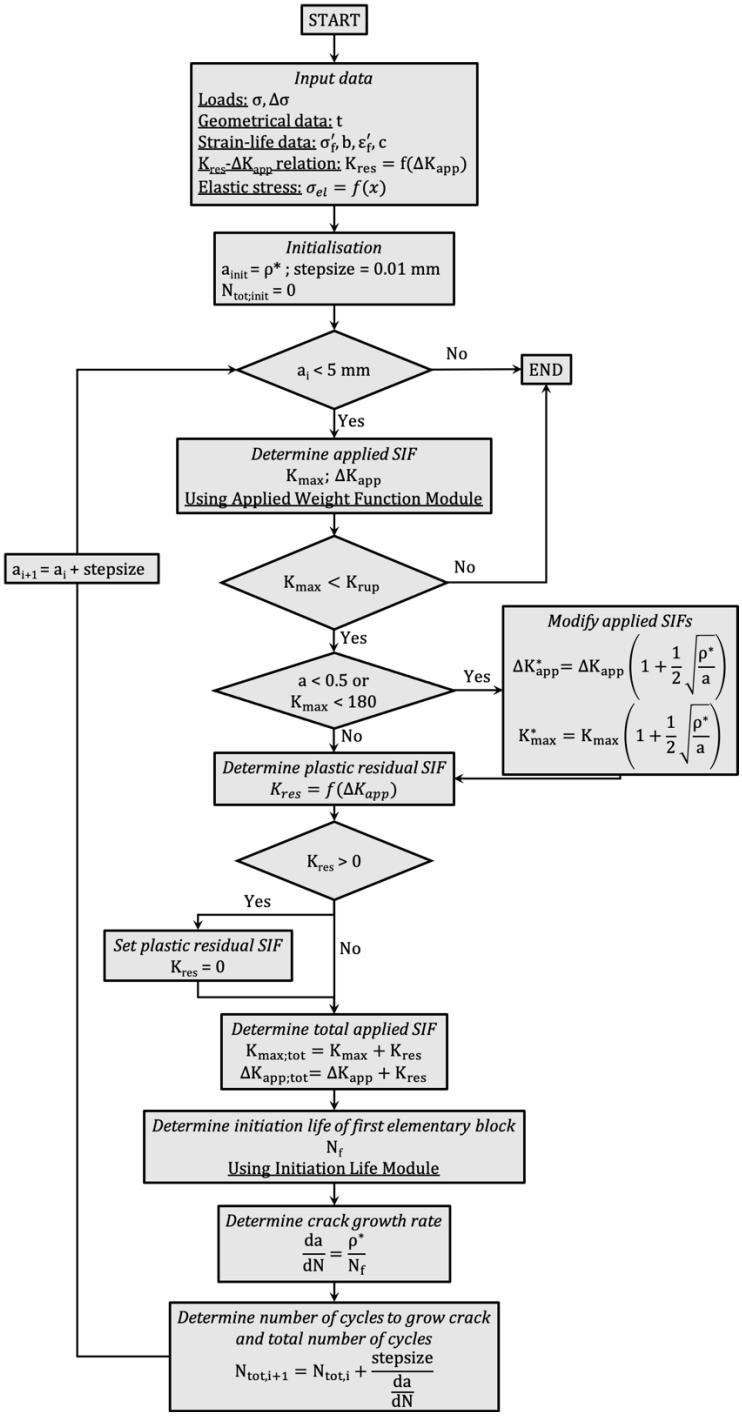

Figure 4.27 Flowchart used for the determination of the total fatigue life of a welded specimen

4.5 Results and discussion

In this section, the results from the analysis that was described in the previous section will be given. It will start with a comparison of the weight function results to FEA results. Then the predicted crack growth speed by the UniGrow method will be given, after which the total fatigue life results are presented. The chapter will end with a discussion of the results.

4.5.1 Weight Function vs. FEA

In this section, the resulting SIFs from the weight function method will be compared to the ones calculated using FEA (ANSYS Fracture Tool). The flat plate case will first be discussed, after which the results for weld geometries are presented.

4.5.1.1 Flat Plate

The calculated SIFs as a function of the crack length for the three methods (Newman-Raju, FEA and weight function) are presented in Figure 4.28. The numerical results for the plates with a thickness of 10 mm and 30 mm are presented in Table 4.7 and Table 4.8 respectively.

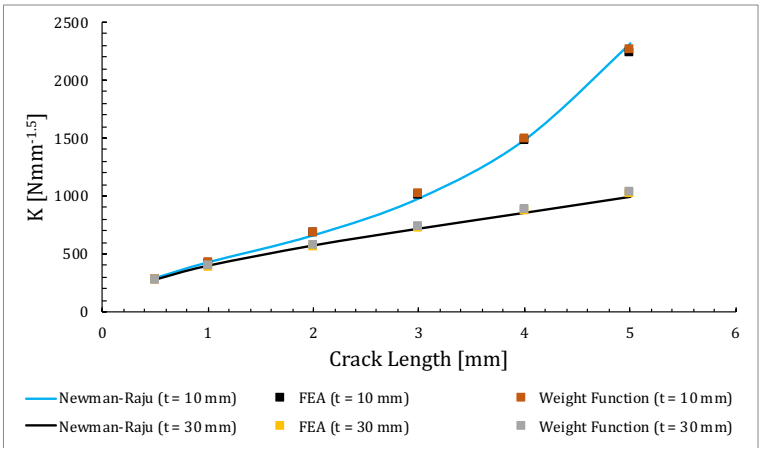

Figure 4.28 Calculated SIF as a function of crack length, determined with three different methods

In general, the results from both methods match very well with the Newman-Raju results. FEA results differentiate from the Newman-Raju results with a maximum of 5% and 3.5% for t = 10 mm and t = 30 mm respectively. Weight function results are slightly poorer and differ from Newman-Raju results with a maximum of 6% and 5.5% for t = 10 mm and t = 30 mm respectively. The fitted equations by Newman-Raju [47] had a maximum error of 5% on the original FEA results. Considering this error, the results obtained using FEA and the WF are approximately within this error range. This indicates proper functioning of both of the methods.

Another interesting thing to take away from Figure 4.28, is that results from FEA and weight function method match very well, the difference being no more than 3.5%. Both methods follow the same global trends for overestimation/underestimation of the SIF when compared to the Newman-Raju solution.

Crack length	SIF Newman-Raju [MPa*mm$^{0.5}$]	SIF FEA [MPa*mm$^{0.5}$]	Difference FEA and NR [%]	SIF WF [MPa*mm$^{0.5}$]	Difference WF and NR [%]
0.5	285.7	285.6	-0.04 %	289.8	1.44 %
1	421.4	414.9	-1.5 %	429.2	1.8 %
2	655.3	683.9	4.4 %	693.2	5.8 %
3	974.3	1018.8	4.6 %	1023.5	5.0 %
4	1479.9	1492.3	0.8 %	1503.8	1.6 %
5	2312.7	2237.6	-3.3 %	2264.4	-2.1 %

Table 4.7 Calculated SIF for a flat plate of t = 10 mm using three different methods

Crack length	SIF Newman-Raju [MPa*mm$^{0.5}$]	SIF FEA [MPa*mm$^{0.5}$]	Difference FEA and NR [%]	SIF WF [MPa*mm$^{0.5}$]	Difference WF and NR [%]
0.5	283.5	279.8	-1,3%	283.2	-0,1%
1	402.1	398.1	-1,0%	404.9	0,7%
2	575.3	574.8	-0,09%	587.8	2,2%
3	718.6	726.3	1,1%	743.4	3,5%
4	853.3	872.8	2,9%	891.9	4,5%
5	989.7	1023.1	3,4%	1042.3	5,3%

Table 4.8 Calculated SIF for a flat plate of t = 30 mm using three different methods

4.5.1.2 Butt-Welded Plate

Similar simulations have also been performed for butt-welded plates excluding the effect of weld residual stresses and only considering Mode I crack propagation. The results for six geometries are presented in Figure 4.30, Figure 4.31 and Figure 4.32. At first glance, it can be noticed that the results for both methods follow the same trend when the weld geometry is varied. This holds for both variations in thickness when going from A10 to A30 and simultaneous variations in weld excess and misalignment when going from A20 to D20. The general effect of weld geometry is portrayed very well by the weight function method.

Looking closer at the results, a very clear trend can be identified: weight function predictions are generally higher than results from FEA. This can clearly be seen from Figure 4.29. Differences between the two methods were found to be as high as 12% for the calculated data points. The relative differences between the methods are smallest when the crack is small but grow larger as it extends. The difference between the methods is quite significant and since the difference between the two methods is mainly present in the propagation regime, the propagation life can be seriously affected by this discrepancy in SIF prediction. The difference between the two methods is also higher than for the flat plate, where the two methods varied a maximum of 3.5%.

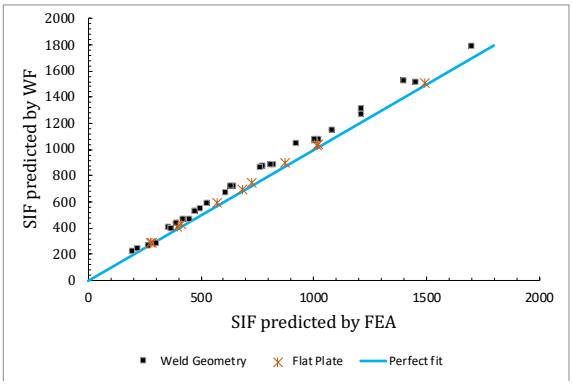

Figure 4.29 Correlation between weight function results and FEA results

Even though the differences between the two methods can be quite significant, accounting for the weld geometry can be done using of the weight function method. Especially for an initial calculation, the method provides accurate enough results. Since this validation has only been performed for edge cracks, the use of the weight function for semi-elliptical cracks to predict SIFs of weld geometries (as done by Mikheevskiy et al [36]) is still not justified. However, based on these results, the expectation is that a similar conclusion can be drawn for this case.

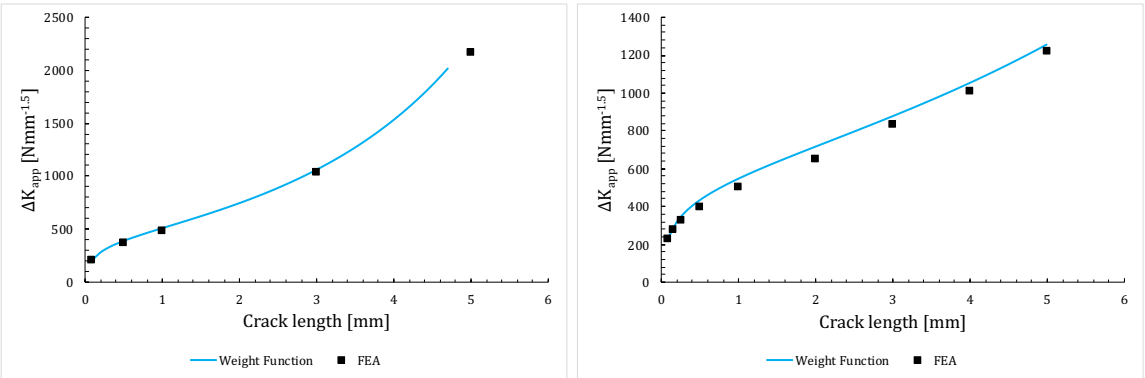

Figure 4.30 Calculated SIF as a function of crack length for weld geometry A10 (left) and A20 (right)

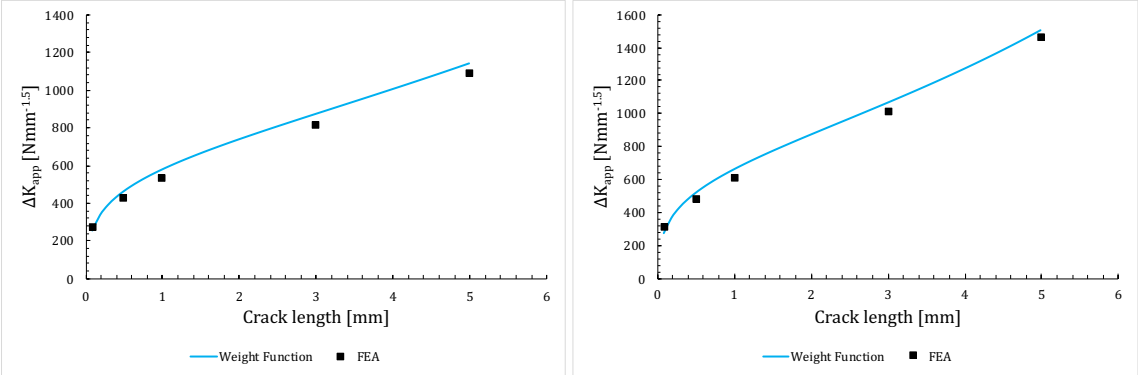

Figure 4.31 Calculated SIF as a function of crack length for weld geometry A30 (left) and B20 (right)

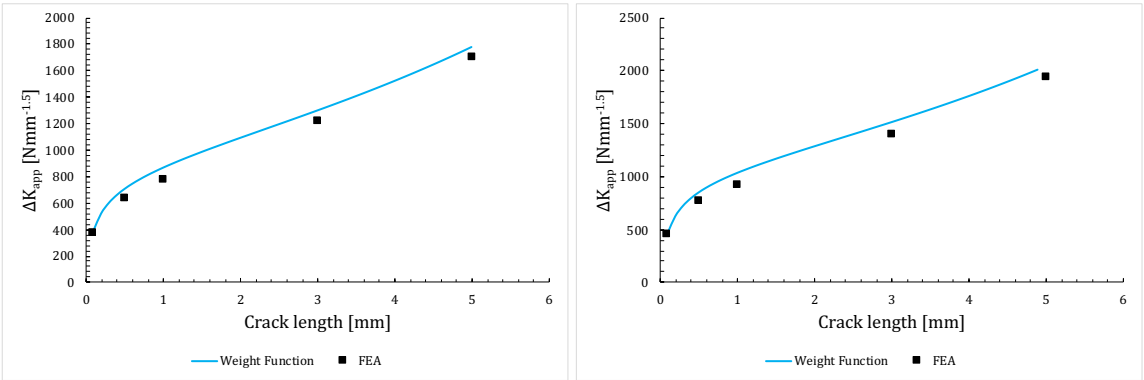

Figure 4.32 Calculated SIF as a function of crack length for weld geometry C20 (left) and D20 (right)

4.5.2 Crack growth speed

From the elastoplastic calculations on a flat plate with a notch, the relation between K_{res} and ΔK_{app} as given in Figure 4.33 has been found. The relation is, again, linear with a high R^2 value of 0.9973. The linearity of this relation matches with the predictions and findings of other authors [10], [53], [54].

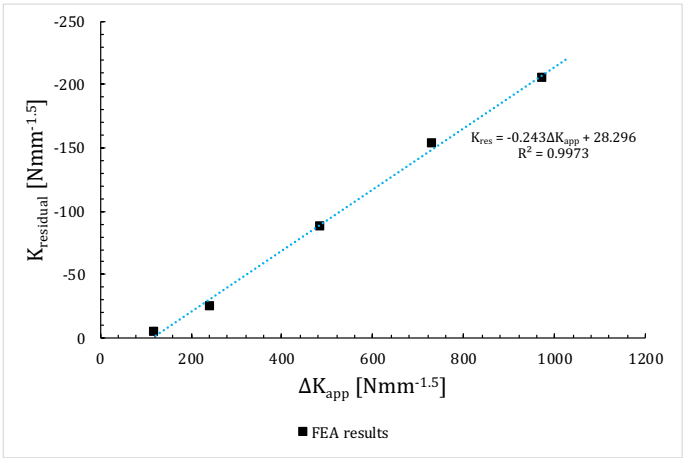

Figure 4.33 Plastic residual SIF as a function of the applied SIF range for R = 0

The relation between K_{res} and ΔK_{app} was determined for an elementary block size of 0.09 mm, which has been found to yield the best crack growth results compared to the Paris crack growth curve that has been used by Röscher et al [64]. Again, looking at the size of the grains in Figure 3.51 from a comparable material (S355 steel from De Jesus et al [11]), this elementary block size in the same order of magnitude as the grains in this material. Reinforcing the suspicion that the elementary block size is in some shape or form related to the material grain size.

Calibrating the UniGrow model to Paris-Law and subsequently using it for validation of fatigue life would, at first, seem to be poor practice. However, in the previous chapter it has been established that the UniGrow

model predicts good crack growth speed results for LC. The main interest of this chapter is how well the UniGrow model performs for the total fatigue life. The fatigue range of interest for SGRE being the High Cycle Fatigue range, where most of the fatigue life is spent on initiating the crack. It is thus valuable to investigate how well the model performs for SC. Fitting the curve to the crack propagation results means that the crack propagation life will match with the life calculated by Röscher et al [64], which means a proper comparison between the predictions of SC growth can be done. Calibrating the model to Paris-Law is justified in this way.

The crack growth speed determined by the model is shown in Figure 4.34. As was also observed in the previous chapter, is that the crack growth curve calculated by the UniGrow method is slightly curved rather than the linear Paris-Law data. This means that, compared to Paris-Law data, the crack growth rates in low and high SIF ranges are overestimated and the crack growth rates in the mid-ranges are overestimated. However, overall, the crack growth results match very well with the Paris-Law crack growth.

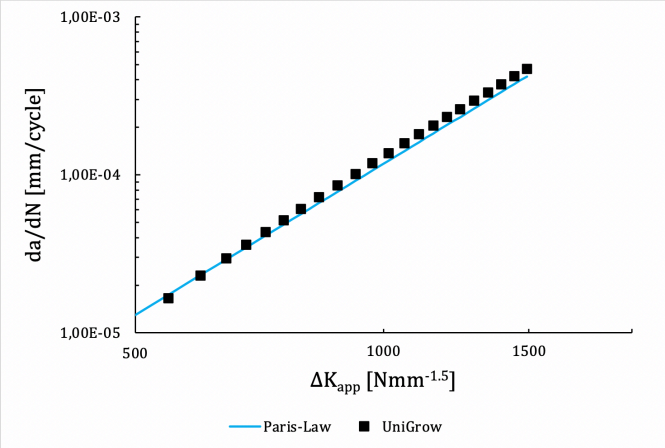

Figure 4.34 Crack growth speed as a function of the applied SIF range for R = 0 compared to Paris Law data from Röscher et al [64]

4.5.3 Crack propagation

In Figure 4.35 the results for the calculation of the crack propagation life using the SIFs calculated by the weight function method can be seen. In Figure 4.35 the S-N curves for crack propagation for the different geometries are given. Crack propagation was defined to start at a crack length of 0.5 mm, with crack growth steps of 0.1 mm to mimic the propagation calculation of Röscher et al [64]. In the determination of the propagation life for these results, no short crack correction factor has been applied. This has been done to assure a proper comparison between the results from the UniGrow method and the Two-Stage-Model.

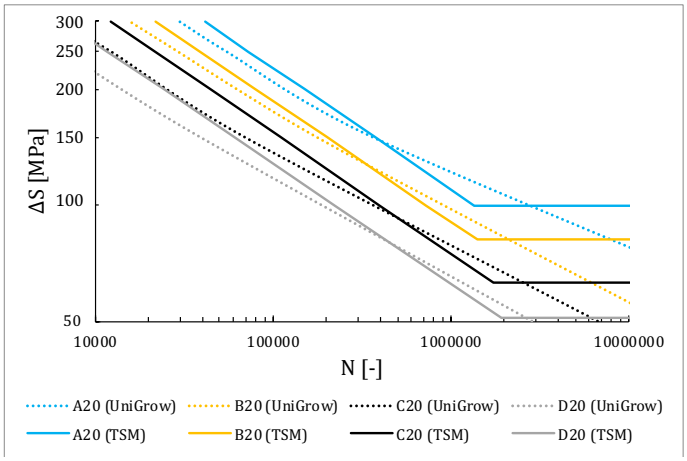

Figure 4.35 S-N curves for crack propagation generated by the Two-Stage-Model and UniGrow model

The results in Figure 4.36 present differences in the predicted fatigue life by the two models. The crack propagation life seems to be underestimated in the LCF region and overestimated in the HCF region. Also, the threshold for crack propagation is absent in the UniGrow method. Three possible causes for the discrepancies between the two models have been identified which will be discussed further:

- **Applied Stress Intensity Factors:** In Figure 4.29 it can be seen that the predicted SIFs by the weight function method are higher than the ones predicted by FEA. This could lead to a shorter prediction of crack propagation life.
- **Predicted crack growth speed:** In Figure 4.34 it can be seen that the crack growth speed is slightly overestimated by the UniGrow model. This could lead to a shorter prediction of crack propagation life. However, since the overestimation is rather small, it is expected to not have a big impact on crack propagation life.
- **Limitations of current model:** The current implementation of the UniGrow model is limited to crack growth in one plane, based on Mode I crack growth only. In the fatigue model used by Röscher et al [64], the crack is allowed to grow freely.

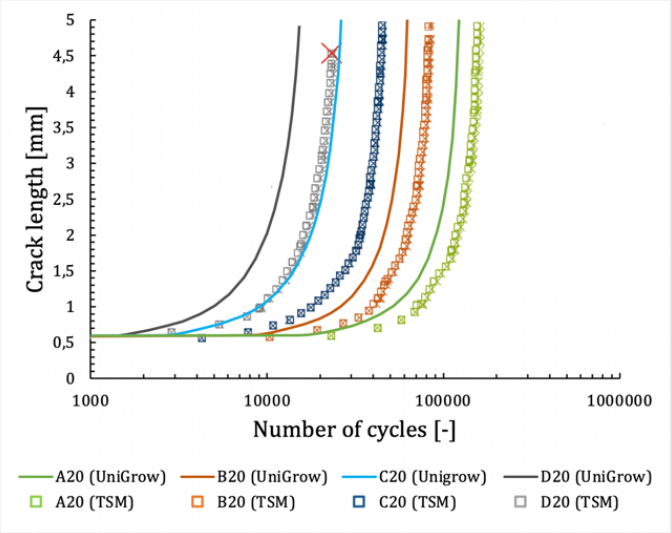

Figure 4.36 Crack length as a function of number of cycles generated by the Two-Stage-Model [64] and UniGrow model

4.5.3.1 Applied Stress Intensity Factors

A cause for the discrepancy between UniGrow and Two-Stage-Model results could be the overestimation of the SIFs by the weight function method, as was determined in the previous chapter. To investigate this effect, the calculated SIFs using FEA as a function of crack length (given in Figure 4.30 - Figure 4.32) has been converted to a curve. This curve was used as input for the UniGrow model.

The S-N curves for crack propagation life can be found in Figure 4.37. From this figure it becomes clear that the results are now much closer to the fatigue propagation lives determined by Röscher et al [64]. This is especially true in the LCF range. However due to the shape of the S – N curve, some difference is found in the HCF range.

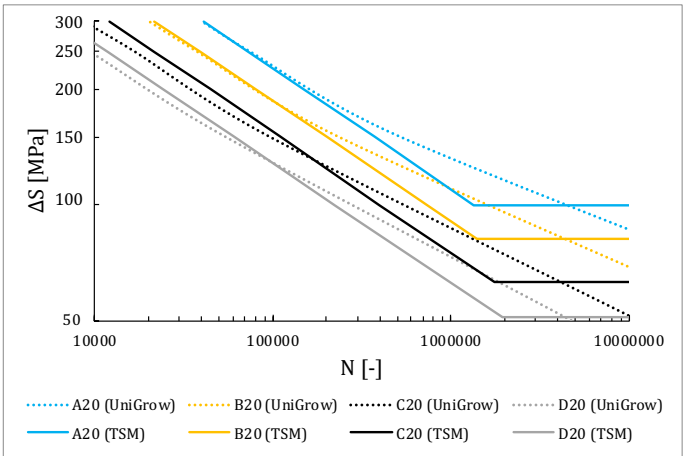

Figure 4.37 S-N curves for crack propagation generated by the Two-Stage-Model and UniGrow model using the SIF from FEA

4.5.3.2 Predicted crack growth speed

The difference from the results by Röscher et al [64] in the HCF range can most likely be explained by the fact that the predictions of crack growth speed by the UniGrow method are not linear like the Paris-Law. Like stated before, the UniGrow model slightly underpredicts crack growth rates for high and low SIFs and lightly overpredicts crack growth rates for medium-range SIFs. In the HCF range, the geometries spent most of their propagation life in lower SIF ranges and thus have a slightly higher propagation life than expected.

If this were true, when the SIFs determined with FEA are used in combination with the Paris-Law results, the propagation life should match closely to the one determined by Röscher et al [64]. The results of this calculation are presented as S-N curves for crack propagation life in Figure 4.38. In this figure, the crack propagation life of the four geometries almost exactly match results by Röscher et al [64]. Still, some slight deviations from the results are present, as can for example be seen in the C20 geometry.

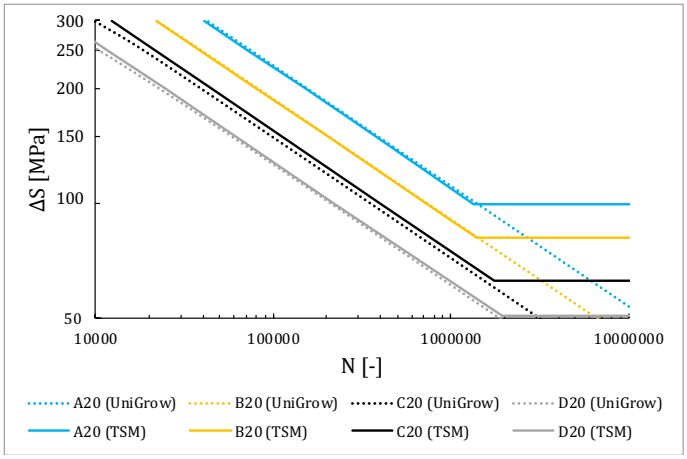

Figure 4.38 S-N curves for crack propagation generated by the Two-Stage-Model and a model that uses SIF from FEA and Paris-Law

4.5.3.3 Limitation of current model

The final contributing factor for differences between the results from the UniGrow method and the Two-Stage-Model are the assumptions on crack growth. In the UniGrow model, it is assumed that the crack grows straight down from the point of initiation. In the Two-Stage-Model, it is assumed that crack grows freely from the point of initiation, with the initial direction being determined by the direction of the principal stresses. The point of initiation is defined as the point in the weld toe where the highest principal stress is found, this is the same in both models.

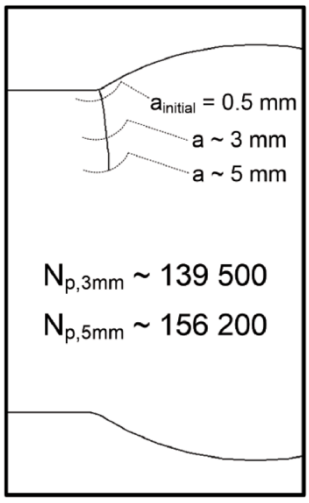

Figure 4.39 Crack shape for A20 geometry predicted by Röscher et al [64]

Due to the weld and the misalignment, some in-plane shear stresses will be present. In-plane shear stresses affect the direction of the crack growth and thus the assumption of pure Mode I crack growth that is used

in the UniGrow method is violated. As can be seen in Figure 4.39, the crack shape predicted by the Two-Stage-Model is lightly curved: the crack doesn't grow in a straight line. However, the deviation from the crack shape predicted by the UniGrow model is limited and therefore it is expected that for geometries with limited misalignment or weld excess, the effect on the fatigue propagation life is minimal.

4.5.4 Total fatigue life

The main interest of this chapter is the ability of the UniGrow method to determine the total fatigue life of welded details. In Figure 4.40 and Figure 4.41, the S-N curves for welds A20, B20, C20 and D20 are given for both total fatigue life (N_f), propagation life (N_p) and initiation life (N_i). These results were calculated using SIFs determined with the weight function method and with the short crack correction method as proposed by Bogdanov et al [3].

4.5.4.1 Total Fatigue Life

The total fatigue life matches very well with the Two-Stage-Model for the Low Cycle Fatigue regime (when $N_f < 10^5 - 10^6$), but in the High Cycle Fatigue regime, the models produce vastly different results. The discrepancy between the two models is mainly caused by the determination of the crack initiation life, as can be seen in Figure 4.40 and Figure 4.41.

For high stress ranges, the weld spends most of its life in crack propagation and therefore total fatigue lives match quite closely to those by Röscher et al [64] (as predicted crack growth rates match very well). For low stress ranges, however, the weld spends most of its life in the initiation phase and therefore total fatigue lives deviate from the ones predicted by the Two-Stage-Model. It can also be seen that as the SCF gets higher (when going from A20 to D20), the stress range where the Two-Stage-Model and the UniGrow method tend to deviate gets lower. This phenomenon can also be explained that for welds with a high SCF, relatively more of its fatigue life is spent on propagation rather than initiation.

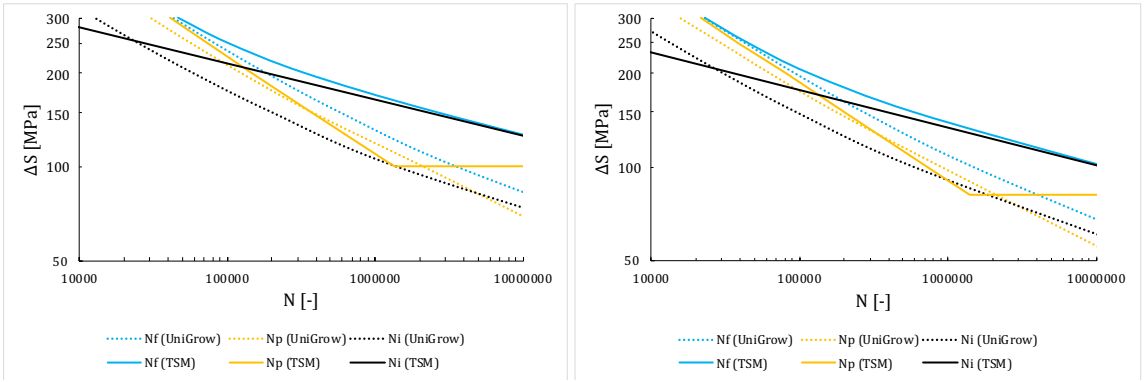

Figure 4.40 S-N curves for crack initiation, propagation and total fatigue life generated by the Two-Stage-Model [64] and UniGrow model for A20 geometry (left) and B20 geometry (right)

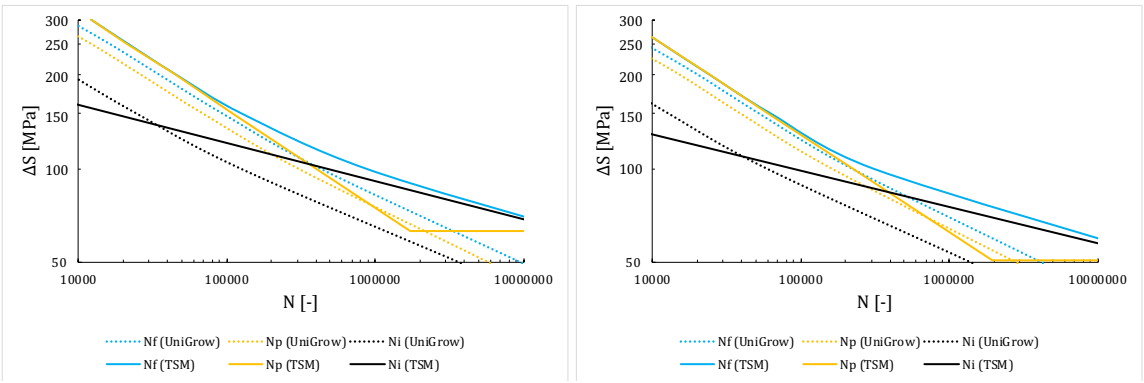

Figure 4.41 S-N curves for crack initiation, propagation and total fatigue life generated by the Two-Stage-Model [64] and UniGrow model for C20 geometry (left) and D20 geometry (right)

As an illustration of the difference between the two results, the total fatigue lives for the different geometries at 50 MPa is given. This is the same order of magnitude that is used as Damage Equivalent Load by SGRE. As can be seen in Table 4.9, the differences between the two methods are very large and deviate as much as two orders of magnitude. This difference does become smaller as the SCF increases, since relatively more life is spent on crack propagation and thus results are bound to match better.

Geometry	Fatigue life UniGrow	Fatigue life Two-Stage-Model
A20	$1.8 * 10^8$	$2.8 * 10^{10}$
B20	$4.8 * 10^7$	$3.6 * 10^9$
C20	$9.8 * 10^6$	$1.4 * 10^8$
D20	$4.3 * 10^6$	$3.6 * 10^7$

Table 4.9 Fatigue life predictions at a stress range of 50 MPa

4.5.4.2 Relative Difference

The relative difference between the S-N curves describes the influence of weld geometry on the fatigue life of the detail. The results for total fatigue life for welds A20, B20, C20 and D20, welds A10, A20 and A30 and C10, C20 and C30 are given in Figure 4.42 and Figure 4.43 respectively.

In Figure 4.42 it becomes clear that the influence of weld geometry, e.g. misalignment, weld toe radius and angle, is accounted for fairly well in the UniGrow model in the higher stress ranges. There, the difference between the S-N curve is in the same order of magnitude as predicted by the Two-Stage-Model. Larger differences between A20/B20 and C20/D20 can be explained by the differences that have been described in the section on crack propagation: a combination of the usage of the weight function method and different crack growth speed prediction.

When looking at the influence of thickness on the S-N curve, it can be seen in Figure 4.43 that the deviation from Two-Stage-Model in the LCF range gets smaller as the thickness increases. The spacing between the curves is less than predicted by Röscher et al [64]. Indicating that the effect of the thickness doesn't seem to be properly accounted for by the UniGrow method. The higher difference between curves for a thickness of 10 mm could partly be the relatively larger role of in-plane shear stresses, altering the direction of crack growth. For all curves, it can be seen that total fatigue lives in the HCF regime are underestimated compared to the Two-Stage-Model. With increasing SCF, the number of cycles where the though the stress

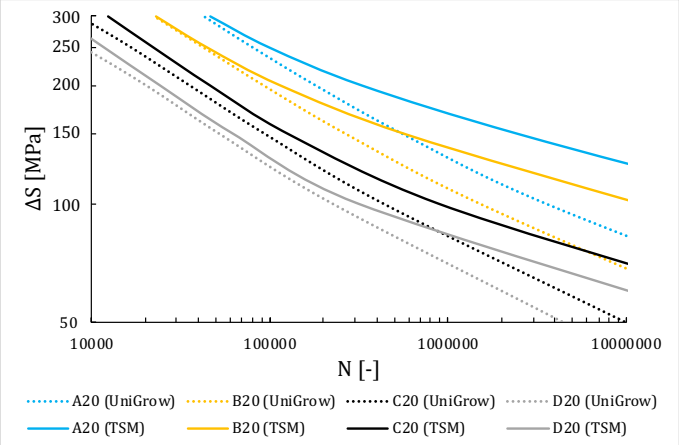

Figure 4.42 S-N curves for total fatigue life generated by the Two-Stage-Model [64] and UniGrow model for using SIF from WF method

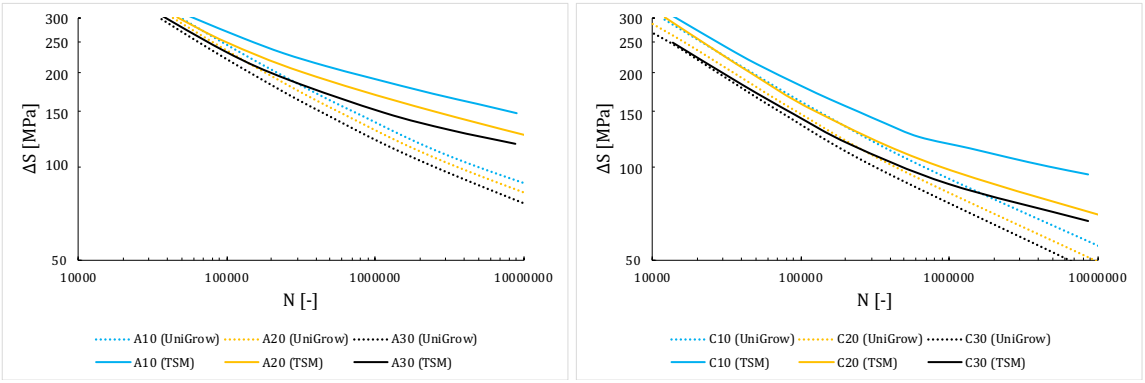

Figure 4.43 S-N curves total fatigue life generated by the Two-Stage-Model [64] and UniGrow model at different thicknesses for A quality (left) and C quality (right) welds using the SIF from WF method

In Figure 4.44 and Figure 4.45, the relative difference in fatigue life between various weld geometries as predicted by the UniGrow method and the Two-Stage-Model are presented. Here, it can be seen that, indeed, at high stress ranges, the two models predict very similar differences between two geometries. However, as the stress range gets lower, the predicted relative difference between two geometries by the two models starts to deviate. This is caused by underestimation of the fatigue crack initiation.

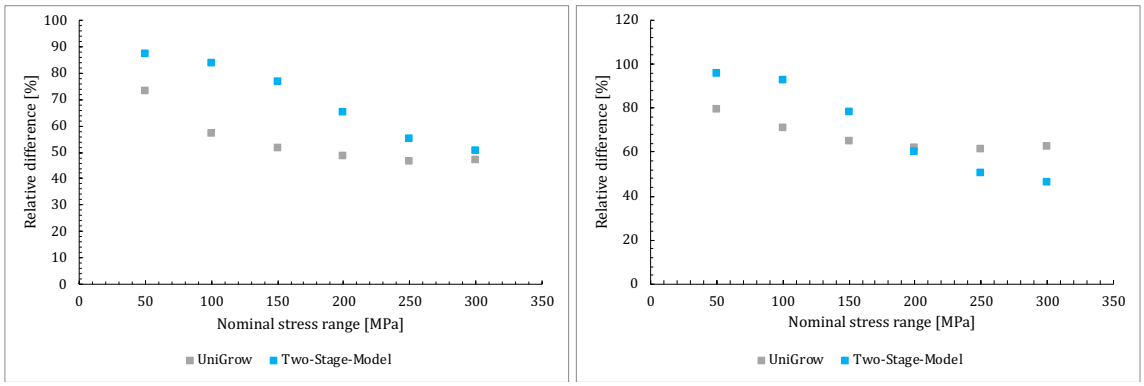

Figure 4.44 Relative difference between predicted fatigue lives of A20 and B20 (left) and B20 and C20 (right) predicted by the UniGrow model and the Two-Stage-Model [64]

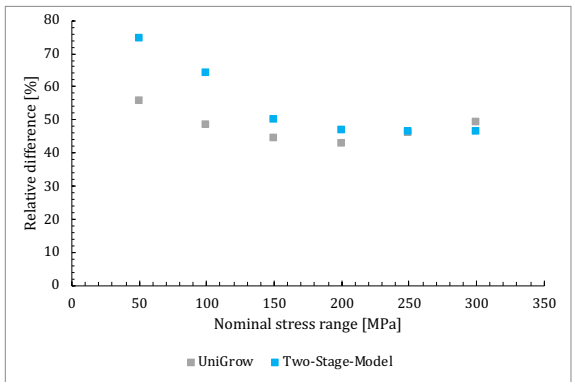

Figure 4.45 Relative difference between predicted fatigue lives of C20 and D20 predicted by the UniGrow model and the Two-Stage-Model [64]

The same effect can be seen when comparing the relative difference between welds of different thicknesses as is depicted in Figure 4.46 and Figure 4.47. Here, the relative difference between the geometries of different thicknesses is vastly underestimated by the UniGrow method for low stress ranges. The different between the two methods is much larger than when comparing geometries of the same thickness. For high stress ranges, however, the two models are in better agreement.

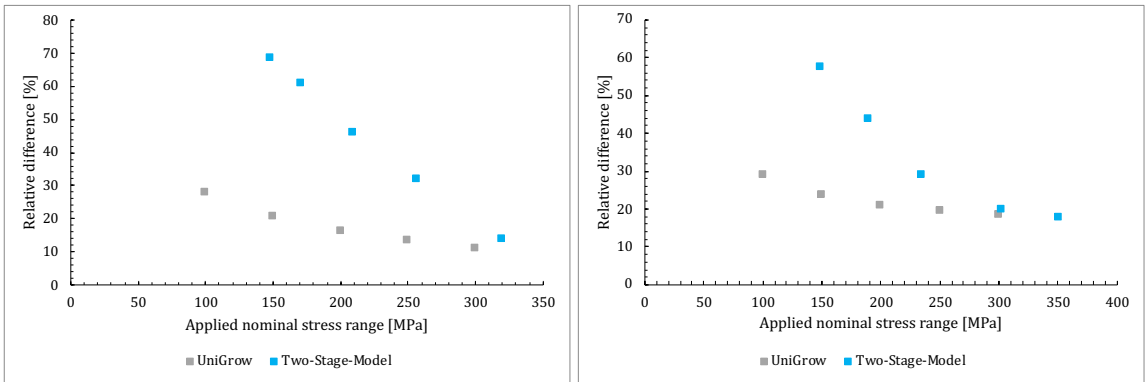

Figure 4.46 Relative difference between predicted fatigue lives of A10 and A20 (left) and A20 and A30 (right) predicted by the UniGrow model and the Two-Stage-Model [64]

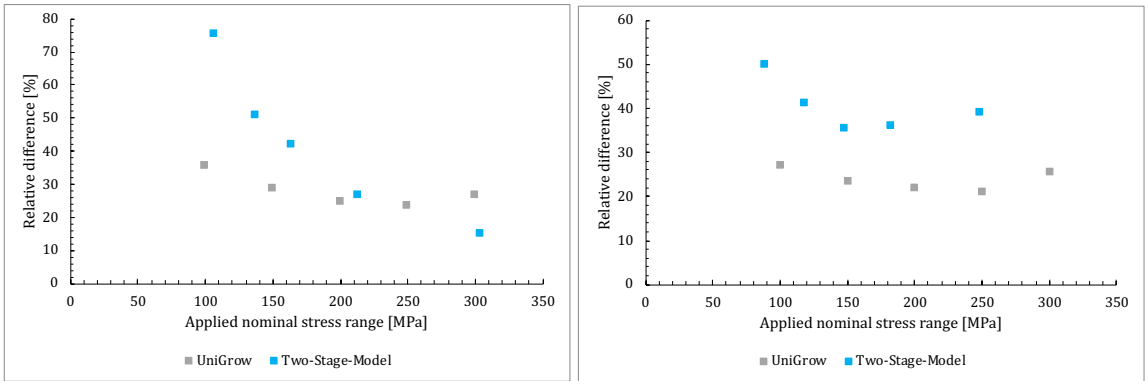

Figure 4.47 Relative difference between predicted fatigue lives of C10 and C20 (left) and C20 and C30 (right) predicted by the UniGrow model and the Two-Stage-Model [64]

4.5.4.3 Discussion

In the previous section, results of the calculations using the UniGrow model have been presented. This section will now present a discussion of those results in two sections: crack growth rates and total fatigue life.

Crack growth rates

From the first section of the results, it was concluded that the differences between the two models are caused by a combination of three factors: the applied SIFs, crack growth speed determination and a simplified crack shape.

The UniGrow model doesn't necessarily perform worse than the Two-Stage-Model in the crack propagation regime: simplifications have also been made on the side of the Two-Stage-Model by e.g. using the Paris-Law to describe the crack growth. Speaking of over- or underestimation when comparing crack growth speed predictions by UniGrow and Two-Stage-Model might thus lead to unjust conclusions. This is because other results (e.g. Figure 3.55) have also shown that experimental crack growth speed curves don't exactly follow the linear log-log Paris-Law but are actually curved.

Differences between the two crack growth speed curves and thus the predicted fatigue crack propagation life can thus be said to be intrinsic to the two methods and is something that cannot be altered. However, something that can be improved is the determination of the applied SIF when using the UniGrow method. Currently, it is recommended to determine this with the weight function method, however it has been shown that the FEA results provide slightly better comparison to results by Röscher et al [64].

Total fatigue life

In section 4.1, several researches where the UniGrow method was used to determine the total fatigue life of a specimen were discussed. From this research, it could be concluded that the UniGrow model was only able to predict satisfactory fatigue lives of specimens which spent most of their life in crack propagation regime (i.e. welded specimens with high SCF and the LCF range for notched specimens).

This hypothesis seems to be further confirmed by the results that have been presented in section 4.1. The UniGrow fatigue life results match quite well with the results by Röscher et al [64] for predicted fatigue lives lower than 10^5. However, between 10^5 – 10^6 cycles, the total fatigue life predictions start to deviate from the Two-Stage-Model. This difference could mainly be attributed to the inaccuracy in predicting the fatigue crack initiation life of the specimens, as the predicted fatigue crack propagation lives matched very well with the Two-Stage-Model (which can be seen in Figure 4.35). This is similar to what was predicted by Bang et al [1].

When talking about the shortcomings of the UniGrow method and thus points of improvement, focus should really be on the SC growth. The general crack growth curve that is generated by using the UniGrow method in combination with the correction method is displayed in Figure 4.48. The shape of this curve, somewhat, resembles that found in experiments. However, still a relatively big jump between the SC and LC regime is found, whereas the two curves should slowly merge. As shown before, short crack growth is very complex: crack growth speeds show more scatter and usually depend on the maximum stress that is applied. Cracks can even fully arrest. Even though the currently implemented model has many similarities with the Unified Approach, at its current state, the model is not capable to fully capture the short crack complexities.

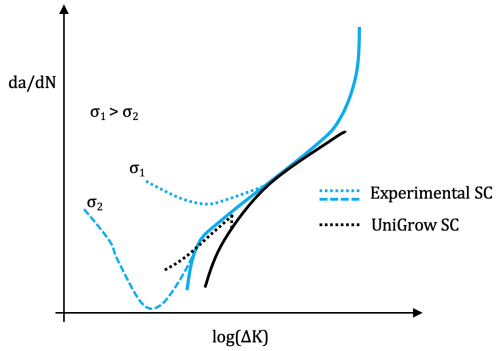

Figure 4.48 Typical crack growth curves for short cracks when using different methods

When looking at the capability of the currently implemented UniGrow method to predict the relative differences between welds of different quality and thickness, the model shows the same trends as predicted by Röscher et al [83]. Similar relative difference between weld qualities have especially been found when comparing the geometries with the same thickness but with different weld qualities, although UniGrow usually predicts a lower relative difference at low stress ranges. This is most probably directly related to the underestimation of the crack initiation life. When the weld quality remains the same, but the thickness changes, UniGrow tends to predict a lower relative difference at low stress ranges compared to the Two-Stage-Model. However, since the Two-Stage-Model is also a model, it is impossible to draw any hard conclusions from this comparison.

Validity limit of the UniGrow model

Based on the current study and the literature that was presented in section 4.1.5, it is reasonable to propose that the UniGrow model for Mode I cracks is solely valid for cracks where crack propagation is a dominant part of the fatigue life. This includes welded details with high SCF as was studied by Bogdanov et al [3] and Mikheevskiy et al [36] and the Low Cycle Fatigue range for notched geometries without weld as was studied by Bang et al [1] and the current study.

For notched geometries, no clear transition point in terms of applied stress can be defined due to varying SCF and materials that have been used. However, from Figure 4.8 and Figure 4.42, the upper bound of the validity of the UniGrow model for notched geometries with various SCF varies between 10^5 and 10^6 cycles. A safe validity limit would in this case be 10^5 cycles, which is often stated as the boundary between LCF and HCF. However, the validity limit could be lower for notches and welds that have a lower SCF. This was observed in Figure 4.42, where the point of deviation shifts to the left as the SCF gets lower (going from D to A weld quality).

For welded geometries, including weld residual stresses, additional research is needed. The model has shown proper functioning for fillet welded details, but it is questionable whether the UniGrow model functions properly for the butt welds used by SGRE, which are generally of quite high quality (i.e. higher contribution of crack initiation to total fatigue life)

5 Parametric Study

Currently, SGRE is working on optimising the design of the turbine towers. One of the governing limit states in design is the fatigue of the welds in the structure. Welds are generally considered to be weak spots due to three aspects:

- Welding causes high tensile residual stresses in the material
- Welding often leaves discontinuities in the material which can decrease the crack initiation life
- The discontinuity in the plates caused by the weld excess causes a stress concentration which locally increases the stresses around the weld toe

Various methods of improvement have been proposed to solve the issues mentioned above. The focus of this chapter will be on the geometry of the weld excess of a butt weld. In section 2.2, four main parameters were found to influence the fatigue life. The influence of three of those parameters (given in Figure 5.1): the weld flank angle, weld toe radius and weld excess height, on the fatigue life of butt-welded geometries will be studied in this chapter. The analysis will be performed with the previously introduced UniGrow method.

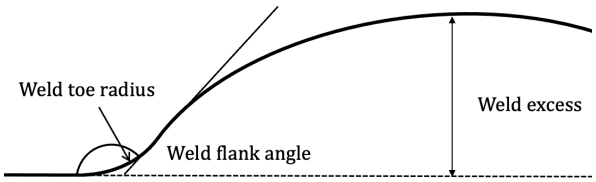

Figure 5.1 Parameters of the weld excess that will be studied in this chapter

In the previous chapter, it was concluded that the UniGrow predict the same trends as the Two-Stage-Model when comparing the relative difference between welds of the same thickness but different quality. Even for stress ranges where the fatigue life was over 10^5 cycles, the UniGrow method predicted similar relative difference, although they were generally lower than predicted by the Two-Stage-Model. With this in mind, the UniGrow model will be used to examine the effect changing the weld toe radius, weld flank angle and weld excess height.

First the data used in the model and the parametric study will be introduced. Subsequently, the implemented UniGrow model and its assumptions will be discussed. This is followed by further explanation of the methods used in this UniGrow method. Lastly, the results are presented and discussed.

5.1 Model data

In this section, the material data used in the parametric study will first be introduced. This is followed by a description of the parametric study that will be done including argumentation as to the bounds of the parameters that are varied.

5.1.1 Material data

The material used in the turbine towers is a mild steel, the parametric study should reflect that. Therefore, the material used in the parametric study will be the S355 steel examined in chapter 4, the same one that was used by Röscher et al [64]. As these material properties were based on the Uniform Material Law from average S355 properties, these will be representative for an average, synthetic S355 steel. Furthermore, this prevents having to redetermine the ΔK_{app} - K_{res} relationship. The material data is given in Table 5.1.

Material parameters		Fatigue parameters	
f_y	355 MPa	σ_f'	735 MPa
f_u	490 MPa	b	-0.087
E	210000 MPa	ε_f'	0.59
ν	0.3	c	-0.58
K'	808.5 MPa	K_{Ic}	2000 N/mm$^{3/2}$
n'	0.15	ΔK_0	180 N/mm$^{3/2}$

Table 5.1 Material parameters for the S355 steel

5.1.2 Parametric study

As discussed before, three parameters will be varied in the parametric study: weld toe radius, weld flank angle and weld excess height. The modelled geometry will have a thickness of 40 mm, as this is representative of the thicknesses used in the turbine towers. The width of the weld is assumed to be equal to the thickness of the plate. This is due to the fact that plates are often bevelled at 45 degrees, resulting in a length width which is approximately the same as the thickness. The global model with the parameters that can be varied is given in Figure 5.2.

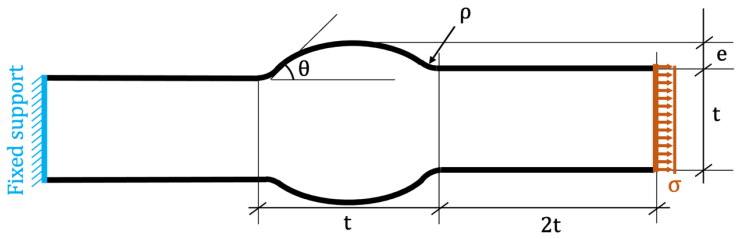

Figure 5.2 Model of weld used in the parametric study

5.1.2.1 Weld flank angle

In theory, the weld flank angle can vary between 90 and 180 degrees. In EN 1090-2:2018, for welds used in structural components, execution class EXC3 is required. This requires the weld angle to be larger than 150 degrees. However, at SGRE internally, for DC90 curves 130 degrees is a manufacturing requirement. Recently, SGRE have proposed a new S-N curve which does require weld flank angles larger than 150 degrees. Based on these values, it was chosen to vary the weld flank angle between 120 and 160 degrees, with increments of 10 degrees. This allows evaluation of the effect of going from 130 to 150 degrees and allows evaluation of what occurs if the weld flank angle is further increased.

5.1.2.2 Weld toe radius

The most commonly assumed value for the weld toe radius is 1 mm. This is taken as center value for the weld toe radius. The weld toe radius has been varied between 0.5 mm and 1.5 mm with increments of 0.25 mm. This range was chosen as it gave approximately the same range of SCF as the other two parameters, which made for good comparison.

5.1.2.3 Weld excess

In EN 1993-1-9 [41], welds in detail class 90 have a limitation on the weld excess maximum 10% of the weld width. Since in this case the weld with is equal to the thickness of the plate, this would be a maximum of 4 mm. This is taken as outer value since welds are not allowed to have a higher excess. The weld excess height has been varied between 2 and 4 mm with increments of 0.5 mm.

5.1.2.4 Overview of modelled geometries

In Table 5.2, an overview of the ranges of the parameters are given. The base case is defined as the weld with all parameters at the middle value. The parametric study will subsequently be done by varying one of the parameters of the base case each time. This will result in 13 different simulations.

Parameter	Low value	Medium-low value	Middle value	Medium-high value	High value	Other parameters
Weld excess	2 mm	2.5 mm	3 mm	3.5 mm	4 mm	Weld toe radius = 1 mm Weld flank angle = 140°
Weld toe radius	0.5 mm	0.75 mm	1 mm	1.25 mm	1.5 mm	Weld excess = 3 mm Weld flank angle = 140°
Weld flank angle	120°	130°	140°	150°	160°	Weld toe radius = 1 mm Weld excess = 3 mm

Table 5.2 Ranges of the parameters used in the parametric study

5.1.2.5 Performance indicator

To determine the performance of the weld geometries, a performance indicator has to be specified. In the section 4.5.4.3, the validity limit of the UniGrow method for notched geometries was specified as lower than 100,000 - 1,000,000 cycles. Since the validity range is given in terms of number of cycles, it is opted to use the applied stress range at a given number of cycles as performance indicator. The stress range resulting in a fatigue life of 100,000 cycles will be determined (as this is the validity limit of the UniGrow method).

Furthermore, stress range resulting in a fatigue life of 2,000,000 cycles will be determined. This is slightly outside the proposed validity limit but is a value that is often used to define the fatigue detail classes. However, it is approximately known how the model behaves for stresses slightly outside of the validity range, which can be used to assess the results.

5.2 Global UniGrow implementation

The crack growth is modelled in a similar way as has been done in chapter 4. This means that the following assumptions will be made:

- **Crack type:** It is assumed that an edge crack is present in the weld. The crack initiates from the point where the principal stresses are the highest and grows straight down (at right angles to the applied stress direction). It is assumed that pure Mode I crack growth is applicable here, even though shear stresses might be present. A comparison of the crack growth predicted by the UniGrow model and the Two-Stage-Model is presented in Figure 4.10.
- **Weld residual stresses:** Weld residual stresses will be neglected in the calculations. Solely the influence of geometry is of consideration in this research.
- **Applied stress:** The applied stress is assumed to have a constant stress range and a stress ratio of R = 0.
- **Material parameters:** The base material, weld material and heat affected zone are assumed to made from the same material and thus have the same material parameters.
- **Failure:** Failure of the specimen is specified as reaching the toughness of the material or a crack length of 20 mm.

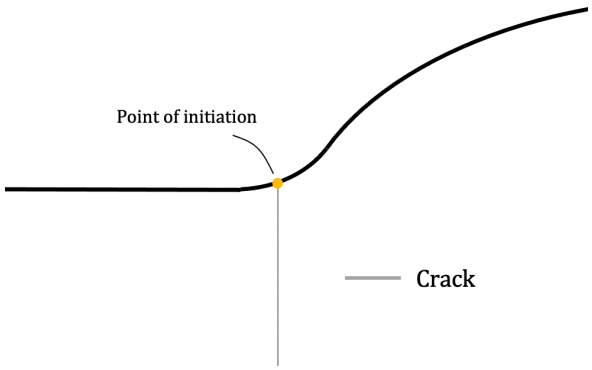

Figure 5.3 Schematic of assumed crack growth in UniGrow method and Two-Stage-Model

In this validation step, the method as given in Figure 5.4 will be used. The calculation procedure is largely the same as the one used in chapter 3.3. The global steps of the UniGrow method will be performed as follows:

1. **Determination of the applied stress intensity factor:** The applied stress intensity factor will be established using the weight function method. The edge crack weight function will be used to determine the SIF. In previous chapter it has been shown to yield proper results. Furthermore, determining the SIF for 13 cracks at multiple crack lengths would require a tremendous amount of time, which is unfortunately not available.

   A linear elastic FEA model will be made to determine the normal stresses (stresses perpendicular to crack direction) in the critical crack cross section. This is the cross section where the principal stress was found to be the highest. This topic will be addressed further in section 5.3.1.
2. **Determination of the elastoplastic stress distribution ahead of the crack tip:** Since the same material has been used as in the previous chapter, the relationship between K_{res} and ΔK_{app} determined in section 4.5.2 will be used.

3. **Determination of the residual stress intensity factor:** Since the same material has been used as in the previous chapter, the relationship between K_{res} and ΔK_{app} determined in section 4.5.2 will be used.
4. **Determination of the elastoplastic stress and strain on first elementary block ahead of the crack tip:** This will be done using the Creager-Paris equations in combination with the Neuber uniaxial plasticity correction. This will not be further addressed in this chapter as this has been discussed before, reference is made to section 3.1.3.4 for background.
5. **Determination of the initiation life of the first elementary block ahead of crack tip:** The initiation life was determined using the Smith-Watson-Topper damage parameter. No use will be made of the Morrow method as this is not valid for SC. This will not be further addressed in this chapter as this has been discussed before, reference is made to section 3.1.3.5 for background.

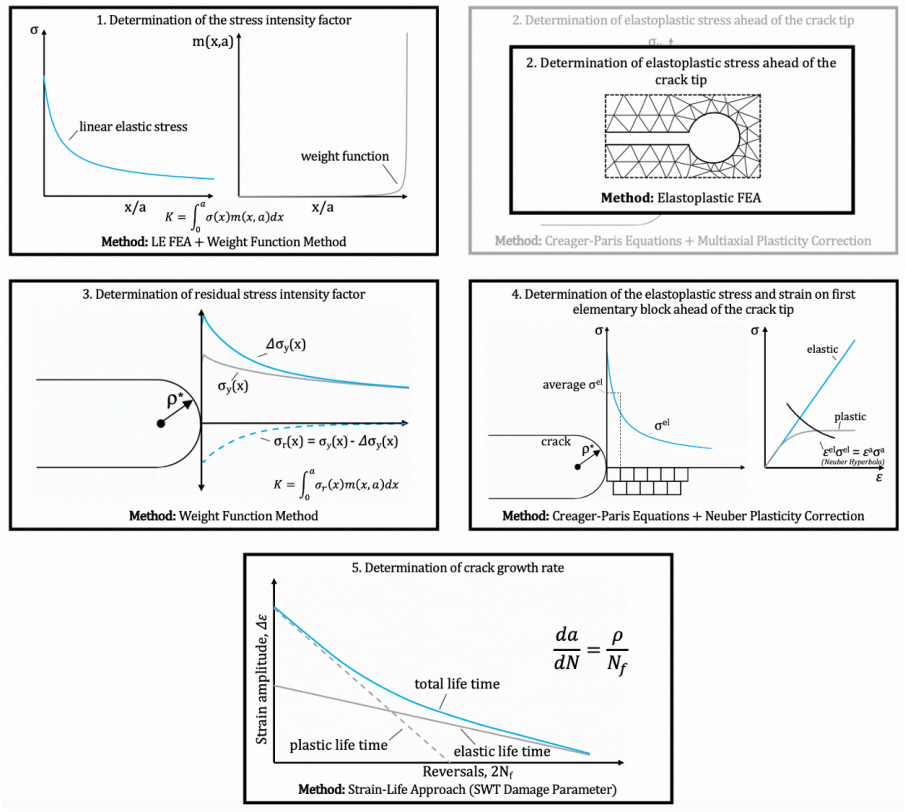

Figure 5.4 Global calculation procedure of the numerical UniGrow method

5.3 Calculation methods

In this section, attention will be given to some methods that are specific to this implementation of the UniGrow method. First, the determination of the stress in the crack plan for the determination of the applied SIF will be discussed, after which the full implementation of the UniGrow model will be presented.

5.3.1 Determination of stress in crack plane

An important part in the determination of the applied SIF is the elastic stress in the crack plane. This section will discuss how the geometries are modelled in the commercial software package ANSYS 18.2.

5.3.1.1 Modelling the geometry

To determine the stress in the critical cross section (i.e. the cross-section perpendicular to the applied stress where the highest principal stress is found), a linear elastic FEA model has been made. The model follows the sizes specified in Table 5.2. Since specific sizes of the weld excess were necessary, it was impossible to model the weld as a perfect arc. A different method using splines was therefore used, as was also proposed by other authors such as Pachoud et al [55].

In this method, first the required weld toe has to be inserted into the model. Subsequently a spline was used to connect either side of the weld. The spline was set to be tangent to the ends of the weld toes as to prevent stress concentrations. At the top of the weld, the spline was set to be tangent to the plates. An example of the spline and the spline points is given in Figure 5.5. It was made sure that the spline controls on the top were always on one horizontal line.

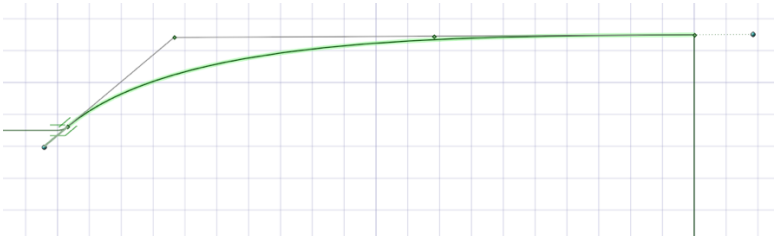

Figure 5.5 Example of spline used to model the weld

Due to symmetry, only a quarter of the weld was required to be modelled. One end of the mode is loaded with a uniform stress. The length of the plate in the model is equal to twice the thickness to ensure proper introduction of the stresses. A summary of the model can be found in Figure 5.6.

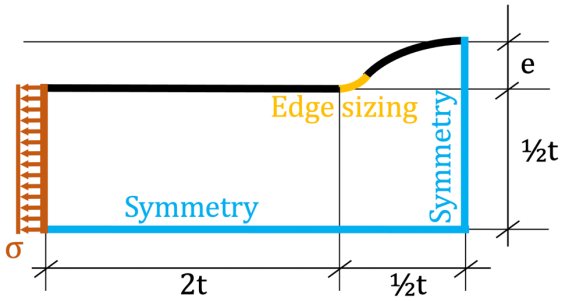

Figure 5.6 Constraints and loads on the linear elastic FEA model of the weld

5.3.1.2 Mesh size

The overall mesh size used in the model was 0.5 mm with a more refined mesh around points where stress concentrations might occur: the weld toes in this case. In the radius of the weld toe, edge sizing has been applied with various sizes until the model had converged as specified in Figure 5.6. The commercial software package ANSYS 18.2 was used to model the welds. Quadratic, triangular plane stress elements have been used due to the limited thickness of the model. Meshing was done using the advancing front method to limit distortion in the elements. A summary of the mesh sizing is given in Figure 5.7.

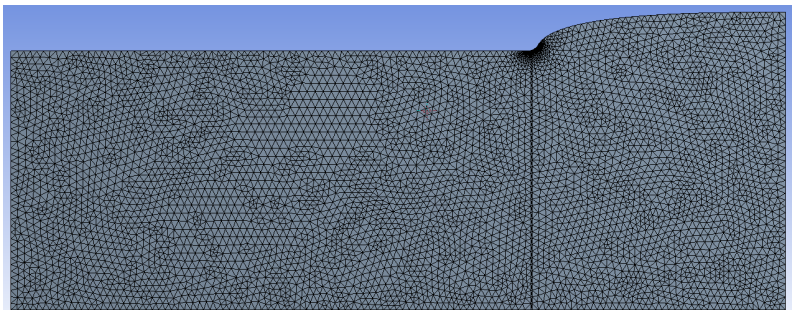

Figure 5.7 Overview of the mesh for the FEA model of the weld

Mesh sensitivity was studied using the 0.5 mm weld toe radius geometry. This geometry was chosen as the transition from the plate to the weld was the most sudden and thus requires the smallest element size. The weld was loaded with a uniform stress of 1 MPa and the element size was varied from 0.5 to 0.025 mm. An overview of the model and mesh in ANSYS is given in Figure 4.14, here, the aforementioned mesh controls can be seen. A more detailed picture of the mesh at the crack tip can be viewed in Figure 4.15 and Figure 4.16. The maximum principal stress reported in each model is reported in Table 4.4. From this, it can be seen that the mesh can be considered to converge at an element size of 0.025 mm.

Element size	σ_1 [MPa]	% change
0.5 mm	2.44	-
0.1 mm	3.08	26,2
0.05 mm	3.11	0,97
0.025 mm	3.11	0,0

Table 5.3 Maximum elastic principal stress for distinct mesh sizes for the geometry with 0.5 mm weld toe radius (σ = 1 MPa)

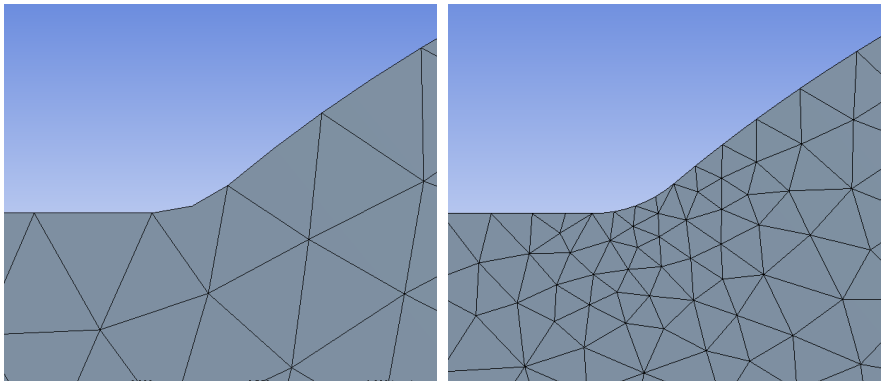

Figure 5.8 Mesh size at weld toe for an edge size of 0.5 mm (left) and 0.1 mm (right)

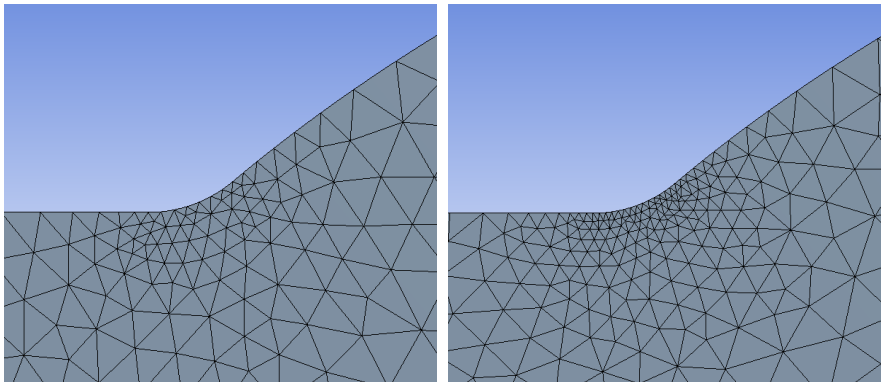

Figure 5.9 Mesh size at weld toe for an edge size of 0.05 mm (left) and 0.025 mm (right)

5.3.2 Implementation in Python

The full implementation of the UniGrow method in Python is the same as the one used in section 4.4.3. The flowchart of the model is given in Figure 4.27 and further background is provided in section 4.4.3. The step size used in the previous model has been changed to 0.1 mm in these calculations.

A large difference between the UniGrow model used in section 4.4.3 and the one used in this chapter is the inclusion of an additional loop around the whole model. This loop allows easy determination of the constant amplitude stress range corresponding to either 100,000 or 2,000,000 cycles. The model starts at an initial maximum stress (the minimum stress is zero, since R = 0) which results in a fatigue life higher than 100,000 or 2,000,000 cycles. The model then increases the nominal stress until the stress range is found at which the fatigue drops below the number of cycles. Linear interpolation is subsequently used to determine the exact constant amplitude stress range at which a fatigue life of the given number of cycles is reached.

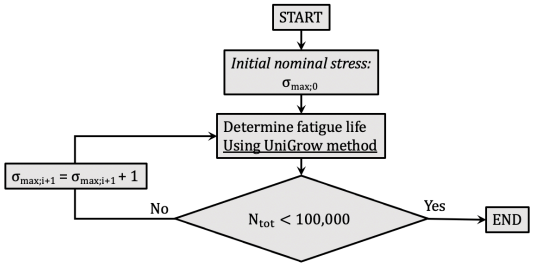

Figure 5.10 Flowchart used for the determination of the total fatigue life of a welded specimen

5.4 Results and Discussion

In this section, the result of the parametric study will be presented and discussed. First, the stress profiles resulting from the various geometries are presented. Followed by the effect of each parameter on the fatigue performance and a comparison of all the parameters on the fatigue performance.

5.4.1 Stress Profiles

The stress profiles of the prospect crack plane resulting from the linear elastic FEA analyses are given in Figure 5.11 - Figure 5.13. The first thing that can be noticed from this is that varying a certain parameter has a very different effect on the stress in the crack plane. Changing the weld toe radius, for example, has a rather local change of the stress concentration (only the first 0.5 mm), whereas changing the weld excess impacts the stress distributions up to a depth of 2.5 mm.

Based on these observations, it is expected that changing the weld excess will have the biggest effect on the total fatigue life, with the weld toe radius having the smallest effect. Furthermore, since the effect of the weld toe radius on the stress distribution is so localized, it is expected that it mainly affects the length of the fatigue crack initiation phase.

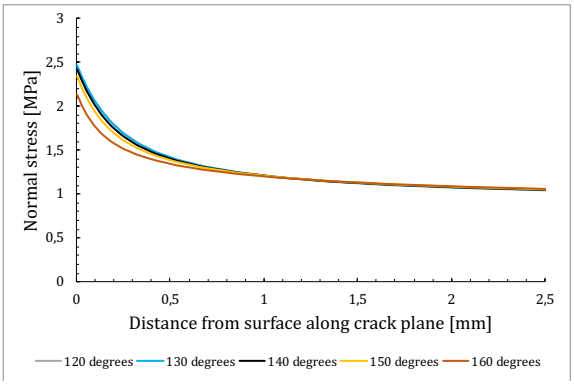

Figure 5.11 Influence of the weld flank angle on the stress concentration in the crack plane

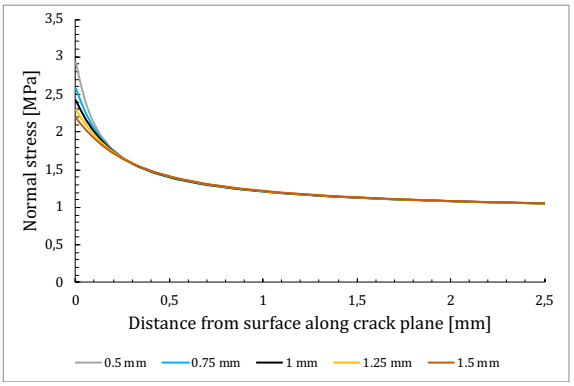

Figure 5.12 Influence of the weld toe radius on the stress concentration in the crack plane

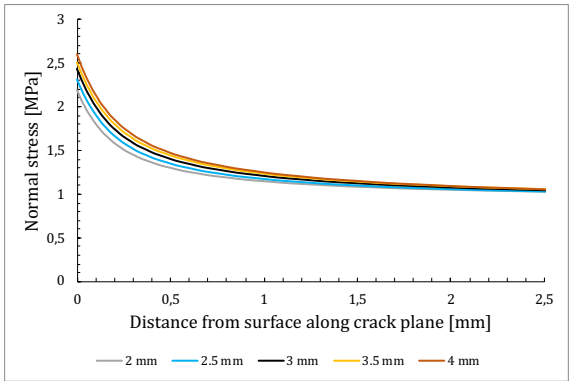

Figure 5.13 Influence of the weld excess on the stress concentration in the crack plane

5.4.2 Influence of geometrical parameters

The weld flank angle, weld toe radius and weld excess height all have varying effects on the fatigue performance of the weld. These effects will be presented in this section, after which the effects will be compared.

5.4.2.1 Weld flank angle

The constant amplitude stress range resulting in a fatigue life of 100,000 and 2,000,000 cycles as a function of the flank angle is given in Figure 5.14. Relative differences have been determined upon comparison to the base case. The change in performance relative to the base case has also been determined. Very little change in the stress range is observed when decreasing the flank angle below 130 degrees, whereas a significant improvement of the fatigue performance is observed for flank angles >150 degrees. Relative results for 100,000 and 2,000,000 cycles are very similar, whereas a relatively larger relative difference between the models is expected at 2,000,000 cycles, which was observed in for example Figure 4.44.

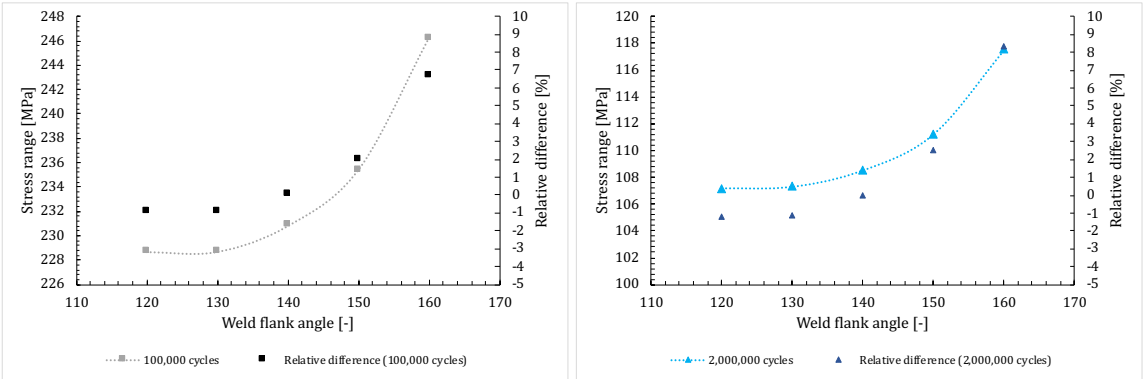

Figure 5.14 Influence of the weld flank angle on the constant amplitude stress range needed to obtain a fatigue life of 100,000 (left) and 2,000,000 cycles (right)

5.4.2.2 Weld toe radius

The constant amplitude stress range resulting in a fatigue life of 100,000 and 2,000,000 cycles as a function of the flank angle is given in Figure 5.15. Relative differences have been determined upon comparison to the base case. The change in performance relative to the base case has also been determined. Very little influence of changing the radius on the fatigue life is observed, just a mere 2% in both directions. Here, the relative difference at 100,000 and 2,000,000 cycles is also very similar.

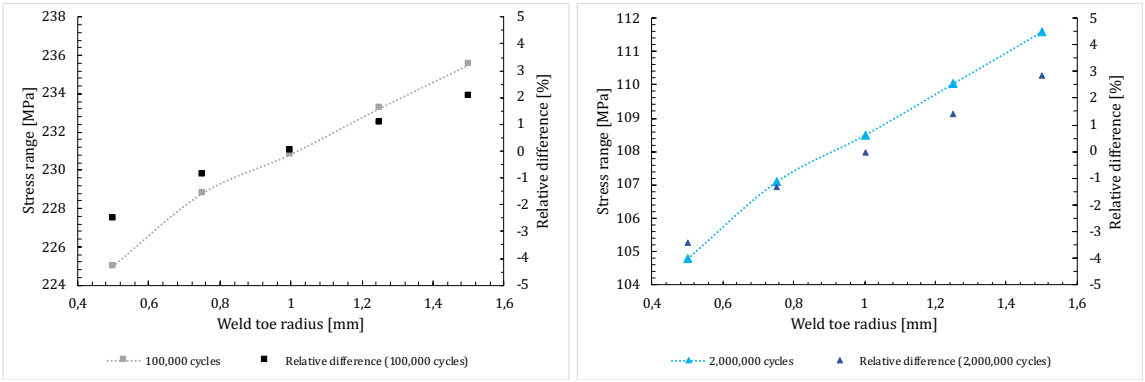

Figure 5.15 Influence of the weld toe radius on the constant amplitude stress range needed to obtain a fatigue life of 100,000 and 2,000,000 cycles

5.4.2.3 Weld excess height

The constant amplitude stress range resulting in a fatigue life of 100,000 and 2,000,000 cycles as a function of the flank angle is given in Figure 5.16. Relative differences have been determined upon comparison to the base case. The change in performance relative to the base case has also been displayed in this figure. Changing the weld excess height has a substantial effect on the fatigue life. Almost a 15% total increase of fatigue performance is observed when reducing the weld excess from 4 to 2 mm. Here, the relative difference at 100,000 and 2,000,000 cycles is also very similar.

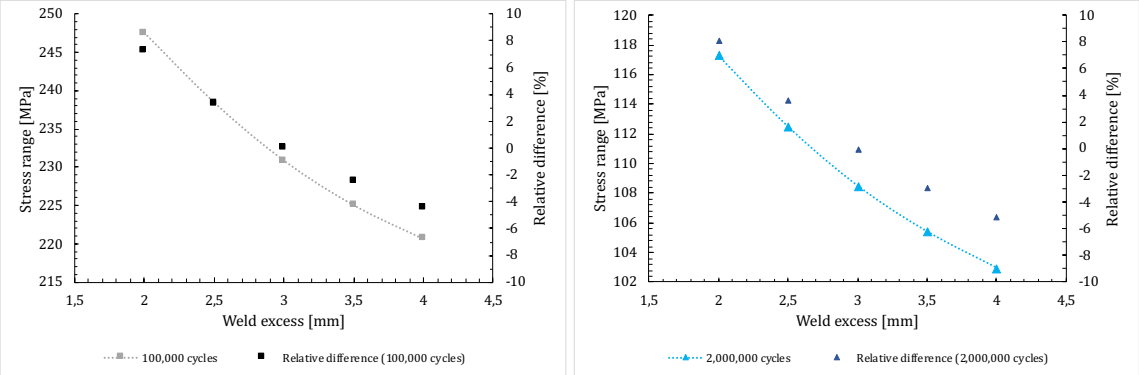

Figure 5.16 Influence of the weld excess on the constant amplitude stress range needed to obtain a fatigue life of 100,000 and 2,000,000 cycles

5.4.2.4 Comparing influence of parameters

As could be seen in the previous section, the parameters have varying influence on the fatigue performance of the weld. To be able to compare the three parameters, the SCF (defined as in Eq. (4.7)) of each geometry was determined. The results are given in Table 5.4. This then allows for comparing the effect of the three parameters. A plot of the stress range required to reach 100,000/2,000,000 cycles as function of the SCF of the weld geometries is given in Figure 5.17 and Figure 5.18. Since the relative differences between the weld geometries was approximately the same at 100,000 and 2,000,000 cycles, the graphs are very much alike.

Parameter	Low value	Medium-low value	Middle value	Medium-high value	High value
Weld excess	2 mm	2.5 mm	3 mm	3.5 mm	4 mm
SCF	**2.3**	**2.44**	**2.55**	**2.66**	**2.75**
Weld toe radius	0.5 mm	0.75 mm	1 mm	1.25 mm	1.5 mm
SCF	**3.1**	**2.76**	**2.55**	**2.41**	**2.3**
Weld flank angle	120°	130°	140°	150°	160°
SCF	**2.66**	**2.64**	**2.55**	**2.43**	**2.19**

Table 5.4 SCF belonging to each of the analysed geometries

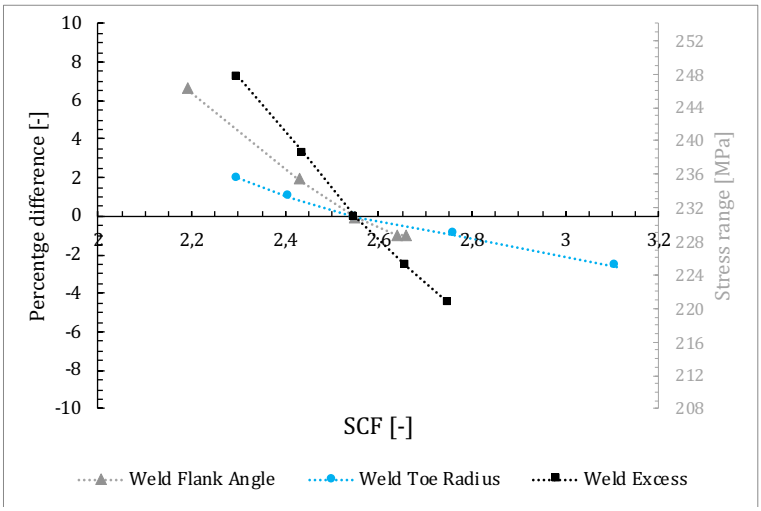

Figure 5.17 Change in constant amplitude stress needed to obtain a fatigue life of 100,000 cycles as function of SCF generated for the various weld geometries

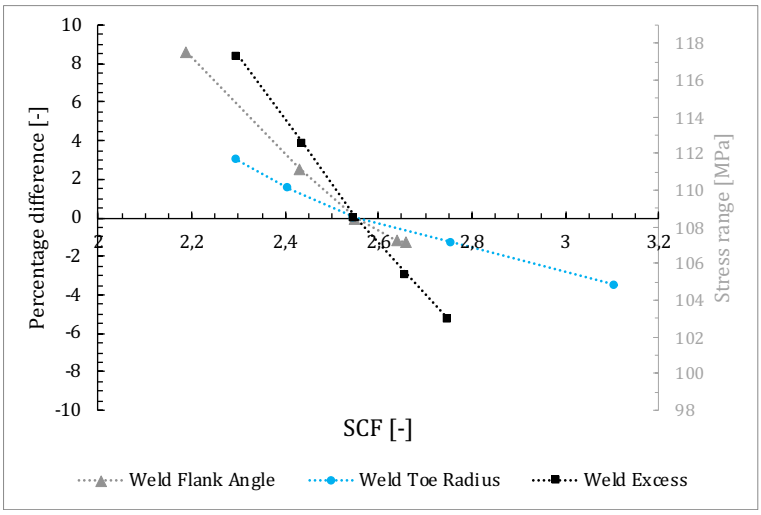

Figure 5.18 Change in constant amplitude stress needed to obtain a fatigue life of 2,000,000 cycles as function of SCF generated for the various weld geometries

In Figure 5.17 and Figure 5.18 it can be observed that even though changing the weld toe radius has a major influence on the local SCF at the weld toe, the UniGrow method predicts that the improvement in fatigue performance is limited. This is due to the fact that the stress only changes very locally at the surface. Changing the weld excess, on the other hand, has limited influence on the observed SCF, but increases the fatigue performance significantly. This is due to the fact that the stress in the crack plane changes to a much deeper depth, influencing more of the crack growth.

5.4.2.5 Contribution of crack growth stages

As stated before, it is expected that the local effect on the stress caused by changing the weld toe radius only affects the fatigue initiation life. To further investigate the effect of changing parameters on the change in fatigue crack initiation and propagation life, all weld geometries were modelled with an applied stress range of 200 MPa (at R = 0). Fatigue crack initiation life was defined as the crack being smaller than 0.5 mm, similar to what was used in chapter 4. Failure was defined similarly as before. The results for each of the parameters are given in Figure 5.19 - Figure 5.21. Relative differences have been determined upon comparison to the base case.

From Figure 5.20, it becomes clear that the weld toe radius indeed only affects the fatigue crack initiation life. The crack propagation life varies very lightly, whereas the crack initiation life changes significantly. For the other two parameters, the highest relative change is also observed in the fatigue crack initiation life. This is due to the fact that the change in the stress distribution only affects the first few mm of crack propagation, therefore the effect on the crack propagation is limited.

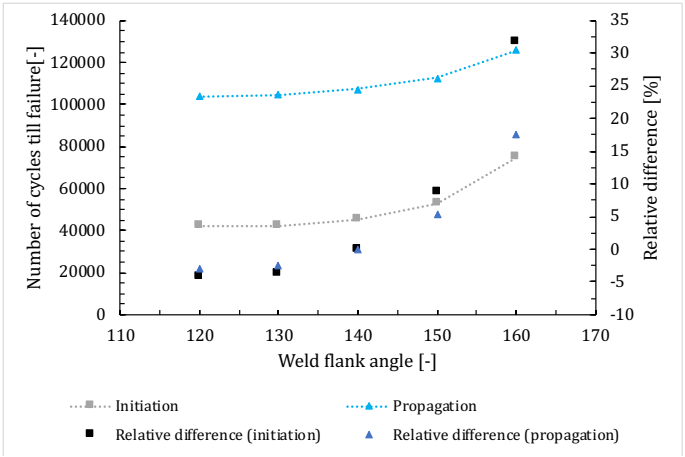

Figure 5.19 Number of cycles till failure in the two crack stages for varying weld flank angles ($\Delta\sigma = 200MPa$, R = 0)

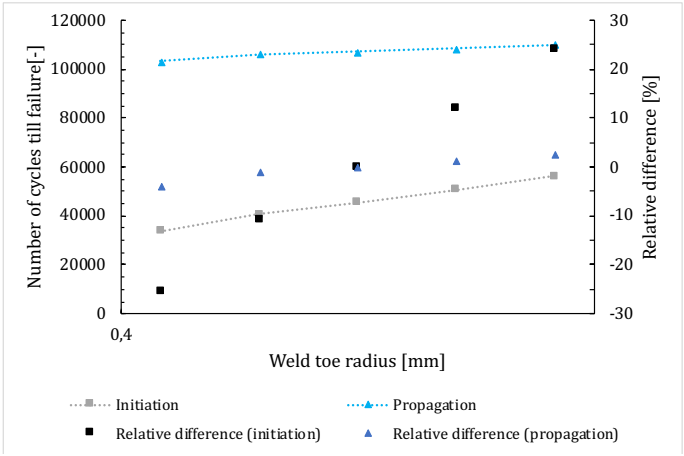

Figure 5.20 Number of cycles till failure in the two crack stages for varying weld toe radius ($\Delta\sigma = 200MPa$, R = 0)

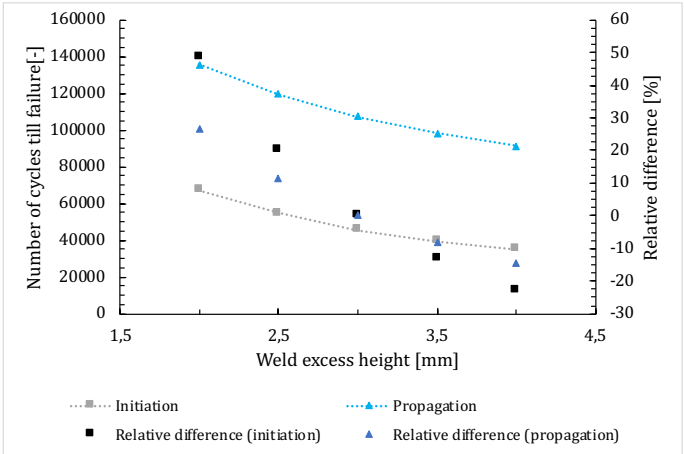

Figure 5.21 Number of cycles till failure in the two crack stages for varying weld excess height ($\Delta\sigma = 200MPa$, R = 0)

5.4.2.6 Comparison to Detail Class curve

To obtain a sense of how much the results produced by the UniGrow method differed from the actual detail class curves, a specimen with weld excess height of 4 mm and weld flank angle of 150 degrees (worst case scenario for a Detail Class 90 butt weld) was modelled. The resulting S-N curve compared to the DC90 curve is presented in Figure 5.22. It can be seen that the curve is in the correct ballpark, albeit not completely accurate due to mentioned effects from using the UniGrow method, neglecting residual stresses and the simplified crack shape and material model.

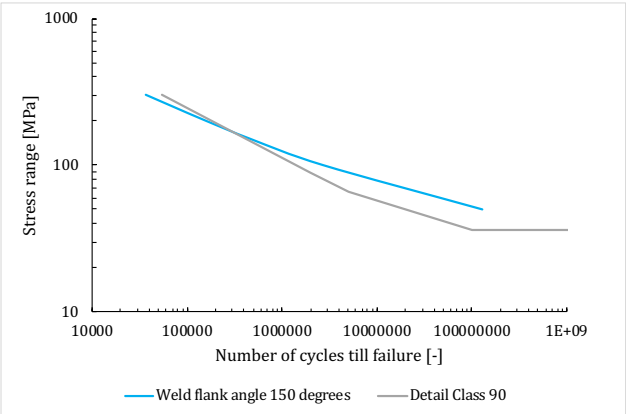

Figure 5.22 S-N curves of the worst-case scenario butt weld modelled with UniGrow compared to the Detail Class 90 curve

5.4.3 Discussion

In this section, the results present in the previous sections will be discussed.

5.4.3.1 Uncertainties in the model

The presented results should be observed with care, as several assumptions and simplifications have been made. Firstly, no weld residual stresses have been accounted for in this parametric study. Weld residual stresses cause an increase of the maximum and minimum SIF and thus locally increase the stress ratio. This usually increases crack rates, and it could lead to a decrease of the contribution of fatigue crack initiation to the total fatigue life. This could therefore influence the effect of parameters on the fatigue performance of welds.

Secondly, the usage of the UniGrow method provides some uncertainty. It has been shown in the previous chapter that the UniGrow method underestimates the fatigue crack initiation lives. This could mean that the effect of parameters that derive the improved fatigue performance from the crack initiation phase (like the weld toe radius) could be underestimated when using the UniGrow method. Furthermore, the relative difference at 2,000,000 cycles is most likely larger than predicted and not exactly the same as the relative difference at 100,000 cycles. This is due to the fact that the UniGrow method tends to predict lower relative differences between curves at a lower stress range, as has been shown in Figure 4.44.

Lastly, in this model, solely an edge crack has been considered. However, in real weld geometries, semi-elliptical cracks are present. The effect of this on the results is unclear and requires further study but has to be considered when the results are interpreted. Another simplification of which the effects are unclear is the modelling of the HAZ, weld material and plate material as the same material. Cracks usually grow in the HAZ, which can have different material properties than the material examined in this chapter. This could have its effect on the influence of the weld geometry parameters on the fatigue performance.

5.4.3.2 SCF of the welded geometry

What has can also be observed in this chapter is that the weld geometries that are usually employed by SGRE have relatively low SCF. They vary around 2.5, which is better than the welded geometries that have been analysed using UniGrow by e.g. Mikheevskiy et al [36] which have shown good results. This could again pose limits on the validity of the UniGrow method, as the better the quality of the welded connection, the more of its life is spent on fatigue crack initiation.

6 Conclusion and Recommendation

6.1 Conclusion

From the research that has been performed, the following conclusions, related to the research questions stated in section 1.3 can be drawn:

- The UniGrow model showed very good correspondence with experimental crack growth speed results of CT specimens made from S355 steel performed by De Jesus et al [11] and Carvalho et al [6]. Good predictions of the crack growth rate were observed for all tested stress ratios except R = 0.25. As was also found by previous research, the UniGrow method is capable of predicting crack growth rates in the crack propagation regime for various stress ratios. It is recommended to use a numerical method (elastoplastic FEA) to determine the plastic residual stresses ahead of the crack tip as this provides more physically accurate results.
- De Jesus et al [10] proposed to use the Morrow method instead of the SWT damage method to determine the fatigue life of the elementary block ahead of the crack tip. Results in this research confirmed the hypothesis that the Morrow method without considering the mean stress yielded better results than the SWT damage parameter in predicting the crack growth rates of the CT specimens. This is because the predicted fatigue initiation lives of the elementary block ahead of the crack are often in the LCF regime ($N_f < 5 * 10^4$cycles). In this regime, the specimen undergoes cyclic stress relaxation. However, for small cracks the fatigue life of the elementary block is much higher and use of the Morrow method without considering residual stresses is not recommended since cyclic stress relaxation does not occur.
- In the studied literature, researchers tend to use the weight function method to determine the SIF in welded geometries. Analysis comparing the weight function method to FEA results showed that for a flat plate, the WF method produced slightly higher (up to 3.5%) SIF predictions than FEA. For welded geometries, the WF method predicted significantly higher SIFs than FEA with difference up to 12%. Usage of FEA to determine the SIF also showed better correspondence between the UniGrow model and Two-Stage-Model. Therefore, it is recommended to use FEA to determine the SIF where precise fatigue life predictions are needed. For an initial estimation, however, the WF can be used without issues, as it is significantly faster and provides relatively accurate results.
- Based on the observations from literature and the comparison to the Two-Stage-Model the validity limit of the currently implemented UniGrow model for Mode I cracks was defined. The current implementation of the UniGrow method produces satisfactory results for cracks where crack propagation is a dominant part of the fatigue life (i.e. welded details or notched specimens in LCF regime). From the analysis of notched geometries with various SCF, the UniGrow model was found to be valid up to a range between 10^5 and 10^6 cycles. The limit seeming to depend on the SCF of the geometry. It is recommended to use the UniGrow method for notched specimens for fatigue lives up to 10^5 cycles. For welded details, no clear conclusion could be drawn yet, as more research specific to butt welded geometries (including weld residual stresses) is required.
- Results of the parametric study have shown that the parameters controlling the shape of the weld excess have various effects on the fatigue life. Changing the weld toe radius mainly led to an increase in the fatigue crack initiation life, whereas changing the weld excess height affected both crack stages quite significantly. The results of the parametric study were, however, subject to a lot of uncertainty from both the UniGrow model and neglecting the weld residual stresses.

6.2 Recommendations

For future research, the following recommendations can be done:

- In order to get a better understanding of the influencing properties of the weld geometry on the fatigue performance of butt welds, a more advanced version of the UniGrow method needs to be implemented. This version should be able to take into account the weld residual stresses and be able to model a semi-elliptical crack instead of the edge crack that was modelled currently.
- This model can then be used to evaluate butt welded geometries used by SGRE. SGRE butt welds are usually of quite high quality and therefore different from the fillet welds used in previous experiments. It is thus recommended to perform additional validation of the UniGrow method for the welded geometries used by SGRE.
- It would be interesting to do further research into the relation between the elementary block size and the grain size, as it could provide a means for using the UniGrow model without calibration to crack growth data. This would mean that the crack growth speed can be predict solely from strain-life tests and measurement of the grain sizes.

7 Bibliography

[1] Bang, D. J., Ince, A., & Tang, L. Q. (2019). A modification of UniGrow 2-parameter driving force model for short fatigue crack growth. *Fatigue & Fracture of Engineering Materials & Structures*, 42(1), 45-60. URL: https://doi.org/10.1111/ffe.12865

[2] Basquin, O. H. (1910). The exponential law of endurance tests. *In Proc Am Soc Test Mater* (Vol. 10, pp. 625-630).

[3] Bogdanov, S., Mikheevskiy, S., & Glinka, G. Draft: The fatigue life prediction methodology based on the UniGrow model. URL: https://www.researchgate.net/profile/G_Glinka/publication/315033663_The_Fatigue_Life_Prediction_Methodology_Based_on_the_Unigrow_Model/links/596e16ac0f7e9bd5f75f60ca/The-Fatigue-Life-Prediction-Methodology-Based-on-the-Unigrow-Model.pdf

[4] Bowness, D., & Lee, M. M. K. (2000). Prediction of weld toe magnification factors for semi-elliptical cracks in T–butt joints. *International Journal of Fatigue*, 22(5), 369-387. URL: https://doi.org/10.1016/S0142-1123(00)00012-8

[5] Bueckner, H. F. (1970). Novel principle for the computation of stress intensity factors. *Zeitschrift fuer Angewandte Mathematik & Mechanik*, 50(9).

[6] Carvalho, D., Silva, A. L. L., Jesus, A. M. P., & Fernandes, A. A. (2015). Fatigue behaviour of structural steels comparison of strain life and fatigue crack propagation data. *Mecanica Experimental*, 25, 67-78. URL: http://www-ext.lnec.pt/APAET/pdf/Rev_25_A7.pdf

[7] Cerit, M., Kokumer, O., & Genel, K. (2010). Stress concentration effects of undercut defect and reinforcement metal in butt welded joint. *Engineering Failure Analysis*, 17(2), 571-578. https://doi.org/10.1016/j.engfailanal.2009.10.010

[8] Correia, J. A. F. D. O., De Jesus, A. M., Moreira, P. M., Calçada, R. A., & Fernández-Canteli, A. (2016). Fatigue Crack Propagation Rates Prediction Using Probabilistic Strain-Based Models. *Fracture Mechanics: Properties, Patterns and Behaviours*, 245.

[9] Creager, M., & Paris, P. C. (1967). Elastic field equations for blunt cracks with reference to stress corrosion cracking. *International journal of fracture mechanics*, 3(4), 247-252. URL: https://link.springer.com/content/pdf/10.1007/BF00182890.pdf

[10] De Jesus, A. M., & Correia, J. A. (2013). Critical assessment of a local strain-based fatigue crack growth model using experimental data available for the P355NL1 steel. *Journal of Pressure Vessel Technology*, 135(1). URL: https://doi.org/10.1115/1.4006905

[11] De Jesus, A. M., Matos, R., Fontoura, B. F., Rebelo, C., da Silva, L. S., & Veljkovic, M. (2012). A comparison of the fatigue behavior between S355 and S690 steel grades. *Journal of Constructional Steel Research*, 79, 140-150. https://doi.org/10.1016/j.jcsr.2012.07.021

[12] Ferreira, J. M., & Branco, C. M. (1989). Influence of the radius of curvature at the weld toe in the fatigue strength of fillet welded joints. *International journal of fatigue*, 11(1), 29-36. https://doi.org/10.1016/0142-1123(89)90044-3

[13] Fett, T., Mattheck, C., & Munz, D. (1987). On the calculation of crack opening displacement from the stress intensity factor. *Engineering Fracture Mechanics*, 27(6), 697-715. URL: https://doi.org/10.1016/0013-7944(87)90159-7

[14] Fett, T., & Munz, D. (1997). Stress intensity factors and weight functions (Vol. 1). *Computational Mechanics*.

[15] Forsyth, P. J. E. (1983). A unified description of micro and macroscopic fatigue crack behaviour. *International Journal of Fatigue*, 5(1), 3-14. URL: https://doi.org/10.1016/0142-1123(83)90002-6

[16] Glinka, G., & Shen, G. (1991). Universal features of weight functions for cracks in mode I. *Engineering Fracture Mechanics*, 40(6), 1135-1146. URL: https://www.researchgate.net/profile/G_Glinka/publication/222584275_Universal_Features_of_Weight_Functions_for_Cracks_in_Mode_I/links/59d2a3e04585150177f64064/Universal-Features-of-Weight-Functions-for-Cracks-in-Mode-I.pdf

[17] Harati, E., Karlsson, L., Svensson, L. E., & Dalaei, K. (2015). The relative effects of residual stresses and weld toe geometry on fatigue life of weldments. *International journal of fatigue*, 77, 160-165. URL: https://doi.org/10.1016/j.ijfatigue.2015.03.023

[18] Hobbacher, A. (1993). Stress intensity factors of welded joints. *Engineering fracture mechanics*, 46(2), 173-182. URL: https://doi.org/10.1016/0013-7944(93)90278-Z

[19] Hussain, K. (1997). Short fatigue crack behaviour and analytical models: a review. *Engineering Fracture Mechanics*, 58(4), 327-354. URL: https://doi.org/10.1016/S0013-7944(97)00102-1

[20] Ibrahim, M. F. E., & Miller, K. J. (1979). Determination of fatigue crack initiation life. *Fatigue & Fracture of Engineering Materials & Structures*, 2(4), 351-360. URL: https://doi.org/10.1111/j.1460-2695.1979.tb01093.x

[21] Ince, A., & Glinka, G. (2011). A modification of Morrow and Smith–Watson–Topper mean stress correction models. *Fatigue & Fracture of Engineering Materials & Structures*, 34(11), 854-867. URL: https://doi.org/10.1111/j.1460-2695.2011.01577.x

[22] Kaya, A. C., & Erdogan, F. (1980). Stress intensity factors and COD in an orthotropic strip. *International Journal of Fracture*, 16(2), 171-190. URL: https://link.springer.com/content/pdf/10.1007/BF00012620.pdf

[23] Koh, S. K., & Stephens, R. I. (1991). Mean stress effects on low cycle fatigue for a high strength steel. *Fatigue & Fracture of Engineering Materials & Structures*, 14(4), 413-428. URL: https://doi.org/10.1111/j.1460-2695.1991.tb00672.x

[24] Lee, Y. L., & Barkey, M. E. (2011). Strain-Based Uniaxial Fatigue Analysis. *Metal Fatigue Analysis Handbook: Practical Problem-solving Techniques for Computer-aided Engineering*, 253.

[25] Lee, Y. L., & Barkey, M. E. (2011). Fundamentals of Cyclic Plasticity Theories. *Metal Fatigue Analysis Handbook: Practical Problem-solving Techniques for Computer-aided Engineering*, 253.

[26] Lee, C. H., Chang, K. H., Jang, G. C., & Lee, C. Y. (2009). Effect of weld geometry on the fatigue life of non-load-carrying fillet welded cruciform joints. *Engineering Failure Analysis*, 16(3), 849-855. URL: https://doi.org/10.1016/j.engfailanal.2008.07.004

[27] Ladinek, M., Niederwanger, A., Lang, R., Schmid, J., Timmers, R., & Lener, G. (2018). The strain-life approach applied to welded joints: Considering the real weld geometry. *Journal of Constructional Steel Research*, 148, 180-188. URL: https://doi.org/10.1016/j.jcsr.2018.04.024

[28] Ladinek, M., Niederwanger, A., Timmers, R., Lang, R., & Osterhuber, D. (2019). Nachweis der Ermüdungsfestigkeit mittels Kerbdehnungskonzept: Eine Einführung für Praktiker–Stand der Technik, Praxiseinsatz und aktuelle Forschung. *Stahlbau*, 88(5), 428-439. URL: https://doi.org/10.1002/stab.201800035

[29] Leggatt, R. H. (2008). Residual stresses in welded structures. *International Journal of Pressure Vessels and Piping*, 85(3), 144-151. URL: https://doi.org/10.1016/j.ijpvp.2007.10.004

[30] Lin, C. K., & Chu, C. C. (2000). Mean stress effects on low-cycle fatigue for a precipitation-hardening martensitic stainless steel in different tempers. *Fatigue & fracture of engineering materials & structures*, 23(7), 545-553. URL: https://doi-org.tudelft.idm.oclc.org/10.1046/j.1460-2695.2000.00324.x

[31] Llavori, I., Etxebarria, U., López-Jauregi, A., Ulacia, I., Ugarte, D., Esnaola, J. A., & Larrañaga, M. (2018). A numerical analysis of multiaxial fatigue in a butt weld specimen considering residual stresses. In *MATEC Web of Conferences* (Vol. 165, p. 21005). EDP Sciences. URL: https://doi.org/10.1051/matecconf/201816521005

[32] Manson, S. S. (1965). Fatigue: a complex subject—some simple approximations. *Experimental mechanics*, 5(4), 193-226.

[33] Mikheevskiy, S. Elastic-Plastic Fatigue Crack Growth Analysis under Variable Amplitude Loading Spectra. *PhD thesis*, University of Waterloo, 2009.

[34] Mikheevskiy, S., Glinka, G., & Algera, D. (2010). Fatigue crack growth analysis of structural components–the UniGrow two-parameter driving force model. In *Proceedings of the ninth international conference on multiaxial fatigue and fracture*, Parma, Italy. URL: http://citeseerx.ist.psu.edu/viewdoc/download?doi=10.1.1.851.9412&rep=rep1&type=pdf

[35] Mikheevskiy, S., Glinka, G., & Algera, D. (2012). Analysis of fatigue crack growth in an attachment lug based on the weight function technique and the UniGrow fatigue crack growth model. *International journal of fatigue*, 42, 88-94. URL: https://doi.org/10.1016/j.ijfatigue.2011.07.006

[36] Mikheevskiy, S., Glinka, G., & Cordes, T. (2015). Total life approach for fatigue life estimation of welded structures. *Procedia Engineering*, 101, 177-184. URL: https://core.ac.uk/download/pdf/82277564.pdf

[37] Miller, K. J. (1991). Metal fatigue—past, current and future. Proceedings of the Institution of Mechanical Engineers, Part C: *Mechanical Engineering Science*, 205(5), 291-304.

[38] Moftakhar, A., Buczynski, A., & Glinka, G. (1994). Calculation of elasto-plastic strains and stresses in notches under multiaxial loading. *International journal of fracture*, 70(4), 357-373. URL: https://link.springer.com/content/pdf/10.1007/BF00032453.pdf

[39] Moftakhar, A., & Glinka, G. (1992). Calculation of stress intensity factors by efficient integration of weight functions. *Engineering Fracture Mechanics*, 43(5), 749-756. URL: https://doi.org/10.1016/0013-7944(92)90005-Y

[40] Nasir, N. S. M., Razab, M. K. A. A., Mamat, S., & Iqbal, M. (2006). Review on welding residual stress. stress, 2(5), 8-10.

[41] NEN-EN 1993-1-9, 2012. NEN.

[42] Neuber H. Kerbspannugslehre. Berlin: Springer; 1985.

[43] Newman, J. C. (1974). Finite-element analysis of fatigue crack propagation--including the effects of crack closure (Doctoral dissertation, Virginia Polytechnic Institute).

[44] Newman, J. C. (1974). Stress analysis of the compact specimen including the effects of pin loading. In *Fracture Analysis: Proceedings of the 1973 National Symposium on Fracture Mechanics, Part II*. ASTM International. URL: https://doi.org/10.1520/STP33136S

[45] Newman Jr, J. C. (1999). Analyses of Fatigue and Fatigue-Crack Growth Under Constant-and Variable-Amplitude Loading. URL: https://ntrs.nasa.gov/citations/20040086775

[46] Newman, J. C., & Annigeri, B. S. (2012). Fatigue-life prediction method based on small-crack theory in an engine material. *Journal of engineering for gas turbines and power*, 134(3).

[47] Newman, J. C., & Raju, I. S. (1983). Stress-intensity factor equations for cracks in three-dimensional finite bodies. In *Fracture Mechanics: Fourteenth Symposium—Volume I: Theory and Analysis*. ASTM International. URL: https://doi.org/10.1520/STP37074S

[48] Newman, J. C., Wu, X. R., Swain, M. H., Zhao, W., & Phillips, E. P. (2000). Small-crack growth and fatigue life predictions for high-strength aluminium alloys. Part II: crack closure and fatigue analyses. *Fatigue & fracture of engineering materials & structures* (Print), 23(1), 59-72.

[49] Nguyen, N. T., & Wahab, M. A. (1996). The effect of undercut, misalignment and residual stresses on the fatigue behaviour of butt welded joints. *Fatigue & fracture of engineering materials & structures*, 19(6), 769-778.

[50] Nguyen, T. N., & Wahab, M. A. (1998). The effect of weld geometry and residual stresses on the fatigue of welded joints under combined loading. *Journal of Materials Processing Technology*, 77(1-3), 201-208. URL: https://doi.org/10.1016/S0924-0136(97)00418-4

[51] Niederwanger, A., Ladinek, M., & Lener, G. (2019). Strain-life fatigue assessment of scanned weld geometries considering notch effects. *Engineering Structures*, 201, 109774. URL: https://doi.org/10.1016/j.engstruct.2019.109774

[52] Ninh, N. T., & Wahab, M. A. (1995). The effect of residual stresses and weld geometry on the improvement of fatigue life. *Journal of materials processing technology*, 48(1-4), 581-588. URL: https://doi.org/10.1016/0924-0136(94)01697-Y

[53] Noroozi, A. H., Glinka, G., & Lambert, S. (2005). A two parameter driving force for fatigue crack growth analysis. *International Journal of Fatigue*, 27(10-12), 1277-1296. URL: https://doi.org/10.1016/j.ijfatigue.2005.07.002

[54] Noroozi, A. H., Glinka, G., & Lambert, S. (2007). A study of the stress ratio effects on fatigue crack growth using the unified two-parameter fatigue crack growth driving force. *International journal of fatigue*, 29(9-11), 1616-1633. URL: https://doi.org/10.1016/j.ijfatigue.2006.12.008

[55] Pachoud, A. J., Manso, P. A., & Schleiss, A. J. (2017). New parametric equations to estimate notch stress concentration factors at butt welded joints modeling the weld profile with splines. *Engineering Failure Analysis*, 72, 11-24. URL: https://doi.org/10.1016/j.engfailanal.2016.11.006

[56] Pang, H. L. J. (1994). Analysis of weld toe radius effects on fatigue weld toe cracks. *International journal of pressure vessels and piping*, 58(2), 171-177. URL: https://doi.org/10.1016/0308-0161(94)90080-9

[57] Paris, P., & Erdogan, F. (1963). A critical analysis of crack propagation laws. *Journal of Basic Engineering*, 85(4), 528–533. URL: https://doi.org/10.1115/1.3656900

[58] Pedersen, M. M. (2019). Thickness Effect in Fatigue of Welded Butt Joints: A Review of Experimental Works. *International Journal of Steel Structures*, 19(6), 1930-1938. URL: https://doi.org/10.1007/s13296-019-00254-y

[59] Petroski, H. J., & Achenbach, J. D. (1978). Computation of the weight function from a stress intensity factor. *Engineering Fracture Mechanics*, 10(2), 257-266. URL: https://doi.org/10.1016/0013-7944(78)90009-7

[60] Prime, M. B. (1999). Measuring residual stress and the resulting stress intensity factor in compact tension specimens. *Materials & Structures*, 22(3). URL: https://public.lanl.gov/prime/CT.pdf

[61] Ramachandra Murthy, D. S., Gandhi, P., & Madhava Rao, A. G. (1994). A model for fatigue life prediction of offshore welded stiffened steel tubular joints using FM approach. *International Journal of Offshore and Polar Engineering*, 4(03).

[62] Ramberg, W., & Osgood, W. R. (1943). Description of stress-strain curves by three parameters. URL: https://ntrs.nasa.gov/citations/19930081614

[63] Rice, J. R. (1972). Some remarks on elastic crack-tip stress fields. *International Journal of Solids and Structures*, 8(6), 751-758. URL: https://doi.org/10.1016/0020-7683(72)90040-6

[64] Röscher, S., & Knobloch, M. (2019). Towards a prognosis of fatigue life using a Two-Stage-Model: Application to butt welds. *Steel Construction*, 12(3), 198-208. URL: https://doi-org.tudelft.idm.oclc.org/10.1002/stab.202070204

[65] Sadananda, K., & Vasudevan, A. K. (1997). Short crack growth behavior. In *Fatigue and Fracture Mechanics: 27th Volume*. ASTM International. URL: https://doi.org/10.1520/STP16240S

[66] Sanders, W. W., Derecho, A. T., & Munse, W. H. (1965). Effect of external geometry on fatigue behavior of welded joints. *Welding journal*, 44(2).

[67] Schreurs, P. J. G. (2012). Fracture Mechanics – Lecture notes. URL: https://www.mate.tue.nl/~piet/edu/frm/pdf/frmsyl1213.pdf

[68] Sha, G. T., & Yang, C. T. (1986). Weight functions of radial cracks emanating from a circular hole in a plate. In *Fracture Mechanics: Seventeenth Volume*. ASTM International. URL: https://doi.org/10.1520/STP17418S

[69] Shen, G., & Glinka, G. (1991). Weight functions for a surface semi-elliptical crack in a finite thickness plate. *Theoretical and Applied Fracture Mechanics*, 15(3), 247-255. URL: https://www.researchgate.net/profile/G_Glinka/publication/256431931_Weight_functions_for_a_semi-elliptical_crack_in_a_finite_thickness_plate/links/59d2aa06aca2721f4369b5cf/Weight-functions-for-a-semi-elliptical-crack-in-a-finite-thickness-plate.pdf

[70] Shen, G., Plumtree, A., & Glinka, G. (1991). Weight function for the surface point of semi-elliptical surface crack in a finite thickness plate. *Engineering fracture mechanics*, 40(1), 167-176. URL: https://doi.org/10.1016/0013-7944(91)90136-O

[71] Smith, E. H. (Ed.). (1994). Mechanical engineer's reference book chapter 7: materials, properties and selection. Oxford: Elsevier Ltd. URL: https://doi.org/10.1016/B978-0-7506-1195-4.50011-7

[72] Smith, K. N.; Watson, P.; Topper, T. H. (1970). A Stress-Strain Function for the Fatigue of Metals. *Journal of Materials*, 5(4), 767–778.

[73] Srawley, J. E. (1976). Wide range stress intensity factor expressions for ASTM E 399 standard fracture toughness specimens. *International Journal of Fracture*, 12(3), 475-476.

[74] Steimbreger, C., & Chapetti, M. D. (2017). Fatigue strength assessment of butt-welded joints with undercuts. *International Journal of Fatigue*, 105, 296-304. URL: https://doi.org/10.1016/j.ijfatigue.2017.09.011

[75] Suresh, S., & Ritchie, R. O. (1984). Propagation of short fatigue cracks. *International metals reviews*, 29(1), 445-475. URL: https://doi.org/10.1179/imtr.1984.29.1.445

[76] Vasudeven, A. K., Sadananda, K., & Louat, N. (1994). A review of crack closure, fatigue crack threshold and related phenomena. *Materials Science and Engineering*: A, 188(1-2), 1-22. URL: https://doi.org/10.1016/0921-5093(94)90351-4

[77] Vishnu Saseendran. Fracture Characterization and Analysis of Debonded Sandwich Composites. PhD thesis, 12 2017.

[78] Wang, C. H. (1996). Introduction to fracture mechanics. Melbourne, Australia: DSTO Aeronautical and Maritime Research Laboratory. URL: https://www.researchgate.net/profile/Chun_Hui_Wang2/publication/277137659_Introduction_to_Fracture_Mechanics/links/5562ce3f08ae86c06b65f6ee/Introduction-to-Fracture-Mechanics.pdf

[79] Westergaard, H. M. (1939). Bearing pressures and cracks. Trans AIME*, J. Appl. Mech*., 6, 49-53.

[80] Xin, H., & Veljkovic, M. (2020). Residual stress effects on fatigue crack growth rate of mild steel S355 exposed to air and seawater environments. *Materials & Design*, 108732. URL: https://doi.org/10.1016/j.matdes.2020.108732

[81] Zhu, S. P., Lei, Q., Huang, H. Z., Yang, Y. J., & Peng, W. (2017). Mean stress effect correction in strain energy-based fatigue life prediction of metals. *International Journal of Damage Mechanics*, 26(8), 1219-1241. URL: https://doi.org/10.1177/1056789516651920

A. Empirical formulas from literature

A.1 Newman-Raju Equation [47]

Newman-Raju proposed to use Eq. (A.1) to determine the SIF of a semi-elliptical crack in a finite width plate.

$$K_I = (S_t + HS_b)\sqrt{\frac{\pi a}{Q}}F\left(\frac{a}{c},\frac{a}{t},\frac{c}{b},\varphi\right) \tag{A.1}$$

The equations below are valid for a/c<1. The complete elliptic integral, Q, may be determined from Eq. (A.2) or from standard tables.

$$Q = 1 + 1.464\left(\frac{a}{c}\right)^{1.65} \tag{A.2}$$

The tension factor F is defined as in Eq. (A.3).

$$F = \left[M_1 + M_2\left(\frac{a}{t}\right)^2 + M_3\left(\frac{a}{t}\right)^4\right] f_\phi g f_w \tag{A.3}$$

Where:

$$M_1 = 1.13 - 0.09\left(\frac{a}{c}\right) \tag{A.4}$$

$$M_2 = -0.54 + \frac{0.89}{0.2 + \frac{a}{c}} \tag{A.5}$$

$$M_3 = 0.5 - \frac{1.0}{0.65 + \frac{a}{c}} + 14\left(1.0 - \frac{a}{c}\right)^{24} \tag{A.6}$$

$$g = 1 + \left[0.1 + 0.35\left(\frac{a}{t}\right)^2\right](1 - \sin\phi)^2 \tag{A.7}$$

f_ϕ corrects for the crack tip plasticity, assuming it is very small. Its value is given in Eq. (A.8).

$$f_\phi = \left[\left(\frac{a}{c}\right)^2 \cos^2\phi + \sin^2\phi\right]^{\frac{1}{4}} \tag{A.8}$$

f_w corrects for the finite width of the plate. Its value is given in Eq. (A.9).

$$f_w = \left[\sec\left(\frac{\pi c}{2b}\sqrt{\frac{a}{r}}\right)\right]^{\frac{1}{2}} \tag{A.9}$$

H is called the bending factor and can be determined by Eq. (A.10).

$$H = H_1 + (H_2 - H_1)\sin^\rho\phi \tag{A.10}$$

Where:

$$\rho = 0.2 + \frac{a}{c} + 0.6\frac{a}{t} \tag{A.11}$$

$$H_1 = 1 - 0.34\frac{a}{t} - 0.11\frac{a}{c}\frac{a}{t} \tag{A.12}$$

$$H_2 = 1 + G_1\left(\frac{a}{t}\right) + G_2\left(\frac{a}{t}\right)^2 \quad \text{(A.13)}$$

$$G_1 = -1.22 - 0.12\frac{a}{c} \quad \text{(A.14)}$$

$$G_2 = 0.55 - 1.05\left(\frac{a}{c}\right)^{0.75} + 0.47\left(\frac{a}{c}\right)^{1.5} \quad \text{(A.15)}$$

A.2 Weight Function Edge Crack [22]

The weight function for an edge crack in a finite width plate as defined by Kaya and Erdogan is given in Eq. (A.16).

$$m(x,a) = \frac{2}{\sqrt{\pi a}} \frac{G\left(\frac{x}{a},\frac{a}{t}\right)}{\left(1-\frac{a}{t}\right)^{\frac{3}{2}}\sqrt{\left(1-\left(\frac{x}{a}\right)^{2}\right.}} \tag{A.16}$$

Where:

$$G\left(\frac{x}{a},\frac{a}{t}\right) = g_1\left(\frac{a}{t}\right) + g_2\left(\frac{a}{t}\right)\frac{x}{a} + g_3\left(\frac{a}{t}\right)\left(\frac{x}{a}\right)^{2} + g_4\left(\frac{a}{t}\right)\left(\frac{x}{a}\right)^{3} \tag{A.17}$$

$$g_1\left(\frac{a}{t}\right) = 0.46 + 3.06\frac{a}{t} + 0.84\left(1-\frac{a}{t}\right)^{5} + 0.66\left(\frac{a}{t}\right)^{2}\left(1-\frac{a}{t}\right)^{2} \tag{A.18}$$

$$g_2\left(\frac{a}{t}\right) = -3.52\left(\frac{a}{t}\right)^{2} \tag{A.19}$$

$$g_3\left(\frac{a}{t}\right) = 6.17 - 28.22\frac{a}{t} + 34.54\left(\frac{a}{t}\right)^{2} - 14.39\left(\frac{a}{t}\right)^{3} - \left(1-\frac{a}{t}\right)^{\frac{3}{2}} - 5.88\left(1-\frac{a}{t}\right)^{5} - 2.64\left(\frac{a}{t}\right)^{2}\left(1-\frac{a}{t}\right)^{2} \tag{A.20}$$

$$g_4\left(\frac{a}{t}\right) = -6.63 + 25.16\frac{a}{t} - 31.04\left(\frac{a}{t}\right)^{2} + 14.41\left(\frac{a}{t}\right)^{3} + 2\left(1-\frac{a}{t}\right)^{\frac{3}{2}} + 5.04\left(1-\frac{a}{t}\right)^{5} + 1.98\left(\frac{a}{t}\right)^{2}\left(1-\frac{a}{t}\right)^{2} \tag{A.21}$$